

**Peptide modified C-dots for  
bioimaging applications**

**by**

**Zachary Thomas Anderson**

A thesis submitted in partial fulfilment for the requirements for the degree of MSc  
(by Research) at the University of Central Lancashire

**June 2019**



## Acknowledgements

I would like to thank my supervisor Dr Antonios Kelarakis and Dr Marta Krysmann for their support and guidance during my research project. I would also like to thank the laboratory technicians in the analytical suite who were always available to help with any problems. Lastly, I would like to thank my family and friends for all their support over this last year.

## Contributors

The pharmacy department at UCLAN did all the sterility, antimicrobial and haemolysis tests. A PhD student from the pharmacy department called Ella Gibbons did all the sterility, haemolysis and antimicrobial testing on all C-dot, K7 peptide and C-dotK7 samples.

## List of Tables

Table 1.....	37
Table 2.....	46
Table 3.....	47
Table 4.....	55
Table 5.....	59
Table 6.....	69
Table 7.....	82
Table 8.....	82

## Lists of Figures

Figure 1.....	1
Figure 2.....	4
Figure 3.....	6
Figure 4.....	7
Figure 5.....	10
Figure 6.....	12
Figure 7.....	13
Figure 8.....	15
Figure 9.....	17
Figure 10.....	19
Figure 11.....	20
Figure 12.....	23
Figure 13.....	23
Figure 14.....	27
Figure 15.....	28
Figure 16.....	29
Figure 17.....	35
Figure 18.....	47
Figure 19.....	50
Figure 20.....	52
Figure 21.....	54
Figure 22.....	56
Figure 23.....	58
Figure 24.....	60
Figure 25.....	62
Figure 26.....	70
Figure 27.....	76
Figure 28.....	77
Figure 29.....	79
Figure 30.....	83
Figure 31.....	85
Figure 32.....	86

## List of Abbreviations

A375 cells = Melanoma tumour xeno grafts via tail vessels

AD = Alzheimer's disease

AEAPMS = N-( $\beta$ -amino ethyl)- $\gamma$ -aminopropylmethyldimethoxysilane

AFM = Atomic force microscopy

APP = Amyloid precursor protein

A $\beta$  (1-42) = Amyloid beta peptides

A $\beta$  = Amyloid beta

Boc = Tert-butyloxycarbonyl protecting group

CaCo-2 cell line = Heterogeneous human epithelial colorectal adenocarcinoma cells

CDCl<sub>3</sub> = Chloroform-d

C-dots = Carbon dots

C-dots-FA = Fluorescent carbon nanodots conjugated with folic acid

C-dots-trans-dox = Carbon dots-transferrin-doxorubicin

CdSe/ZnS = Cadmium selenide / Zinc sulphide

CEE = Cross link-enhanced emission

Cervical cancer cells taken for a patient who died of cancer in 1951 called Henrietta Lacks from HeLe

CLSM = Confocal laser scanning microscopy

CNT = Carbon Nanotubes

CPPs = Cell penetrating peptides

CQDs = Carbon based quantum dots

DCM = Dichloromethane

DHLA = Dihydrolipoic acid

DIC = Differential interference contrast

DIEA = N-ethyldiisopropylamine

DLS = Dynamic light scattering

DMF = Dimethylformamide

DOX = Doxorubicin

DOX-CD = Doxorubicin conjugated with carbon dots

E.coli = Escherichia coli

EDC = (1-Ethyl-3-(3-dimethylaminopropyl)-carbodiimide

EPR effect = Enhanced permeability and retention

Fmoc = Fluorenylmethoxycarbonyl group

FR = Folic receptor

FTIR = Fourier Transform Infrared Spectroscopy

GQDG = Neuroprotective peptide to graphene quantum dots

HBTU = (2-(1H-benzotriazol-1-yl)-1,1,3,3-tetramethyluroniumhexafluorophosphate

HEPES = (4-(2-hydroxyethyl)-1-piperazineethane sulfonic acid) = HEPES

HPLC = High performance liquid chromatography

iRGD = Tumour-homing penetration peptide (CRGDKGPDC)

K7 poly-Lysine = Seven chained peptide sequence of Lysine amino acids attached together

M/z = Molecular ion ( $M^+$ ) peak

MCF-7 = Human breast cancer cell line

MEPs = Multi-walled carbon nanotubes epsilon polyLysine

Mg = Magnesium

Mg-CQDs = Magnesium-carbon quantum dots

MSCs = Living mesenchymal stem cells

MTT assay = Colorimetric assay for assessing cell metabolic activity

MWCO = Molecular weight cut off

MWNTs = Multi-walled carbon nanotubes

N-C-dots = Nitrogen-doped carbon dots

NHS = N-hydroxysuccinimide

NIH-3T3 cells = Mouse embryonic fibroblast cell line

NIR = Near Infrared region

NLS = Nuclear localization sequence peptide

NMP = 1-methyl-2-pyrrolidinone

NMR = Nuclear magnetic resonance

ORR = Oxygen reduction reaction

PDs = Polymer dots

PEG = Polyethylene glycol

PEGylated C-dots = Polyethylene glycol

PL = Photoluminescence

QDNPs = Quantum dot nanoparticles

QDs = Quantum dots

QY = Quantum Yield

RBFs = Round bottom flasks

RGD peptides = Arginine-glycine-aspartic

RGD-dQDs = Arginine-glycine-aspartic dendrimer-modified cadmium selenide quantum dots

ROS = Reactive oxygen species

S, C-dots = Sulphur-doped carbon dots

SHSY5Y is a human derived cell line, original cell line called SK-N-SH from which it was isolated from a bone marrow biopsy taken from a four-year-old female with neuroblastoma

SPPS = Solid Phase peptide synthesis

SQDs = Semiconductor quantum dots

Tat peptide = derived from the transactivator of transactivator transcription (TAT) of human immunodeficiency virus

TEM = Transmission Electron Microscopy

TFA = Trifluoroacetic acid

TFR = Transferrin receptors

ThT = Thioflavin

TIS = Triisopropylsilane

TPM = Two-photon microscopy

UV light = Ultraviolet light

UV-Vis = Ultra-violet visible spectroscopy

WST-1 Assay = Colorimetric assay designed to measure the relative proliferation rates of cells in culture

## Table of Contents

Declaration of work.....	ii
Acknowledgments and contributors.....	iii
List of tables .....	iv
List of figures .....	v
List of Abbreviations.....	vi
Abstract.....	xii
1. Introduction.....	1
1.1. Top-down and bottom-up methods of C-dot synthesis .....	2
1.2. Characterisation of C-dots.....	3
1.3. Tuning the photoluminescence properties of C-dots.....	4
1.3.1. Size control.....	4
1.3.2. Surface functionalization.....	4
1.3.3. pH solvent.....	5
1.3.4. Elemental content.....	6
1.4. Toxicity and bioimaging of C-dots.....	7
1.5. Bioimaging of C-dots.....	10
1.6. Conjugation with bioactive compounds.....	11
1.7. Toxicity of Quantum dot.....	11
1.8. Toxicity of C-dots.....	12
1.9. Biomedical applications of C-dots conjugation with peptides.....	14
1.10. Solid phase peptide synthesis (SPPS).....	22
1.10.1. Steps carried out in SPPS using Fmoc Strategy.....	23
1.10.2. Advantages and Disadvantages of SPPS.....	24
1.10.3. K7 peptide.....	25
1.11. Peptide Quantum dot conjugation.....	26
1.12. Summary of the introduction.....	29
2. Experimental Section.....	30
2.1. Materials.....	30
2.2. Synthesis of C-dot.....	30
2.3. Synthesis of K7 peptide.....	31

2.3.1. Cleaving off polymeric support resin from K7 peptide chain.....	32
2.4. C-dotK7 conjugates.....	33
2.4.1. Synthesis of C-dotK7A.....	33
2.4.2. Synthesis of C-dotK7B.....	34
2.5. Diagram of the method for K7 peptide attachment to C-dot.....	35
2.6. Purification method using HPLC analysis.....	35
2.7. Analytical characterisation methods.....	36
2.7.1. Elemental Analysis.....	36
2.7.2. Fluorescence spectroscopy.....	37
2.7.3. Infra-red spectroscopy.....	38
2.7.4. UV-Vis.....	38
2.7.5. Nuclear magnetic resonance.....	39
2.7.6. Dynamic light scattering using a Nano 300 series Zetasizer.....	39
2.7.7. Contact angle.....	40
2.8. Sterility Test Method.....	40
2.9. Liquid Antimicrobial Method.....	41
2.9.1. General Culturing Method.....	41
2.9.2. Testing Method.....	41
2.9.3. Plate Counting Method.....	41
2.10. Haemolysis Test Method.....	42
3. Analysis and discussion.....	43
3.1. Structural characterisation of C-dot, K7 peptide and conjugate...44	44
3.1.1. HPLC purification of K7 peptide.....	44
3.1.2. NMR for K7 peptide.....	52
3.1.3. Infra-red spectroscopy.....	57
3.1.4. Zetasizer.....	60
3.1.5. Contact Angle Measurement.....	61
3.2. Optical properties of C-dot, K7 peptide and conjugates.....	64
3.2.1. Fluorescence spectroscopy.....	64
3.2.2. UV-VIS analysis.....	75
3.3. Sterility Test.....	77
3.4. Haemolysis Test Method.....	78
3.5. Nanoparticles with both bioimaging and antimicrobial properties.....	79
3.6. Antimicrobial behaviour of C-dot, K7 peptide and conjugates.....	80
3.7. Comparison of results to literature data.....	84

4. Conclusion.....	88
5. Future Work.....	90
6. References.....	92

Appendix 1.....	103
Appendix 2.....	103
Appendix 3.....	104

## Abstract

The aims of this project included, synthesis and characterisation of Carbon dots (C-dots), surface modification of the C-dots to secure cell penetration and enhance Photoluminescence (PL) properties and the development of peptide C-dot conjugation to improve cell selectivity.

Fluorescent C-dots were prepared by the pyrolysis treatment of citric acid monohydrate and ethanolamine at 300°C. PL studies reveal that C-dots display excitation-dependent behaviour, show a high level of conjugation on the surface and can disperse well in water. A cell penetrating peptide (K7) made up of seven-lysine amino acids was synthesized using a semi-automated peptide synthesizer and purified using HPLC analysis. Based on the as-prepared C-dots, the K7 peptide was attached onto the surface of the C-dot via two methods to form two conjugated systems, C-dotK7A and C-dotK7B, respectively. Method A relies on the covalent attachment of C-dot at the end of the uncleaved peptide as grown in the synthesizer, whereas in method B the cleaved peptide is used for the conjugation.

Both conjugated systems demonstrate very low levels of haemolytic activity. A synergistic effect noticed for both C-dotK7A and C-dotK7B materials when tested against *E.coli* and *Staphylococcus* bacteria. At very low concentrations (0.01 mg ml<sup>-1</sup>) both materials effectively suppress bacteria colonies. The C-dotK7A material killed 43% of *E. coli* and *Staphylococcus* colonies and the C-dotK7B material killed 63% of *E.coli* colonies and 43% *Staphylococcus* colonies. Their unique photoluminescent behaviour, their antimicrobial properties and their supreme optical properties, makes C-dotK7 promising materials for bioimaging applications

## 1. Introduction

Bioimaging is a relatively new diagnostic tool used in research and the medical field and allows *in vivo* imaging of biological processes within a living organism, as well as molecular and cellular signalling/interactions and the movement of molecules through membranes. It is a highly informative method and can accurately track metabolites used as biomarkers for identifying diseases, progress of diseases and treatment response. However, there are some drawbacks to the currently available materials (Quantum dots (QDs) and organic dyes) used in bioimaging such as, toxicity issues, photobleaching, low quantum yields, and excitation only in the ultra violet (UV) light region etc.

Described below in Figure 1, are uses of bio imaging applications for a variety of synthesized C-dots, with brief descriptions of other potential applications such as drug delivery.

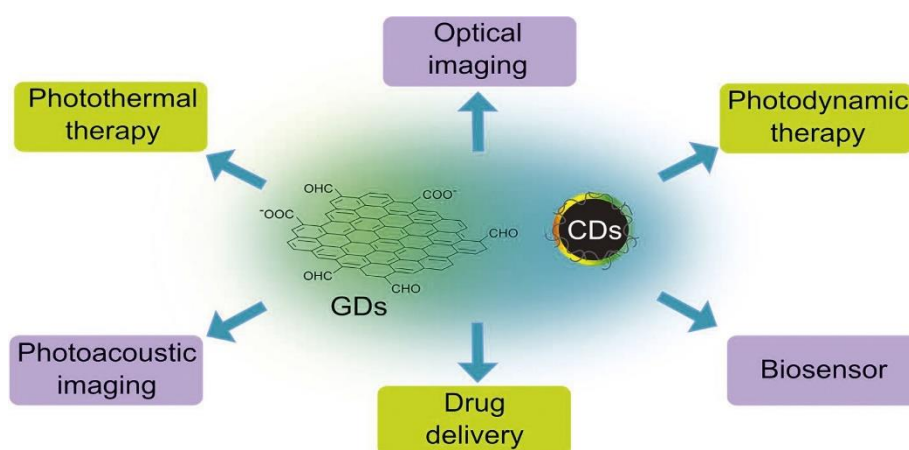


Figure. 1 – Some of the major bio applications of C- dots.<sup>1</sup>

C-dots represent a new type of fluorescent material that has the potential to replace traditional materials such as QDs and organic dyes. C-dots are now being synthesized using greener methods and show lower toxicity levels, greater biocompatibility, higher quantum yields and improved colloidal stability. With

respect to bioimaging applications, emphasis is given to the synthesis of C-dots with improved quantum yield in the deep-red and near infrared region that ideally also exhibit advanced cell selectivity.<sup>1,2</sup>

PL compounds are used in many important applications such as bio-imaging, photovoltaics, biological labelling, printing inks, chemical imaging and photocatalysis.<sup>3</sup> For these PL compounds to be used in more demanding applications (*in-vivo* imaging), they need to display good structural and photo stability in harsh environments, have a high affinity for certain proteins or cells in the body, high absorption, and provide high quantum yields but low toxicity levels.<sup>4</sup>

Moreover, C-dots show colour tuneability, easy chemical modifications, photo bleaching and up-conversion emission.<sup>5</sup> Structurally, the carbogenic core can be graphitic or amorphous carbon. The elemental composition of C-dots all have carbon, hydrogen and oxygen, some also consist of nitrogen, phosphorus and sulphur. Carbonyl, epoxy and carboxyl groups are typically found on the surface.<sup>1</sup> By modifying their size, structure and chemical composition, the PL properties of C-dots can be tuned with respect to their applications.<sup>2</sup>

### 1.1. Top-down and bottom-up methods of C-dot synthesis

In general, the synthetic methods for producing carbon-based quantum dots (CQDs) are divided into two approaches; “top-down” and “bottom up”. The top-down approach looks at synthesizing C-dots from materials like graphite, graphene, carbon nanotubes (CNT), carbon black, by reducing their sizes until the products show characteristics of PL nanoparticles. This can be done by electrochemical carbonization/oxidation, oxygen plasma treatment or chemical oxidative cutting/ablation.<sup>1</sup> Whereas, the bottom-up approach, focuses on carbon-rich precursors such as grass, fruit juice, carbohydrates that can be

pyrolyzed under suitable conditions.<sup>1</sup> In principle, it is an energy efficient approach to create PL carbon-nanoparticles with enhanced colloidal stability and fine-tuned surface chemistry.<sup>6</sup>

An important characteristic of C-dots to be used in applications is their PL emission. In “bottom-up” synthetic methods, the PL properties depend on the synthesis pathway, which determines the size and surface functionalisation of the resulting nanoparticle. *Wei et al*, prepared C-dots by using different amino acids with glucose followed by microwave pyrolysis. Different amino acids produced different sized C-dots and had different wavelength emissions such as blue, green and yellow.<sup>1</sup>

## 1.2. Characterisation of C-dots

C-dots can be characterised using various techniques, in which some are described below. Raman spectroscopy is an analytical technique that could be used to differentiate whether the carbon core is graphitic or amorphous. X-ray photoelectron spectroscopy (XPS) is a surface-sensitive quantitative spectroscopic technique that measures the elemental composition and can characterise the detailed bonding structure of the C-dots. Elemental analysis also can measure the elemental composition. Fourier Transform Infrared Spectroscopy (FTIR) is typically employed for the characterization of the surface functionalities.<sup>7</sup> Transmission Electron Microscopy (TEM) provides information about the size and morphology of the nanoparticles. The size distribution can be narrowed through post-treatment e.g. dialysis, oftentimes resulting in well-defined nanoparticles. For example; the pyrolysis reaction of citric acid and ethanolamine at different temperatures (230°C and 300°C), give rise to nanoparticles with average diameter 19 and 7 nm, respectively, as shown in Figure 2.<sup>4</sup>

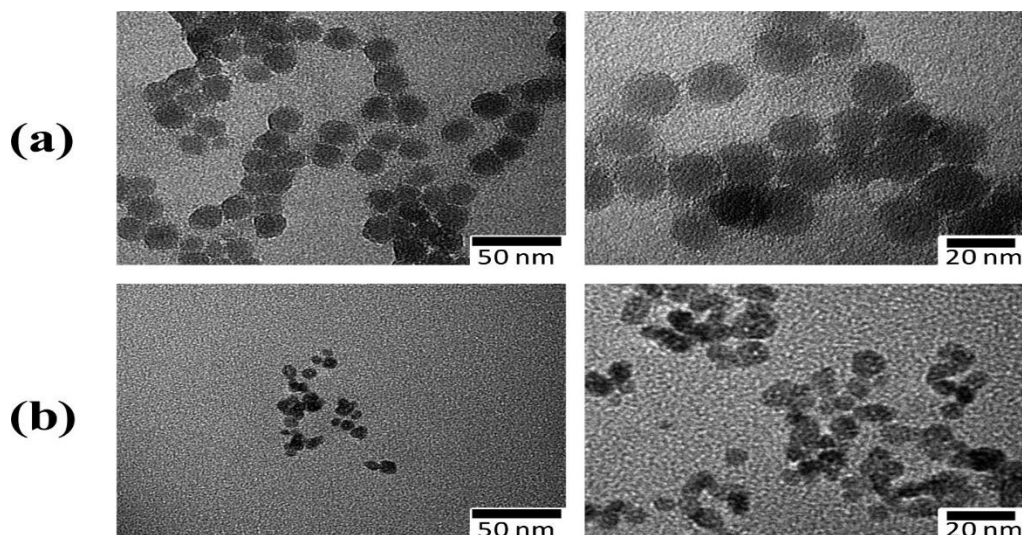


Figure 2. TEM images of (a) CNP230 and (b) CNP300 produced by pyrolytic treatment of citric acid and ethanolamine at 230 and 300 °C, respectively.<sup>4</sup>

### 1.3. Tuning the photoluminescence properties of C-dots

#### 1.3.1. Size control

Graphene “is a single-atom thin two-dimensional sheet consisting of hexagonally-packed carbon atoms”.<sup>8</sup> Recent studies have found that when graphene shrinks to zero dimension (nanoscale lateral dimensions) it can fluoresce, and it exhibits size-dependent emission.<sup>9</sup> The anticipation of CQDs to replace current organic dyes, semiconductor quantum dots (SQDs) and fluorescent proteins in many biomedical applications, is an exciting prospect because of their tuneable PL properties, molecular sizes and good biocompatibility with living tissue to not produce a toxic response. etc.<sup>8</sup>

#### 1.3.2. Surface functionalization

C-dots can have PL emissions even without any surface passivation, albeit the intensity tend to be rather low. Surface passivation with organic or polymeric materials attached onto the surface of C-dots, can help enhance the PL properties considerably. The emissions of passivated C-dots can broadly range

from the visible region and extend to the near infrared (NIR) region.<sup>10</sup> C-dots emitting in the NIR region (red) are important for bioimaging applications, since this NIR light can penetrate deep body tissue.<sup>1</sup>

Examples of C-dot surface functionalization;

It has been found by Sun *et al*, that doping the surface of the carbon nanoparticles with inorganic salts Zinc Oxide, Zinc Sulfide (ZnO, ZnS) can increase the quantum yield and the brightness of fluorescence emissions, compared to undoped C-dots.<sup>11</sup>

Goh *et al*. described in vivo and cellular bioimaging of PEG diamine capped C-dots made via the pyrolysis of citric acid in hot solvent. The C-dots were functionalised by linking hyaluronic acid to the surface to improve receptor-mediated endocytosis and specific delivery into cells of the body.<sup>12</sup>

Qiao *et al*. established a general and simple method to prepare multicolour PL C-dots. C-dots prepared by treatment of nitric acid with amorphous activated carbon and then the C-dots were passivated using amine-terminated compounds. The C-dots were good materials for a live-cell fluorescent imaging agent.<sup>13</sup>

### 1.3.3. pH solvent

The synthesis of sulphur-doped C-dots (S, C-dots) using waste frying oil as the precursor has shown pH sensitive PL. It was deduced, when the pH levels increase from 3 to 9, the deprotonation degree of the S, C-dots increases, producing higher concentrations of carboxyl functional groups on the surface of the S,C-dots, enhancing the PL intensity.

This can be viewed in Figures 3a and b. As the concentration of carboxyl groups reaches a maximum point, the PL intensity will begin to decrease and this can be

determined by measuring the pH value, which will be between (9-12). The pH response of PL intensity has been shown to be reversible. S,C-dots are capable fluorescent probes for pH monitoring in biomedical applications.<sup>14</sup>

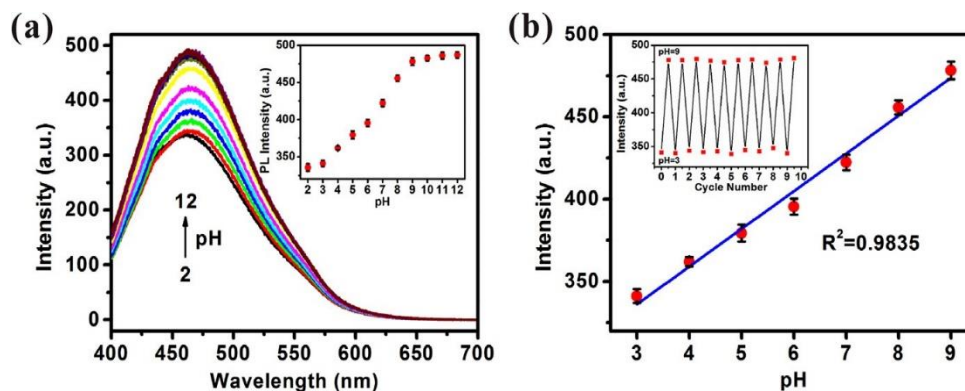


Figure. 3 – (a) PL spectra of the S, C-dots dispersion at different pH values (from 2 to 12) with excitation at 380nm. (b) A linear relationship between the PL intensity and pH (from 3 to 9).<sup>14</sup>

#### 1.3.4. Elemental content

The addition of heteroatoms via pre-doping or post-doping can affect the luminescence of C-dots.<sup>14</sup> Post-doping refers to treatments that aim to include heteroatoms to the surface of already prepared C-dots, pre-doping aims to include heteroatoms during the C-dot generation. An example of this is known as surface functionalization, where the surface of the C-dots is oxidized such as attaching amine groups. In a study by Liu et al, a Mg/N doping strategy was introduced that produced highly luminescent CQDs with a quantum yield (QY) of 83%. After hydrothermal treatment, Mg-carbon quantum dots (Mg-CQDs) were synthesized. The introduction of Magnesium (Mg) helped preserve majority of carboxyl groups on the surface and with the nitrogen-passivation lead to the high increase in the PL of the final CQDs.<sup>15</sup> It was also found, that nitrogen-doped C-dots (N-C-dots) had improved fluorescent intensity, compared to un-doped C-dots and N-C-dots were successful at detecting  $Fe^{3+}$ .<sup>16</sup>

#### 1.4. Toxicity and bio imaging of C-dots

Fluorescent imaging is a widely used technique, to view biological processes taking place in living cells, due to its high sensitivity, lack of radioactivity threat, better spatial resolution and greater throughout capability.<sup>17</sup> Therefore, C-dots are a promising prospect for the field of bioimaging, having interesting characteristics such as low toxicity, photostability, up-conversion PL, high solubility, multicolour wavelength tuned emission and resistance to photo-bleaching. C-dots are also promising in applications like drug and gene delivery, biosensors and optoelectronic devices.<sup>18</sup>

In a study by Sun *et al*, they first used C-dots for bioimaging by labelling *E. coli* cells using the PEG<sub>1500</sub>N-passivated C-dots. The fluorescent staining of the *E. coli* bacteria cells occurred when they were incubated with the PEGylated C-dots. The confocal microscopy images of Figure 4, show that the endocytosed C-dots were mostly present in the cytoplasm, with only a small amount penetrating the cell nucleus.<sup>11,19</sup>

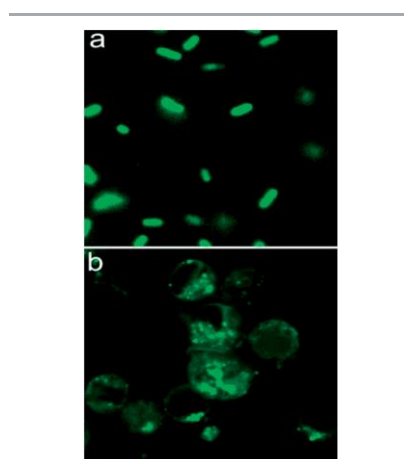


Figure. 4 – Confocal fluorescence microscopy images (488 nm excitation) of (a) *E. coli* and (b) *Caco-2* cells labelled with C-dot.<sup>11</sup>

Two kinds of C-dots using citric acid with 1, 2-ethylenediamine (CD-1) and N-( $\beta$ -aminoethyl)- $\gamma$ -aminopropyl methyltrimethoxysilane (AEAPMS) (CD-2) were synthesized and found to be excellent “turn off” fluorescent probes. They both

displayed quantum yields as high as 50-65%, which can be attributed to the heteroatom doping on the surface of the dots. The C-dots had low-level cytotoxicity and good cell permeability, thus lead to the successful fluorescence imaging of NIH-3T3 cells.<sup>20</sup>

The synthesis of green C-dots derived from apple juice, have been investigated for the imaging of bacteria (*Mycobacterium* and *Pseudomonas aeruginosa*) and fungal cells (*Magnaporthe oryzae*) and showed intracellular wavelength tuned emission.<sup>21</sup> Furthermore, highly soluble nitrogen-doped C-dots were synthesized from ethylenediamine tetraacetic acid using hydrothermal treatment. The study by *Shi et al* found a way to boost carbon-carbon double bond synthetic yields and show ultrahigh yield synthesis of N-doped C-dots via hydrothermal carbonization.<sup>22</sup> The group proved that the uptake and metabolism of N-doped C-dots (mostly in the digestive system) in zebrafish, where the N-doped C-dots showed excellent down-regulation effects for reactive oxygen species (ROS), and good protection against H<sub>2</sub>O<sub>2</sub>-induced oxidative stress (the ROS content in N-doped C-dots treatment groups was reduced by 68%).<sup>22</sup> Overall, the anti-oxidative and low toxic N-doped C-dots of this application, could be a step in the right-direction for helping age-related diseases.<sup>22</sup>

Zheng's group attached a platinum(VI) based anti-cancer pro drug oxidised oxaliplatin (Oxa(VI)-COOH) onto the surface of C-dots via chemical coupling.<sup>23</sup> These CQDs were taken up by cancer cells through endocytosis and the Oxa(VI)-COOH is reduced to oxaliplatin(II). The fluorescence signals of the CQDs can monitor the distribution of the pro-drug conjugated CQDs, to help adapt the injection time and dosage of the medicine. Lastly, the green method of hydrothermal treatment (180°C) of soy milk, which not only exhibits intriguing PL

properties, but also displays good electro catalytic activity towards the oxygen reduction reaction (ORR).<sup>24</sup>

Fluorescent carbon nanodots conjugated with folic acid (C-dots-FA) were synthesized to distinguish folate-receptor-positive cancer cells from normal cells. Confocal laser scanning microscopy was used to investigate the uptake of C-dots-FA by HeLa cancer cells. The images (Figure 5a-f) below show that the HeLa cells incubated with C-dots-FA show bright fluorescence in both the cytoplasm and membrane, but not the nucleus. Weaker fluorescence was observed when comparing Folic acid receptor (FR)-negative MCF-7 breast cancer cells, suggesting C-dots-FA can be transported into cells via a receptor-mediated endocytosis. No damage to the cells was observed and the colorimetric assay for assessing cell metabolic activity (MTT assay) shows the cell viability remained intact upon treatment with C-dots-FA, indicating the C-dot material has low cytotoxicity.<sup>25</sup> The targeting and detection of cancer cells from normal cells was successfully completed by culturing and analysing a model cell mixture of NIH-3T3 and HeLa cells. NIH-3T3 cells lack FR, while HeLa cells prominently overexpress FR. HeLa cells gave bright fluorescent images, whereas, NIH-3T3 cells did not express any fluorescence.<sup>25</sup>

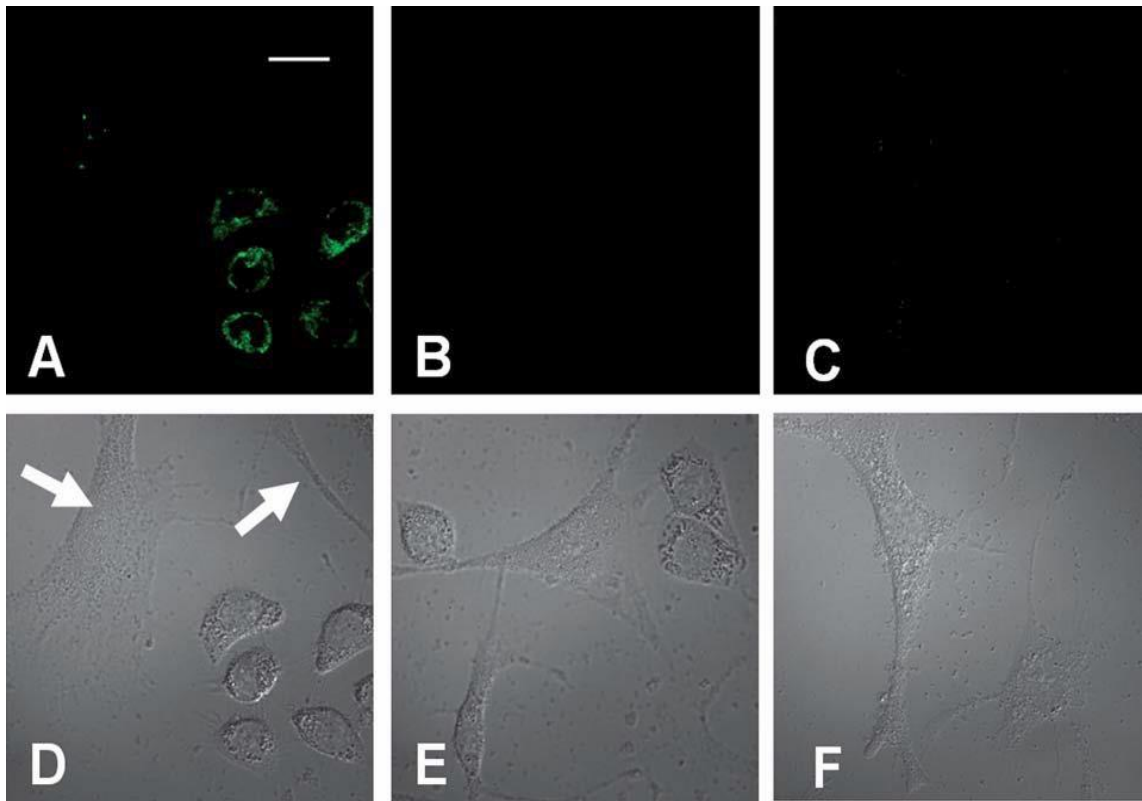


Figure 5: fluorescence images of different cell samples. A= NIH-3T3 and HeLa cells after incubation for 6h. B= control mixture of C-dots-FA ( $50 \mu\text{g mL}^{-1}$ ). C= only NIH-3T3 cells incubated with C-dots-FA at  $37^{\circ}\text{C}$  for 6h. Differential interference contrast (DIC) images of the corresponding samples (D-F), white arrows represent NIH-3T3 cells.<sup>25</sup>

### 1.5. Bioimaging of C-dots

Additionally, C-dots passivated with PPEI-EI agent for two-photon microscopy was reported by Cao *et al.*<sup>19</sup> The passivation leads to surface defects on the carbon particle surface acting as excitation energy traps, which allow human breast cancer MCF-7 cells be brightly illuminated under the microscope with excitation at 800nm. The C-dots were able to label both the cell membrane and cytoplasm of MCF-7 cells without reaching the cell nucleus in a considerable manner.<sup>19</sup>

#### 1.6. Conjugation with bioactive compounds

Carbon-dot-transferrin-doxorubicin covalent conjugate (C-dot-trans-Dox) was synthesized and investigated for the possibility of delivering the anticancer drug doxorubicin to treat pediatric brain tumours, via possible transferrin receptor-mediated transcytosis.<sup>26</sup> Four pediatric cell lines (CHLA-200, Daoy –tumour specimen at diagnosis), (CHLA-226, SJGBM2-tumor specimen from patients post chemotherapy) studied to compare the efficacy of C-dots-trans-Dox and Dox alone.<sup>26</sup> Studies reveal that the transferrin receptors (TFR) are overexpressed in many tumours.<sup>27</sup> The results from the *in vitro* studies show better uptake of the C-dot-trans-Dox material compared to Dox alone, likely due to high levels of transferrin receptors on these tumour cells.<sup>26</sup>

The experiment indicated that C-Dots-Trans-Dox at 10 nM was considerably more cytotoxic than Dox alone, reducing the cell viability by 45% for some of the pediatric brain tumour cell lines.<sup>26</sup>

#### 1.7. Toxicity of Quantum dots

An issue regarding QDs for use in biomedical applications has been their toxicity levels. Heavy metals such as Cadmium, Selenide and Zinc Sulphide used to synthesize quantum nanoparticles cause the materials to become very toxic.<sup>38</sup> Therefore, when the QDs introduced into the human body to target and kill particular cancer/diseased cells, they will unfortunately also destroy normal, healthy cells. Some of the methods mentioned in section 1.11, explained how

QDs –peptide conjugation is successful, but high toxicity is a great cause for concern.

### 1.8. Toxicity of C-dots

Carbogenic nanoparticles also named as “C-dots” where first discovered back in 2004 by Xu et al<sup>29</sup> and are environmentally friendly and biocompatible, without heavy metal centres or use of toxic elements.<sup>5</sup> Toxicity evaluations have been performed for C-dots and generally show encouraging results.<sup>11</sup> In a study by Yang et al, cytotoxicity evaluations on PEGylated C-dots were performed, and found that these dots were generally non-toxic to the cell lines.<sup>11</sup> The investigation by Tao et al, indicated no obvious toxic effects were present in blood tests or haematology readings for the in vivo toxicology of C-dots, observed in female balb/c mice for 90 days.<sup>11</sup> Hela cells were exposed to concentrations between 0-160 µg/mL of graphene quantum dots. As seen in Figure 6, over 95% of Hela cells survived after 24h incubation, even when the concentration of GQD increased to 160 µg/mL.<sup>30</sup>

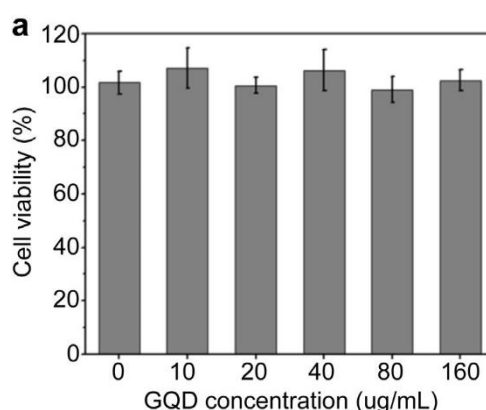


Figure 6. – Colorimetric assay ( WST-1-assay) the relationship between the GQD concentration and the cell viability.<sup>30</sup>

In one study, polyethylene glycol (PEG) anchored carbon nitride C-dots synthesized by a one-step hydrothermal treatment, then functionalized with a Nuclear Localization Sequence (NLS) peptide, by using a standard (1-Ethyl-3-(3-dimethylaminopropyl)-carbodiimide/N-Hydroxysuccinimide (EDC/NHS) coupling, for targeting the cell nucleus. The *in vitro* cytotoxicity study on the CDs@PEG and NLS-CDs using a MTT assay to assess the cell metabolic activity. In figure 7, it shows the cell viability of Hep G2, MCF7, A549 and L929 cells incubated with various concentrations of NLS-CDs. Roughly, 90% of all cells tested remained alive after a 24 h incubation with NLS-CDs, even after increasing the concentration of NLS-CDs to  $0.5\text{ mg mL}^{-1}$ . The cell viability is still above 75% even when the concentration of NLS-CDs is increased to  $2\text{ mg mL}^{-1}$ . Therefore, the as-prepared NLS-CDs and CDs exhibit very low cytotoxicity at the tested dose, which is also higher than the concentration usually required for cell imaging.<sup>31</sup>

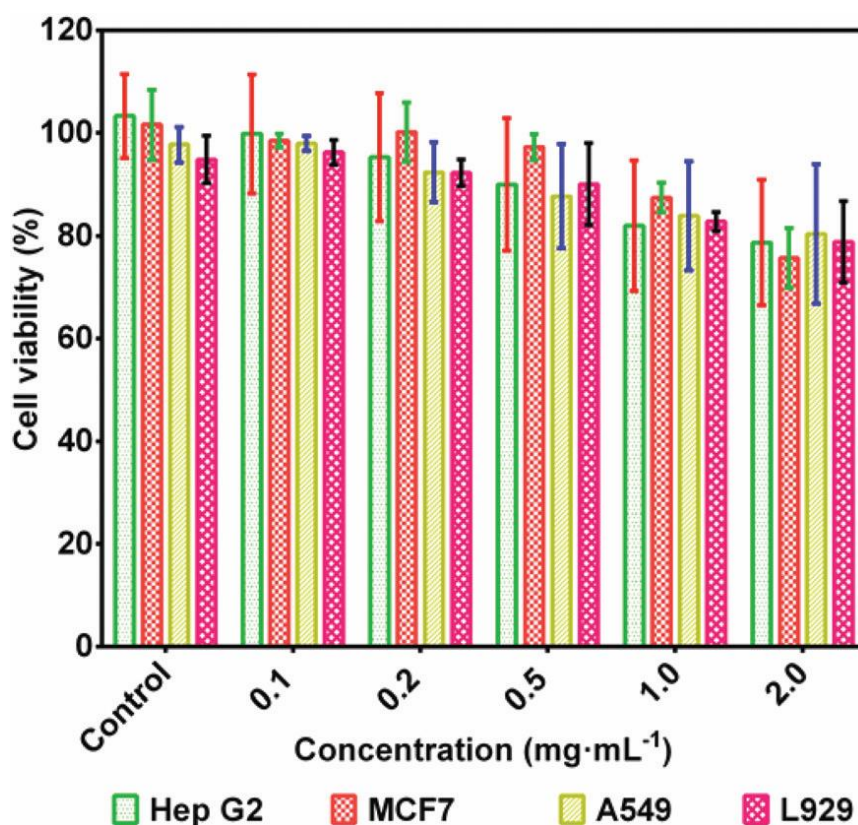


Figure 7. The viability of Hep G2, MCF7, A549, and L929 cells incubated with various concentrations of NLS-CDs for 24 h.<sup>31</sup>

A tumour-homing penetration peptide iRGD (CRGDKGPDC) conjugated with red shift emissive C-dots (iRGD-CDs). C-dots were synthesized by dissolving and heating melanin in deionized water and the iRGD added to the cooled solution. Different concentrations of iRGD-CDs used to incubate 4T1 mouse breast cells for a 24-hour period. Concentrations as high as 64 µg/mL, showed no difference between the control and iRGD-CDs treated cells after 24 hours, suggesting iRGD-CDs have low cytotoxicity consistent with C-dots. Increasing the concentration to 128 µg/ml could inhibit the growth of 4T1 mouse breast cells, meaning the iRGD-CDs could be useful at slowing down the cancer cells.<sup>33</sup>

#### 1.9. Biomedical applications of C-dots conjugated with peptides

Alzheimer's disease (AD) is one of the leading cause for dementia and is estimated to be a large health risk as society ages. Amyloid plaques found in the extracellular matrix are plaques mainly formed by the self-fibrillation of peptides known as amyloid beta (A $\beta$ ) peptides. Those peptides are produced by proteolytic cleavage of a transmembrane protein called the amyloid precursor protein (APP).<sup>34</sup> The mechanism linking A $\beta$  peptides and the growth of Alzheimer's disease is not fully clear, but it has been widely accepted that the fibrillation of A $\beta$  peptides is closely related to their neurotoxicity and development of AD.<sup>35</sup>

As mentioned above, one of the most widely accepted theories of AD is the amyloid hypothesis, involving aggregation and fibril formation of amyloid- $\beta$  (A $\beta$ ) peptides.<sup>37</sup> A research group led by Sun *Yet sen* designed a new nanomaterial (GQDG) conjugating a neuroprotective peptide to graphene quantum dots (GQDs). The *in vitro* assays including TEM and ThT (figure 10 a-b) performed to

investigate the inhibition effects of GQDs and GQDG in the aggregation of A $\beta$ 42. Both GQDs and GQDG exhibited better inhibitory effects on A $\beta$ 42 aggregation at a concentration of 200  $\mu$ g/mL compared to the reference compound resveratrol. TEM used to confirm the inhibitory effect of GQDs and GQDG. The TEM images show high-density long linear A $\beta$ 42 fibrils for the samples of untreated A $\beta$ 42 peptides. Whereas, the A $\beta$ 42 peptide samples incubated with GQDs and GQDG contained only a few short linear fibrils or few amount of amorphous aggregates. Thus, GQDs and GQDG could inhibit the aggregation of A $\beta$ 42 fibrils.<sup>37</sup>

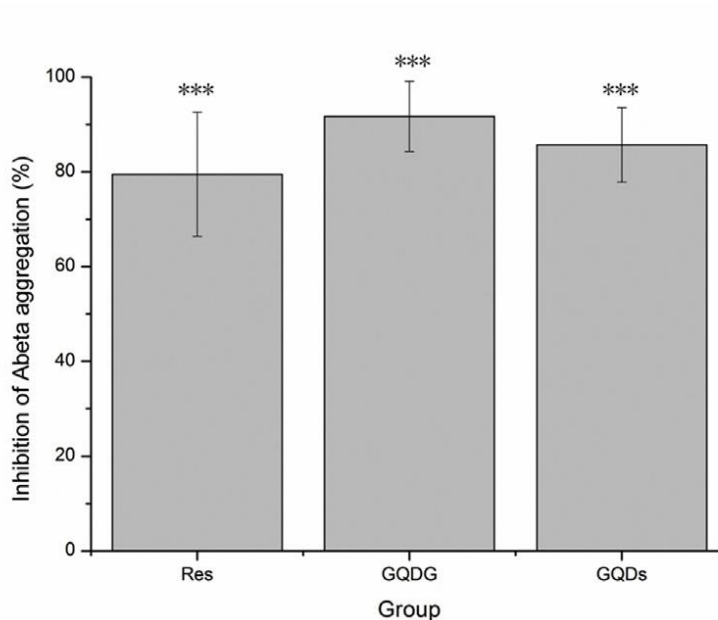
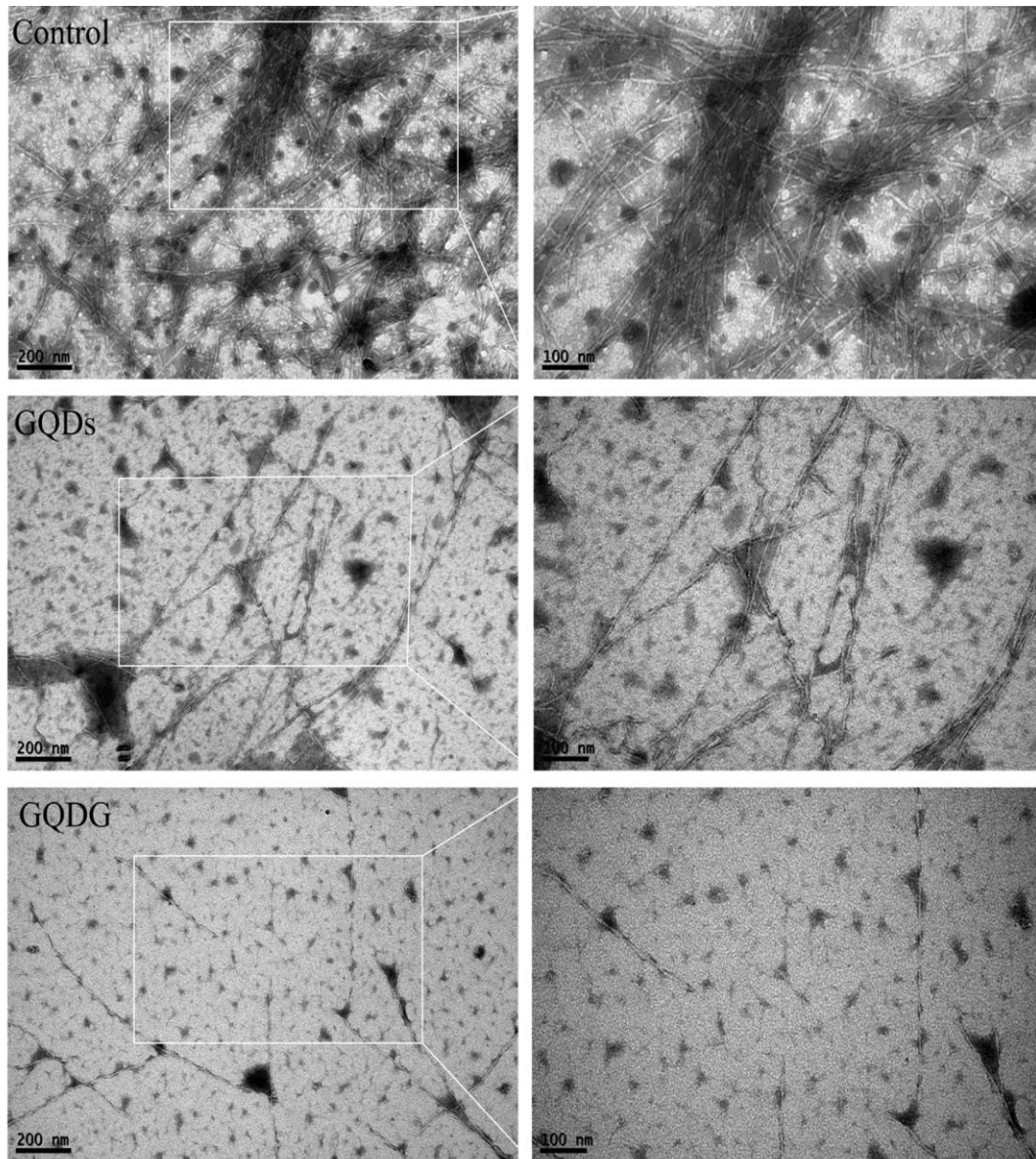


Figure 8a: ThT fluorescence assay to determine the inhibition of A $\beta$ 42 peptide aggregation when incubated with resveratrol, GQDG and GQDs at a concentration of 200  $\mu$ g/mL.<sup>37</sup>



*Figure 8b: The morphology effect of GQDG and GQDs on A $\beta$ 42 using TEM. Long linear fibrils present for the control sample of A  $\beta$ 42, whereas the sample of GQDs incubated with A $\beta$ 42 show fewer shorter fibrils and the GQDG incubated sample shows even fewer short fibrils.<sup>37</sup>*

In a study by a research group from Singapore, they synthesized C-dots by hydrothermal pyrolysis of sucrose in the presence of Polyethylene Glycol 1500 (PEG 1500) as a surface passivation and were conjugated with amyloid beta 42 peptides (A $\beta$ 42). The functionalized C-dots were assessed with regards to their ability to inhibit the amyloid fibrils.<sup>35</sup> The C-dots were incubated with SHSY5Y neuroblastoma cells to test their biocompatibility and even at a high concentration of 2 mg/ml, the cell viability is above 90%. The confocal images (Figure 8) of the

SHSY5Y cells below proves the C-dots can be internalized by the cells and localized in the cytoplasm.<sup>35</sup> The C-dots were mixed with A $\beta$ 42 peptides and the fibrillation process observed by using Thioflavin (ThT) staining. At its free state, ThT exhibits weak fluorescence, but when bound to amyloid fibrils the fluorescence increases greatly.<sup>36</sup> As shown in figure 9 (a-c), the ThT fluorescence signals are much lesser for C-dots treated with A $\beta$ 42 compared to the fluorescence signals of the control group (A $\beta$ 42 alone), implying that the fibrillation process is delayed significantly. The difference between the fibrillation process can be viewed in the TEM images between untreated A $\beta$ 42 fibrils in figure 9b and C-dots treated A $\beta$ 42 fibrils in figure 9c. The inhibition of amyloid fibrils shows the affinity between C-dots and A $\beta$ 42 peptides as the fluorescence intensities are lower. <sup>35</sup>

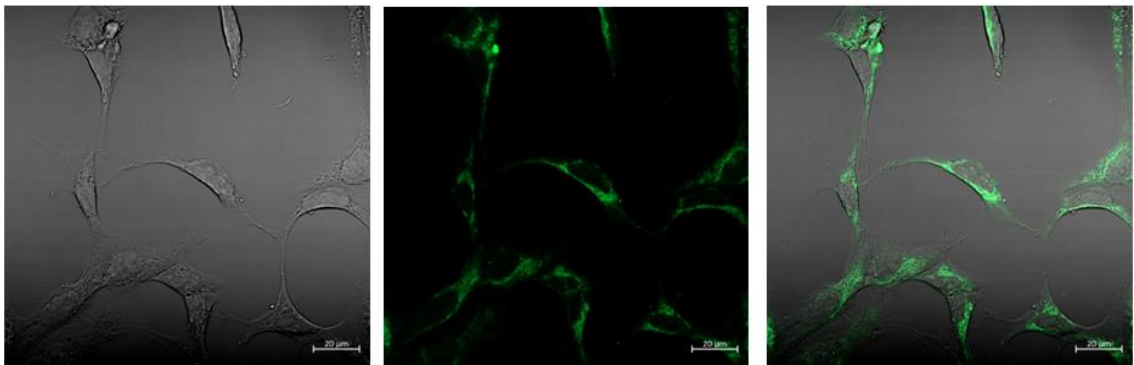


*Figure 9a): Labelling of SHSY5Y cell using C-dots, bright field image, fluorescence image and merged image.<sup>35</sup>*

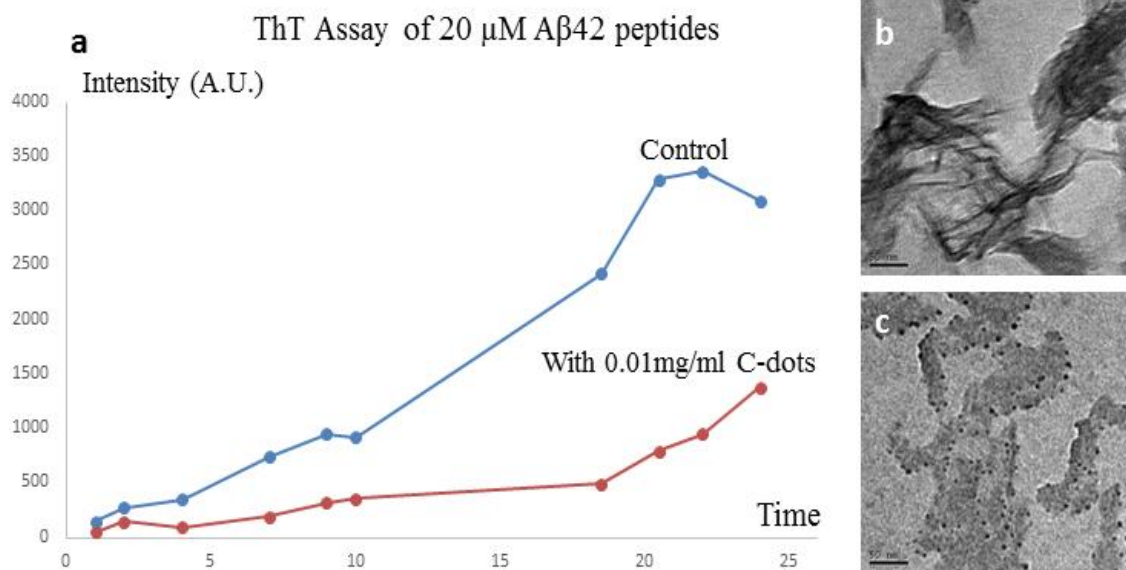


Figure 9b). (a) ThT assay of 20  $\mu$ M A $\beta$ 42 incubated with or without 0.01mg/ml of C-dots, and TEM images of untreated A $\beta$ 42 (b) and C-dots treated A $\beta$ 42 (c) after 24 hours incubation.<sup>35</sup>

In comparison, a similar study by *Garima Thakur et al* proved that amyloid beta (A $\beta$ ) peptides mixed with and conjugated to dihydrolipoic acid - (DHLA) capped CdSe/ZnS QDs can be used to reduce the fibrillation process. The QDs mixed or conjugated to A $\beta$  (1-42) show a decrease in the fibrillation as compared to pure A $\beta$  (1-42), when incubated at 37°C for seven days. The morphology and length of A $\beta$  (1-42) fibrils vary for the samples viewed in the TEM images (figure 10 a-d). Large number of short and long-length fibrils (30-1730 nm) observed in the pure A $\beta$  (1-42) sample. For the sample, having A $\beta$  (1-42) mixed with QDs the TEM exhibited longer fibrils with sizes of 2 micron. Whereas, shorter and thicker length fibrils (30-80nm) observed in the sample of A $\beta$  (1-42) conjugated to QDs. Analysis using AFM and ThT fluorescence assay also demonstrate that mixed or conjugated QDs with A $\beta$  (1-42) successfully inhibit the fibrillation process.<sup>38</sup>

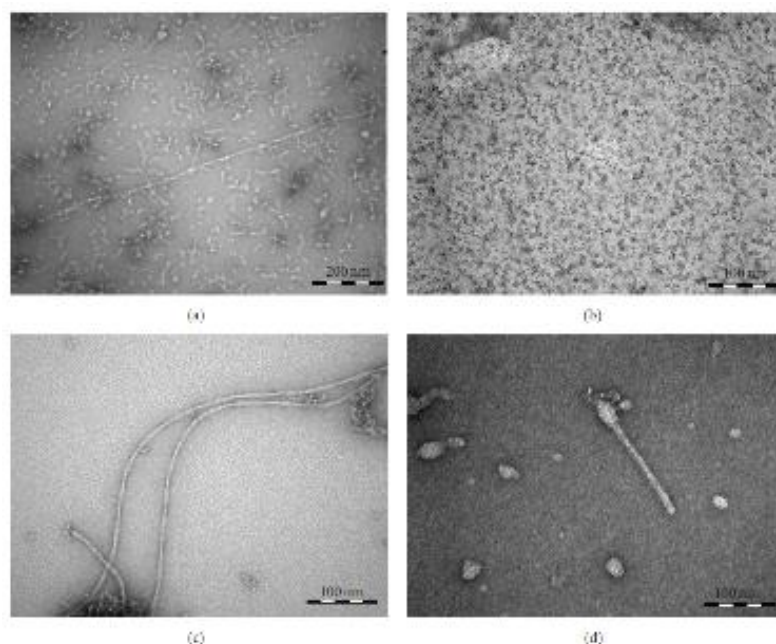


Figure 10: TEM images: (a) A $\beta$  (1-42) (b) DHLA-capped QDs (c) A $\beta$  (1-42) mixed with DHLA-capped QDs (d) A $\beta$  (1-42) conjugated to DHLA-capped QDs all sample contained in a buffer solution of PBS (pH 7.4).<sup>38</sup>

In another study, C-dots were functionalized with an NLS peptide (NLS-CDs) and were tested to transport the anticancer drug Doxorubicin (DOX) into A549 cancer cells to inhibit their activity. The survival rate of A549 cells when testing the cytotoxicity of Doxorubicin –C-dots (DOX-CD) showed it was over 90% at low concentrations ( $0.01-1 \mu\text{g mL}^{-1}$ ) after 24 hours exposure.<sup>32</sup>

The cellular uptake of DOX-CDs was analysed through flow cytometry and visualized using confocal laser scanning microscopy. It was interesting to find out that the DOX-CD complex group, had an increased cellular uptake compared with DOX by itself, and the fluorescence intensity of the complex group was 1.7 times higher than DOX after 4 hours incubation. <sup>32</sup>

Moreover, the DOX-CDs could efficiently induce cell death of A549 cells and decrease the free-DOX-induced necrosis. From the figure below, both DOX-CDs and free DOX could destroy tumour growth, while DOX-CD group showed higher inhibition levels than the free DOX group. The growth inhibition levels were calculated to be 41.6% (DOX) and 60.9% (DOX-CD) according to the tumour weight. <sup>32</sup> The higher tumour inhibition of DOX-CDs could be due to their ability for targeted delivery and efficient accumulation at tumour sites via the enhanced permeability and retention (EPR effect).<sup>28</sup>

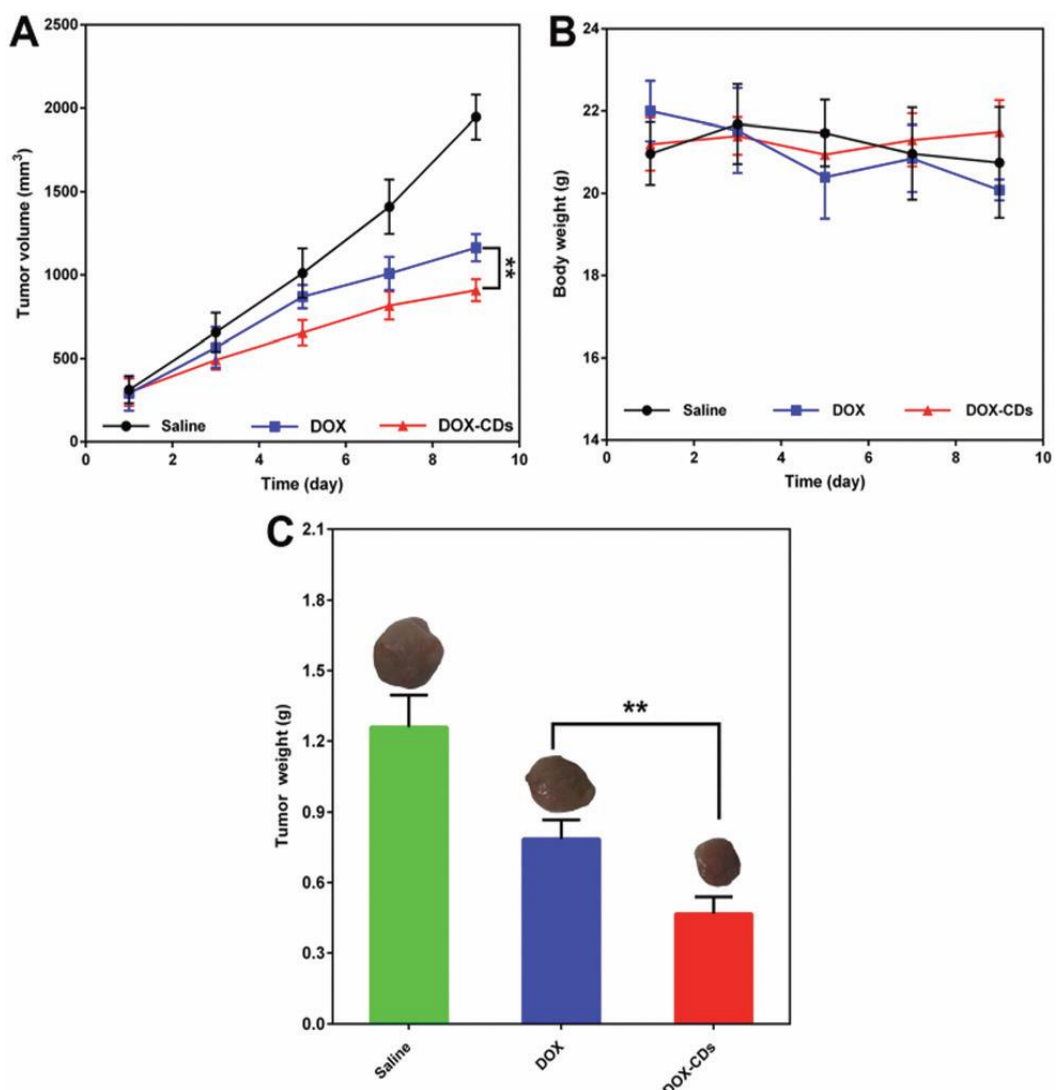


Figure 11: In vivo antitumor efficacy of DOX-CDs in BALB/c mice bearing A549 tumor. (A) The tumor growth curve of mice treated with free DOX and DOX-CDs, and mice given saline as a control, (B) mice body weight, and (C) tumor weight in different groups.<sup>40</sup>

There are only a few reports regarding C-dots for cell nucleus imaging.<sup>17</sup>

However, researchers have put forward a surface-functionalization method to try and effectively target the nucleus by attaching a NLS peptide to a nanoparticle.<sup>39</sup>

The NLS peptide was conjugated to the surface of the C-dots for binding to the importin and the complex could potentially pass through the core of the nucleus and eventually localize in the cell nucleus. The scheme below shows the possible method for NLS-CDs complex endocytosis and localisation to the nucleus.

A confocal laser microscope was used to observe the cellular localization of NLS-CDs incubated inside MCF7 and then A549 cells. NLS-CDs could enter into the cells easily even in the first 0.5 h of incubation and provides a blue light at 405nm. The fast uptake of NLS-CDs can be attributed to the small size as well as the good biocompatibility of C-dots and they can enter into the cells by means of endocytosis.<sup>40</sup> It involves the capture of the material from the surface of a cell and transport into the cytoplasm. The NLS-CDs brought into the cell inside membrane-bound endocytic vesicles that are formed from the phospholipid bilayer of the cell's plasma membrane. The NLS peptide was able to deliver the C-dots to cross the nuclear pore and be internalized into the nuclei. Moreover, the incubation time was gradually increased in which the cell nucleus exhibited a higher fluorescence intensity in the merged images providing a build-up of NLS-CDs in the nuclei. Large quantities of CDs penetrated into the nucleus and gave a stronger blue fluorescence after 4 h incubation compared to at 0.5 h, suggesting they gather inside the nucleus. <sup>40</sup>

## 1.10. Solid phase peptide synthesis

To improve the synthesis of peptides, a new synthetic method known as “solid-phase peptide synthesis” (SPPS) was first developed in the 1960s.<sup>41</sup> SPPS is a step-wise construction of a peptide chain attached to an insoluble polymeric support resin. SPPS allows unreacted reagents to be removed by washing with solvent, without loss of product. Using a macroscopic solid support matrix (resin/bead) to attach successive amino acids is a main feature in SPPS. Most of the solid supports are made from small beads of polystyrene plastic approximately 70-400 microns in size. Attached to each functional site of the polystyrene core is a linker. There are many linker molecules on the surface of each bead, and the number is normally selected by the millimoles of linker per gram of beads (mmol/g).<sup>42</sup> There are different types of linkers which can control the properties of the final product and what particular chemicals the resin bound peptide can handle during the reactions and cleavage stage. Wang and Rink are the most commonly used linkers in Fmoc-peptide synthesis. The Rink resin has a polystyrene core with Rink linkers attached and will form a peptide amide (CONH<sub>2</sub>), whereas the Wang resin has Wang linkers attached to the core and produces a peptide acid (COOH). The first amino acid attaching to a Wang resin is different from the successive amino acid-to-amino acid attachments.<sup>43</sup> To minimize forming racemic mixtures of amino acids and to make the synthesis easier, SPPS techniques synthesize peptides starting from the C-terminus.<sup>42,44,45</sup> The hydroxyl group highlighted in the figure 13 of Wang resin below is the point of attachment through an ester linkage to the C-terminal amino acid in the peptide chain. The remaining amino acids attach one by one to complete the peptide chain.

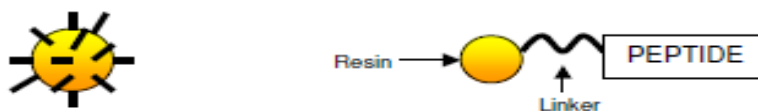


Figure 12: Linkers (in black) attached to functional sites of resin bead and close up of a single linker (black wavy line) linking resin to peptide.<sup>43</sup>

Every amino acid consists of both a carboxylic acid and amine functional group in which they potentially can react with each other during synthesis. To stop these two groups from reacting together and to make the precise peptide sequence, protecting groups need to be enforced. A good strategy known as “Fmoc Strategy” involves controlling the coupling reaction by protecting the amine-end of the amino acids with a Fluorenylmethoxycarbonyl (Fmoc) group. This prevents the amine-end of the amino acid from reacting, therefore only the carboxylic acid group on the incoming amino acid and the terminal amine group on the resin will couple. The scheme down below shows the general reaction of the Fmoc group attaching to amine-end of amino acid.

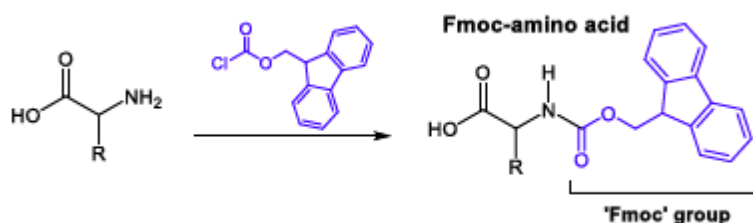


Figure 13: Synthesis of Fmoc-protected amino acids.<sup>42</sup>

#### 1.10.1. Steps carried out in SPPS using Fmoc Strategy

The fmoc-lys (boc)-Wang resin used has a lysine amino acid already attached. Thus, the resin must first be “deprotected” by removing the Fmoc group on the first amino acid (C-terminal amino acid) using a base such as piperidine.<sup>44,45</sup> The second Fmoc-protected amino acid is then attached using a coupling reagent to help the reaction (coupling reagents discussed further down). The Fmoc-group

removed with pyridine to deprotect the second amino acid, and then a third Fmoc amino acid can be coupled. The process continues until the peptide chain length has been reached. Then, the peptide undergoes a final deprotection step and can be isolated from the solid support. The peptide is cleaved off the Wang resin linker using trifluoroacetic acid (TFA) and the carboxylic acid terminus regenerates. Lysine has a side chain containing an amine group, which needs protecting during the synthesis to prevent any side-reactions from occurring. Tert-butyloxycarbonyl (Boc) is a good group to protect the side chain groups, as it prevents degradation due to good stability in basic conditions. In addition, Boc groups are unstable in acid, so they work well with Wang resins as they can be removed during the final cleavage of peptide.<sup>42</sup> To obtain an efficient reaction between an amine group and carboxylic acid to form a peptide bond, a “coupling reagent” or “activator” is used. The coupling reagent helps to convert carboxylic acids into “activated esters” prior to the reaction in order to aid displacement of the O-H by the  $-NH_2$  on the end of the growing peptide. The coupling reagent is used because the O-H functional group is a poor leaving group.<sup>46</sup>

#### 1.10.2. Advantages and Disadvantages of SPPS

Firstly, a large excess of reagents at high concentrations can be used to push coupling reactions to completion since the peptide is anchored to a solid support and only has one reactive end. Another advantage of SPPS is that filtration and washing steps can simply remove side products and excess reagents used after each coupling phase.<sup>42</sup>

The cost of the solid support resin, the repeated stepwise synthesis and the partial number of “linker” groups on the surface of the beads are some

disadvantages of SPPS. Nevertheless, “peptide synthesizers” are commercially available instruments which will speed up the procedure. With SPPS, only peptides having 30 amino acids or less are synthesized. Even though the reaction conditions are quite efficient, if you receive a high percentage of the coupled product at each step, after the addition of 30 amino acids, not all of the product will have the correct sequence. Longer sequences of peptides tend to be achieved through expression by bacterial cells such as *E.coli*.<sup>42,44</sup>

### 1.10.3. K7 peptide

Short-chained polyLysine peptides known as cell penetrating peptides, have the ability to pass through the cellular membrane and deliver types of cargo.<sup>47</sup> The “cargo” e.g. C-dot is related with the peptide either through chemical linkage via covalent bonds or through non-covalent interactions. The cell penetrating peptides function to deliver the cargo to cells for use in biomedical applications. Poly-Lysine increases electrostatic interaction between negatively charged ions of the cell membrane and positively charged surface ions of attachment factors on the culture surface. Hence, when the K7 peptide adsorbs to the surface of a cell culture, the number of positively charged sites should increase and be available for cell binding.<sup>48</sup> For the research study “Synthesis of C-dots conjugated with a K7 poly-Lysine peptide for biomedical applications” it was interesting to design and synthesize a peptide that could help promote transfer through the cell membrane of a cell and then attach to solid surfaces in biological applications. In addition, for the peptide to conjugate to the surface of a nanoparticle and assist in fluorescence imaging. Therefore, designed in this project, a K7 poly-Lysine peptide made up of seven-lysine amino acids.

### 1.11. Peptide Quantum Dot conjugation

C-dots are a new field of research, there are only a limited amount of research papers available, describing C-dot to peptide conjugation. However, there are close related QD nanoparticles that people have used to conjugate to peptide. A few examples are discussed below.

Polyethylene glycol (PEG) encapsulated Cadmium selenide/Zinc Sulfide CdSe/ZnS (QDs) conjugated with a Tat peptide and introduced into living mesenchymal stem cells (MSCs). The PL intensity of the QDs coupled with the Tat peptides improves significantly by over 40%.

The fluorescent images in figure 14 show that MSCs incubated with QD-Tat peptides emit fluorescence. A two-step synthetic route designed to create the CdSe/ZnS QDs.<sup>49</sup> In contrast, the coated QDs were directly incubated with MSCs without the attached Tat peptides, leading to no intracellular QD fluorescence observation in the MSCs. In addition, the QDs were attached to a random peptide but no cellular uptake was observed, meaning the Tat peptide is better at labelling MSCs with the attached QDs, than the random peptide. Moreover, the Tat-QDs labelled stem cells were further injected into the tail veins of nude mice and the tissue distribution of the labelled cells was studied by fluorescence spectroscopy. The characteristic fluorescence of QD-Tat peptides was observed mainly in the lung, the spleen, and the liver, with no or little QD accumulation in the kidney, heart or brain. Therefore, fluorescent imaging can be used to view the labelled stem cells and the Tat-QDs could potentially be used in stem cell transportation.<sup>50</sup>

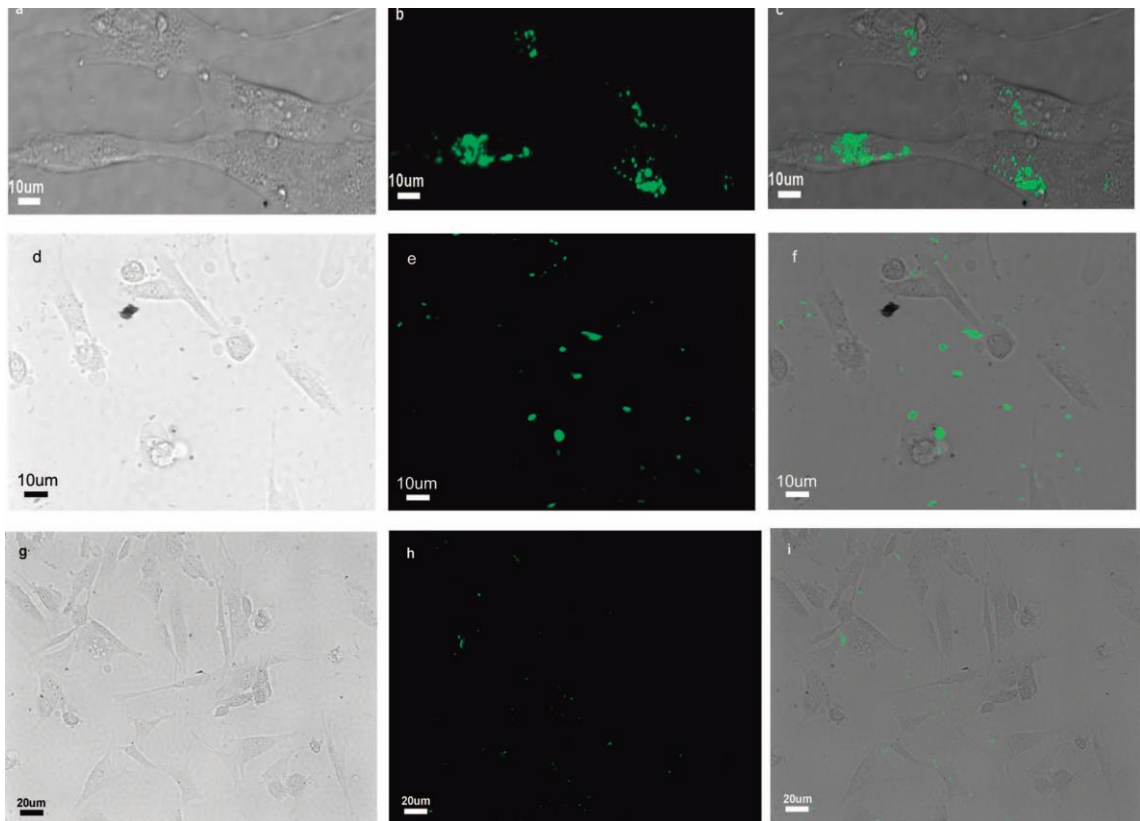


Figure 14: Fluorescent microscopy images of MSCs incubated with DSPE-PEG-coated QDs. MSCs labelled by the green QD-Tat peptides are shown in parts a-c. DSPE-PEG coated QDs were directly incubated with MSC without the assistance of Tat peptides, the images are shown in parts d-f. A control experiment was completed to use QDs with a random peptide, and the images are shown in parts g-i. a, d and g are images in the bright field, b, e and h are the corresponding fluorescent images and c, f and i are the merged images.<sup>50</sup>

In a different study but also using CdSe-ZnS QDs, an insect neuropeptide known as allatostatin 1, conjugates to streptavidin-coated CdSe-ZnS QDs. It transfects living NIH 3T3 and A431 human epidermoid carcinoma cells and transports QDs inside the cytoplasm and even the nucleus of the cells. Allatostatin could be useful for high-efficiency cell transfection and nucleus-specific cell labelling and transport of QDs inside the nucleus.<sup>51</sup>

One research group synthesized dendrimer-modified CdSe QDs and conjugated them to arginine-glycine-aspartic (RGD) peptides. The nanoprobe were injected into nude mice loaded with melanoma (A375) tumour xenografts via tail vessels. The arginine-glycine-aspartic dendrimer modified cadmium selenide quantum

dots (RGD-dQDs) nanoprobe can target tumour tissues, the bio distribution shows as time increases, the amounts of nanoprobe in blood slowly reduce, but the amounts slowly increase in the tumour tissues and are maximised after 3 hours. This is similar when comparing the *in vivo* imaging of nude mice, the fluorescent signal intensity in tumour sites becomes stronger as time passes. Therefore, with RGD-dQDs showing low cytotoxicity and high stability in biological environments, they have likely application in tumour diagnosis and therapy.<sup>52</sup>

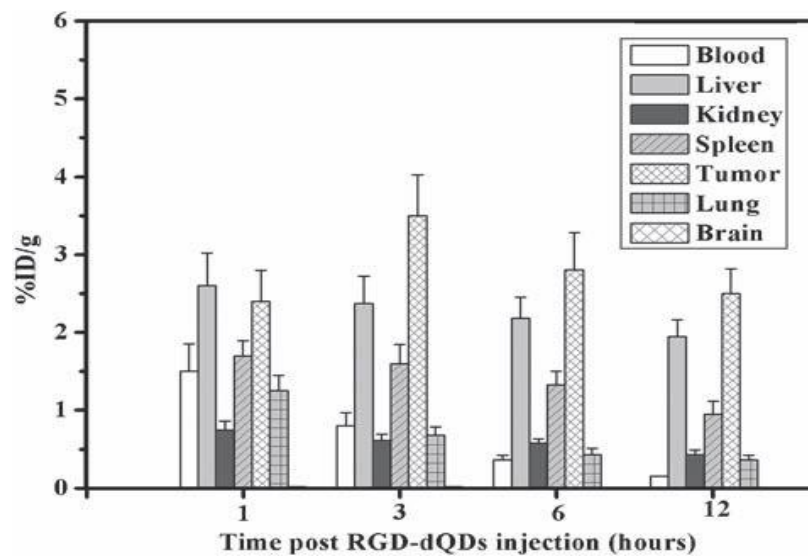


Figure 15: Biodistribution of RGD-dQDs nanoprobe in nude mice bearing melanoma.<sup>52</sup>

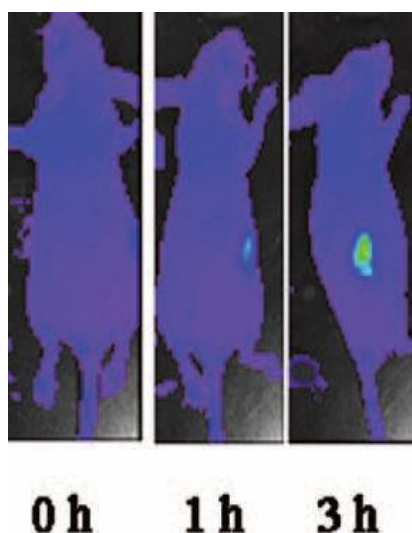


Figure 16: The images of mice in test group at 0, 1, 3-hour post-injection of 30 pmol RGD-dQDs nanoprobe.<sup>52</sup>

### 1.12. Summary of the introduction

One of the objectives of the research project is to synthesize and characterise C-dots. Part of the introduction chapter includes research about different ways C-dots are being synthesized. The materials used in C-dot synthesis are greener and renewable compared to QDs, leading to lower toxicity levels. A second objective, to modify the surface of the C-dot to secure cell penetration and enhance the PL properties. It was of interest, to discover how the surface of the C-dot can be modified to tune the PL properties. From literature, the size control, surface functionalisation and elemental content were a few techniques incorporated into the C-dot synthesis to try and increase the PL intensity, and to potentially lead to better cell detection. Another main objective is to develop peptide/C-dot conjugation to improve cell selectivity. It was interest to research other studies from literature to find out how C-dots can possibly be attached to a peptide and how the conjugated systems could potentially be used in bioimaging applications. Overall, the literature research described in the introduction chapter, provides helpful knowledge for the project work mentioned in the experimental and results chapters.

## 2. Experimental Section

### 2.1. Materials

All chemicals used in the research project purchased and supplied from either Sigma Aldrich or Alfa Aesar.

Citric acid monohydrate, Ethanolamine, Nitric acid (S.G. 1.42 70%), Fmoc-Lys (Boc)-Wang resin (loading mass = 0.4-0.6 mmol), Hydrochloric acid (S.G. 1.16 32%), Sodium hydroxide, Methanol, Acetonitrile (HPLC graded  $\geq 99.8\%$ ), Methionine, Chloroform-d all supplied from Sigma Aldrich.

Nepsilon-Boc-Nalpha-Fmoc-L-lysine, Triisopropylsilane (TIS, 98%), Trifluoroacetic acid (TFA, HPLC graded  $\geq 99\%$ ), (2-(1H-benzotriazol-1-yl)-1,1,3,3-tetramethyluroniumhexafluorophosphate, Tert-butyl-methyl ether (99%), 1-methyl-2-pyrrolidinone (NMP, 99+%), Dimethylformamide (DMF, 99.9%), Dichloromethane (DCM, 99+%), Piperidine (99%), N-ethyl-diisopropylamine (DIEA), Formic acid (97%) all supplied from Alfa Aesar.

### 2.2. Synthesis of C-dot

The synthesis of the C-dots follows a previously described method, which involves the reaction of citric acid monohydrate (30.2122g) and ethanolamine (28.3032g) in a molar ratio 1 to 3.<sup>4</sup> The mixture was stirred at 180°C for 30 mins under reflux in air, then the temperature was increased to 230°C and the reaction continued for 30 minutes without the reflux condenser. Next, the mixture was heated inside the furnace for one hour at 300°C for further decomposition. Then, the product is oxidised thus dispersing in distilled water (200 mL) and a 3M

concentration of nitric acid (200 mL), and heated under reflux for 16 hours at 100°C. Subsequently, the product cools to room temperature and placed in a snakeskin 3.5K MWCO dialysis tube membrane for twelve weeks, with the intention of removing any impurities or by-products that are smaller than 3.5K. Finally, the water removed via freeze-drying for 5 days to obtain the pure carbogenic product.<sup>4</sup>

### 2.3. Synthesis of K7 peptide

A Biotage Initiator + SP Wave semi-automated machine was used to synthesize K7. The insoluble polymeric support resin used in this synthesis is a pre-loaded fmoc-lys (boc)-Wang resin that comes with one lysine amino acid already attached. 0.1996g of the resin weighed into reactor syringe and placed inside the reactor holder of the machine. The resin swells for an hour to allow for expansion and opening of active sites for availability. Next, amino acids solutions prepared by adding 1.5 mL of NMP solvent to each vial of 0.14g lysine and 1.425 mL of NMP to each vial of 0.11g HBTU. All the solutions dispersed using a vortex to make sure all solid dissolved and then, HBTU solutions mixed with lysine solutions. After swelling of the resin, it must first be “deprotected” by removing the Fmoc group on the first amino acid to allow the second amino acid to join. Before, attaching the second amino acid solution, it requires the addition of 0.285 mL of DIEA stock solution (consists of 3.484 mL DIEA/ 6.516 mL NMP) which allows the carbon moiety of the residue to activate. After five minutes, the slightly yellowish solution is pipetted into the reactor syringe to undergo a “coupling with MW-deprotection reaction.” Each of the lysine amino acids have a blocking group attached known as a FMOC group. The  $\alpha$ -amino group of the incoming residue is temporarily blocked in order to prohibit peptide bond formation at this site. The

residue is un-blocked at the start of the next synthesis cycle and the cycle repeats until all amino acids attach.<sup>53</sup>

### 2.3.1. Cleaving off polymeric support resin from K7 peptide chain

The peptide batches split equally into glass vials. A stock solution of TFA: TIS: H<sub>2</sub>O (95:2.5:2.5) were prepared and 15 mL poured into each glass vial. The pale, yellow solutions placed inside the shaker and incubated for 3 hours at room temperature (30°C, rpm: 105). Then, using glass teat pipettes with a small amount of cotton wool blocking the insides, the precipitated solutions were pipetted into round bottom flasks (RBFs) trapping the solid beads inside the glass teat pipettes. Using the rotary evaporator roughly halved the amount of TFA stock liquid from the peptide solutions and placed the RBFs inside an ice-bath to remain cool. Added to the reduced volumes of TFA, a good squeeze of cold tert-butyl-methyl ether (no more than 40 mL). Each of the solutions gave a white precipitate and the solutions transferred to separate labelled falcon flasks, making sure RBFs washed out with extra cold ether to obtain all peptide solid. Next, decanted off as much of the TFA/ether solution without losing any of the solid. Then, added cold ether to each of the falcon flasks and weighed them to attain the same weights, before placing them into the centrifuge. Centrifuge settings: 4000 rpm, 3 minutes, 20°C. Once the flasks were removed from the centrifuge, decanted off all or most of the ether solution and left to dry.<sup>54</sup>

## 2.4. C-dot-K7 conjugates

Two protocols established in order to attach the C-dot to the K7 peptide. One protocol was aiming to attach the C-dot at the end of the peptide chain. Whereas, the other protocol will try to allow the peptide to ravel around the C-dot to shield it.

### 2.4.1 Synthesis of C-dotK7A

Following a similar method of attaching lysine amino acids to the support resin, the C-dot attaches to the end of the peptide chain. Firstly, the peptide batch containing the already attached lysines have been deprotected to help swell the peptide. Next, the solution of 0.11g HBTU in 1.425 mL NMP and solution of 0.0021g C-dot in 1.5 mL NMP dispersed and mixed. Both solutions combined with stock solution of 0.285 mL DIEA, left for 5 minutes to help activate the carbonyl functional group for attachment to peptide. C-dot then attaches via a coupling with MW reaction. The polymeric support resin cleaved exactly the same way as mentioned above in section 2.1.1. The carbon dot-K7 (C-dotK7) residue dispersed in water (20 mL) purifies using a dialysis membrane snakeskin, which allows larger, impure materials to disperse from the snakeskin bag, leaving the pure C-dotK7 material inside. The snakeskin bag placed into a large beaker (3L) filled with e-pure water and the water replaced daily for around 3 months, removing any impurities. Finally, the solution freezes to allow sublimation through freeze-drying obtaining the carbon dot-K7 peptide material.

#### 2.4.2 Synthesis of C-dotK7B

A solution of 0.0039g of C-dot dispersed in 5 mL of NMP, a solution of 0.2202g of HBTU dispersed in 5 mL of NMP and a solution of K7 peptide residue dispersed in 10 mL of NMP were prepared. All three solutions were combined together into a 45 mL syringe bottle. Then, 0.570 mL of DIEA solution was added and the bottle was placed inside the shaker for one hour at room temperature to mix thoroughly. The solution of C-dot-peptide from the bottle is transferred into a dialysis membrane snakeskin bag. The snakeskin bag is placed into a large beaker (3L) filled with e-pure water and the water replaced daily (over a 3-month period), removing any impurities. Lastly, the solution freezes to allow sublimation through freeze-drying obtaining the pure C-dot-peptide material.

## 2.5. Diagram of the method for K7 peptide attachment to C-dot

The figure 17 below shows a possible method for the attachment of K7 peptide to the surface of the C-dot. One method suggests that the N-terminus end of the K7 peptide will react with a possible oxygen based group on the surface of the C-dot and attach in an orderly fashion. The second method explains that more than one area of peptide reacts with the surface of the C-dot and the peptide wraps itself around its surface. Lastly, two units of the peptide may attach to the C-dot to form a dimer.

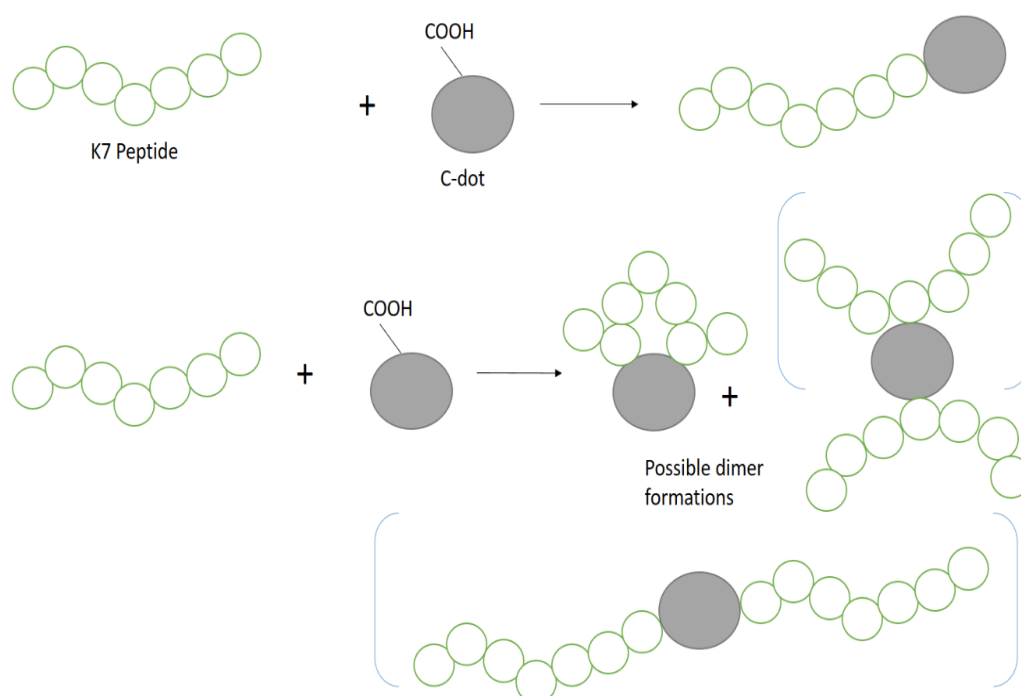


Figure 17: Protocol reaction scheme for C-dot-K7 peptide attachment.

## 2.6. Purification method using HPLC analysis

High performance liquid chromatography (HPLC) is the analytical technique used to separate and purify the K7 peptide. The crude K7 peptide contains some contaminants from the synthesis reagents, so passing the peptide solution through a column under high pressure helps to separate out the individual components/analytes. A mobile phase passes through the material in the column,

which is called the stationary phase. When the analytes in the K7 peptide pass through the column, they interact at different rates with both the stationary and mobile phases, predominantly because of the different polarities.<sup>55</sup> Therefore, the analytes that interact least with the stationary phase or interact most with the mobile phase will leave the column fastest. By adjusting the percentages of mobile phases and therefore the polarities, will help to separate all components of K7 peptide. A UV detector coupled to the HPLC apparatus to characterize the analytes as they separate. The first objective of HPLC analysis is to achieve a good separation of peaks on the chromatogram in which the pure sample of K7 peptide can be identified. Once the intensity peak of K7 peptide has been identified, the solution containing the pure component can be isolated at the time the peak begins and until the peak ends. After five injections, the pure peptide solution to be injected into the mass spectrum to obtain the molecular weight of peptide. A second objective, to establish a short timed method, to be replicated onto the semi prep scale so that several, larger injections can be performed in order to achieve a higher yield of pure K7 peptide.

## 2.7. Analytical Characterisation methods

### 2.7.1. Elemental Analysis

Elemental analysis is an analytical technique to gain information about the elemental composition of an unknown material. Firstly, using Flash 2000 organic elemental analyser (CHNS-O analyser) sample of C-dot burned through combustion to determine the carbon, nitrogen, hydrogen and sulphur element percentages of the material. A known amount of substance is converted to simple, known compounds containing the element required to be analysed. For

example, carbon and hydrogen will be determined in the materials by conversion through combustion to carbon dioxide and water. In table 1, the C-dot material listed displays the percentage of each element present.<sup>56</sup> The pyrolysis of C-dots at 300°C using citric acid and ethanolamine (same as method in section 2.2) reported and the element composition tested using elemental analysis. The percentage of the elements of the C-dot material were similar to the C-dots prepared in section 2.2, (50.5% C, 3.7% H, and 13.1% N).<sup>4</sup>

Table 1: Percentage of element composition of C-dot.

Percentage of Element Composition (%)				
Sample	Nitrogen	Hydrogen	Carbon	Sulphur
C-dot	13.53	7.16	60.14	0

### 2.7.2. Fluorescence Spectroscopy

Fluorescence spectroscopy measures the intensity of photons emitted from a sample after it has absorbed photons. When a beam of ultraviolet light shines onto the sample solution, it excites the electrons of certain molecules within the sample and causes them to emit light. For the C-dot, C-dotK7A and C-dotK7B samples, 4 mL of each solution placed into a clear cuvette. The cuvette placed into the holder inside the Horiba Jobin Yvon fluoromax-4-spectrofluorometer and a wavelength range of 350-500 nm set, for the incident photon source to shine light onto the solutions.

The species (related to the sample material) is excited into a higher electronic state by absorbing a photon. The excited molecule will then start to lose vibrational energy as it collides with other molecules until it reaches the lowest vibrational state of the excited electronic state. The molecule will eventually drop

back down to the ground state by emitting a photon. Emission happens from the ground vibrational level of the excited electronic state and goes to an excited vibrational state of the ground electronic state. The fluorescence also measured for all of the samples by changing the pH value.<sup>57</sup> Hydrochloric acid (32%) used to lower the pH of each solution, whereas Sodium hydroxide (1M concentration liquid) used to increase the pH values.

### 2.7.3. Infra-red spectroscopy

Infra-red (IR) spectroscopy involves the interaction of infrared radiation with material. A very small amount of solid material is placed onto a sample holder and a beam of IR light is passed through the sample.<sup>58</sup> When the frequency of the IR matches the vibrational frequency of a bond or collection of bonds in the material<sup>58</sup>, then absorption occurs and this is observed in graph with transmittance (%) versus wavenumber ( $\text{cm}^{-1}$ ). In the analysis section, the IR spectrums of all the samples are presented showing the main functional groups.

### 2.7.4. UV-Vis

Ultra-violet spectroscopy refers to the absorption or reflectance spectroscopy in the ultraviolet-visible spectral region. The samples dispersed in water (0.1 mg/ml) and each solution poured into a 4 ml UV quartz cuvette. Firstly, a blank (just water) was ran on the UV spectrometer used as a control/reference point, then each sample placed into the holder and UV light is radiated onto each solution. The absorbance or reflectance of UV light directly affects the apparent colour of the chemical solution. The absorbance of UV light radiation is related with excitation of electrons, in molecules and atoms from lower to higher energy levels.<sup>59</sup>

### 2.7.5. Nuclear magnetic resonance

Nuclear Magnetic Resonance (NMR) spectroscopy is an analytical technique for determining the molecular structure of materials.<sup>60</sup> Several nuclei have spin and all nuclei are electrically charged. An energy transfer can be possible between the base energy to a higher energy level, if an external magnetic field is introduced. The energy transfer takes place at a wavelength that links to the radio frequencies and when the spin returns to its base level, energy is emitted at the same frequency. The energy transfer will match a signal and is processed in order to yield an NMR spectrum.<sup>60</sup>

### 2.7.6 Dynamic light scattering using a Nano 3000 series Zetasizer

Dynamic light scattering (DLS) is a technique that can be used to measure the size of particles suspended within a liquid.<sup>62</sup> The Brownian motion is measured by the DLS and with time, this helps to identify the size of the particles present in the liquid. Brownian motion is described as the random movement of particles due to their collisions with other atoms and molecules such as solvent molecules.<sup>63</sup> These particles diffuse at a speed related to their size, smaller particles diffusing faster than larger particles.

A Nano series Zetasizer (Malvern Instruments) was used to measure the size of the particle species present in the K7 peptide. The K7 peptide filtered into a UV cuvette through a minisart (0.45 $\mu$ m) filter unit to remove any dust or fine particles. The cuvette is placed inside the zetasizer sample holder and a laser beam illuminates the K7 solution. The laser beam allows the measurement of the rate at which the intensity of the scattered light fluctuates. The rate at which these intensity fluctuations happen will depend on the size of the K7 particles.

### 2.7.7. Contact angle

When an interface exists between a liquid and a solid, the contact angle can be calculated between the surface of the liquid and the outline of the contact surface. The contact angle is the measure of the wettability of a solid by a liquid.<sup>64</sup> A contact angle of  $0^\circ$  shows complete wetting and a complete spread of the liquid evenly against the solid surface. An angle between  $0^\circ$  and  $90^\circ$  shows the solid is wettable and an angle above  $90^\circ$ , the solid is not wettable. The lower the contact angle, the greater the hydrophilic interaction of the solid surface with water and other polar groups. The contact angle above 90 degrees describes the solid surface exhibiting hydrophobic interactions.<sup>64</sup>

The method used to measure the contact angles for the solutions of C-dot, K7 peptide, C-dotK7A and C-dotK7B is the sessile drop technique. In this technique, a droplet of each test solution is placed onto a micro glass slide's surface and an image taken using a camera that is fixed into a stationary place to provide an accurate image of the droplet. The image of the droplet for each solution is viewed onto a screen and the contact angle calculated.

*The pharmacy department at UCLAN did all the sterility, antimicrobial and haemolysis tests. A pH student from the pharmacy department called Ella Gibbons did all the sterility, haemolysis and antimicrobial testing on all C-dot, K7 peptide and C-dotK7 samples.*

### 2.8. Sterility Test Method

A single, sterile loop of solution was streaked onto a nutrient agar plate in a zigzag manner. The plates incubated at  $37^\circ\text{C}$  and checked after 24 hours and 48 hours for any signs of bacteria growth. The absence of growth indicates sterility, which is a necessary property in order to carry out antimicrobial testing.

## 2.9. Liquid Antimicrobial Method

### 2.9.1 General Culturing Method

25 ml of nutrient broth is poured into 250 ml Erlenmeyer flasks and they were inoculated with a single colony of bacteria for 24 hours in an orbital shaker set to 200 rpm and 37 °C. Next, cultures were prepared by transferring them into 25 ml falcon tubes, balanced within 0.1g of each other and then centrifuged at 4000 rpm for 10 minutes. The supernatant is removed and 20 ml of a ¼ strength Ringer's solution (solution of several salts dissolved in water for the purpose of creating an isotonic solution relative to the body fluids of an animal). is added and the tubes vortexed. Then, the falcon tubes were centrifuged for a further 10 minutes at 4000 rpm and the supernatant is removed. Another 2 ml of ¼ strength Ringer's solution is added to each tube and they were vortexed. Finally, the re-suspended cultures were diluted by a factor of either 1000 for *E.coli* or 2000 for *Staphylococcus* to obtain an absorbance reading of between 0.05 and 0.08.

### 2.9.2. Testing Method

100 µL of bacterial culture was added to Eppendorf's containing 800 µL of nutrient broth and either 100 µL of a ¼ strength Ringer's solution (control) or 100 µL of 0.1 mg/mL test sample (test). The samples were incubated in an orbital shaker at 200 rpm and at 37 °C for 20 hours.

### 2.9.3. Plate Counting Method:

Consecutively, 100 µL of each sample was diluted into 900 µL ¼ strength Ringer's solution, 6 times, to obtain dilutions down to 10<sup>-6</sup>. 100 µL of respective sample was spread onto a nutrient agar plate and each dilution being plated in a

triplicate layout. The plates were incubated for 20 hours at 37 °C, and then each plate counted for number of bacteria colonies. Plates with 30-300 colonies were recorded alongside the respective dilution factor. The % decrease of colonies compared to the control was calculated for each test sample.

## 2.10. Haemolysis Test Method

The round end of a blue sterile pipette tip was used to create wells in a horse blood agar dish. Each well was filled with 100 µL of the desired test solution. A control test was set up using a ¼ strength Ringer's solution as the negative control and 1% Triton X-100 as the positive control. The positive control is always there to show what it looks like if the haemolysis is successful and it is most important in experiments with lower levels of difference between the positive and negative result. Next, the plates were incubated for 20 hours at 25 °C to observe for any haemolytic activity. Results were recorded as either α-haemolysis (partial haemolysis), β-haemolysis (complete haemolysis), or γ-haemolysis (no haemolysis).<sup>61</sup>

### 3. Analysis and Discussion

Firstly, it is important for the research project, to synthesize a C-dot with brilliant surface functionality, for the ability of the C-dots surface to be available for the attachment of surface functional groups. Described in section 3.1 of “structural characterisations of C-dot, K7 peptide and conjugates,” are results in which the surface of the C-dot is successfully modified to allow the attachment of K7 peptide to form two C-dotK7 conjugates. Secondly, materials which are intended to be used in biomedical applications, should possess good optical properties and photoluminescence. In section 3.2 of “optical properties of C-dot, K7 peptide and conjugates,” the results of both the fluorescence spectroscopy and UV-VIS analysis show that the conjugated materials have excellent optical properties. Many materials especially nanoparticles used in bioimaging, also express good antimicrobial properties, allowing them to be useful at killing bacteria. In part of the results chapter, it describes how certain nanoparticles can have both bioimaging and antimicrobial behaviour. The C-dotK7 conjugates have very good antimicrobial activity against both gram-positive and negative bacteria and the statistical results can be seen in section 3.6. Also, in the results section it clarifies the conjugates having minimal haemolytic activity however, further cytotoxicity tests would need to be performed to assure the materials express no or little toxicity.

### 3.1 Structural characterisation of C-dot, K7 peptide and conjugates

#### 3.1.1 HPLC purification of K7 peptide

HPLC was used to separate and purify the K7 peptide. The crude K7 peptide contains some contaminants from the synthesis reagents, so passing the peptide solution through a column under high pressure should help to separate the impurities from the peptide, to allow isolation of just pure K7 peptide.

Free peptides are less responsive to mass-spectrometric analysis and some peptides are volatile and can be ionised in the gas phase by electron impact in the mass spectrometer. Usually the molecular ions formed in this particular way are fragmented in a characteristic way because of the removal of amino-acid groups from the C-terminus end of the chain.<sup>65</sup> The investigation of predicting the electron impact mass spectra for peptides starts with the identification of a positively charged site in the molecule that has undergone electron impact. In the peptide, the atom with the lowest ionization potential (electron is most easily lost) becomes the positive site known as the molecular ion.<sup>65</sup> By comparing the ionization potentials among common functional groups, the oxygen atom of a carbonyl group in a carboxylic acid has the lowest ionization potential. Therefore, for a peptide the C-terminal carbonyl group is the more favourable site at which a positive charge forms. When a positive site has been established in a peptide molecule through electro impact, the molecule will start to break down quickly into different fragments known as daughter ions ( $m_1^+$ ,  $m_2^+$  etc.).<sup>65</sup> In standard mass-spectrometric analysis, only positive ions are verified on the spectrum graph. These ions are formed by fragmentation of the C-terminus of the peptide, and the mass spectrum can be viewed to determine and understand the structure of the peptide.

K7 peptide analysed using the HPLC Agilent Technologies 1220 Infinity II LC. The HPLC method (shown in Table 2) researched from literature and used to run a sample of K7 peptide. The first sample run which provides results in figure 18a, shows a broad peak at a retention time of 18, it is not very narrow or clear it appears to merge. The peptide sample diluted down with water (50:50). The first dilution of (1:1) had similarity to figure 18a) with a merged peak at the 18<sup>th</sup> retention minute, but the peak slightly narrower. After further diluting the peptide sample (25:75 K7: Water) the peak width continued to decrease but remained merged for the initial runs (figure 18c). However, after repeating the sample run continuously, the merged peak divided into two clear peaks between 15-20 min. The mass spectroscopy data mentioned later in the HPLC section, suggests that the separation of the peaks could be due to protonation of the peptide.

In figure 18d), the two peaks at 15 min and 17 min were isolated out separately into glass vials. A direct mass injection of the two samples provided mass data for K7. In figures 19a) and 19b), it shows the mass spectrums of the two isolated peaks and the fragmentation of these peaks. The assumption is that the first peak separated out at the 15 min is the K7 peptide as it exhibits an m/z value of 915, matching the molecular weight of the peptide. In addition, the mass spectrum exhibits fragment masses, which calculate as cleavage areas of the peptide structure. The pattern of mass fragmentation of K7 peptide show similar characteristics as explained in the text at the start of the previous page. At certain locations on the K7 structure, bonds are broken at either side of the carbonyl groups and this shows up in the mass spectrums. (Shown in figure 20). For example, in figure 19a), drawn on the mass spectrum is structures of the fragments cut off from the peptide sequence. The first peak has structures with

molar masses of 915 (m/z), 771, 628, 572 and 514 whereas, in figure 19b), it has structures with molar masses of 626 and 578.

Peaks at 628, 572 and 514 shown in figure 19a) and some of the peaks in figure 19b), have thicker line widths lower down on the spectrum, which suggests fragmentation occurs near and around the peaks. As K7 peptide consists of side chains with amine groups attached, these groups may become protonated during analysis on the mass-spectrometer. Therefore, the possible protonation of the peptide molecule is a good explanation why two separated peaks present during HPLC analysis. The second peak on the HPLC chromatogram in figure 18d) only shows two relevant fragment masses linking to the peptide sequence and the molar masses slightly shift via the loss/gain of H<sup>+</sup> protons. (628-626, 572-578).

Both mass spectrums have a peak at 458 that does not seem to elucidate to a cleavage area on the peptide sequence but with peptides, they may consist of isotopes forms and these masses vary and are present in the spectrums but not relatable to the K7 peptide structure.

Table 2: HPLC gradients.<sup>66</sup>

<b>Method 1</b>		
<b>Time (min)</b>	<b>A [%]</b>	<b>B [%]</b>
<b>0</b>	98	2
<b>24</b>	5	95
<b>24.1</b>	98	2
<b>26</b>	98	2

Table 3: Conditions used for HPLC analysis.

<b>Column</b>	<b>bioZen 3 µm Peptide PS-C18, LC Column</b> <b>150 x 4.6 mm</b>
<b>Mobile phases</b>	A – 0.1% TFA in water B – 0.1% TFA in acetonitrile
<b>Flow rate</b>	0.2 ml/min
<b>UV Detector</b>	220 nm
<b>Max Pressure Limit</b>	400 Bar
<b>Peptide sample injection</b>	50 µL

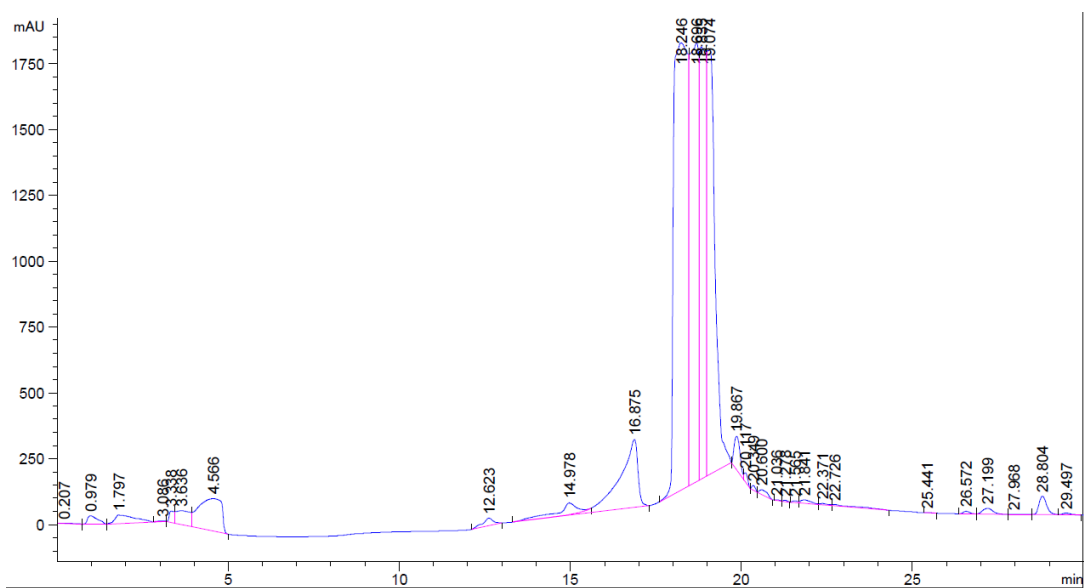


Figure 18a: HPLC chromatogram of K7 peptide first run.

Dilution scheme:

Firstly, the K7 peptide dissolved in 5 ml of water. For the dilution scheme in figure 18b), 1ml of peptide from the solution consisting of peptide dissolved in 5ml, mixed with 1ml of water (50:50).

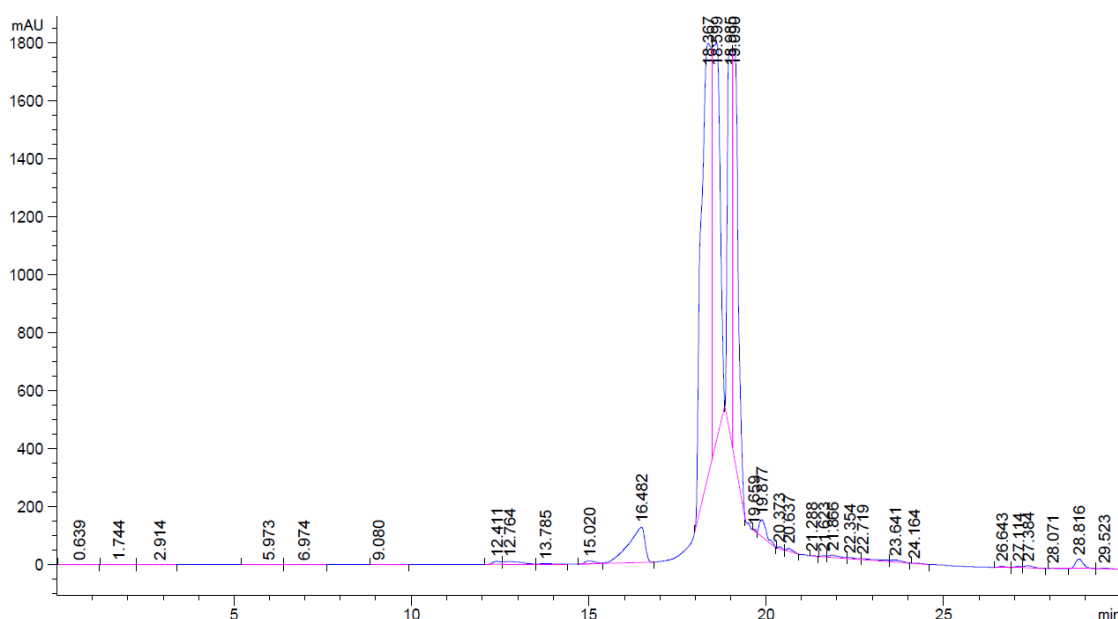
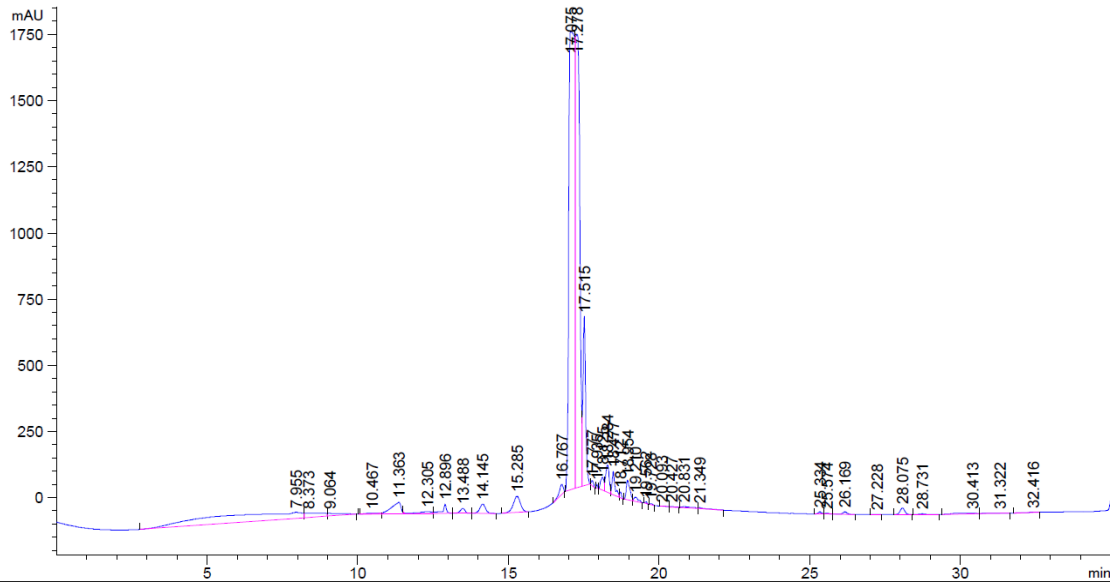


Figure 18b): HPLC chromatogram of K7 peptide using (50:50) dilution scheme

For better separation of the peak, 1ml of peptide was added (from the original solution of peptide in 5ml) to 3 ml of water (25:75) and injected into the HPLC. Initially, the first couple of method runs show one peak at around the 17<sup>th</sup> min but it appears merged. However, once the method has been ran a few times on the HPLC, the merged peaks separate out and figure 18d) show two clear separated peaks.



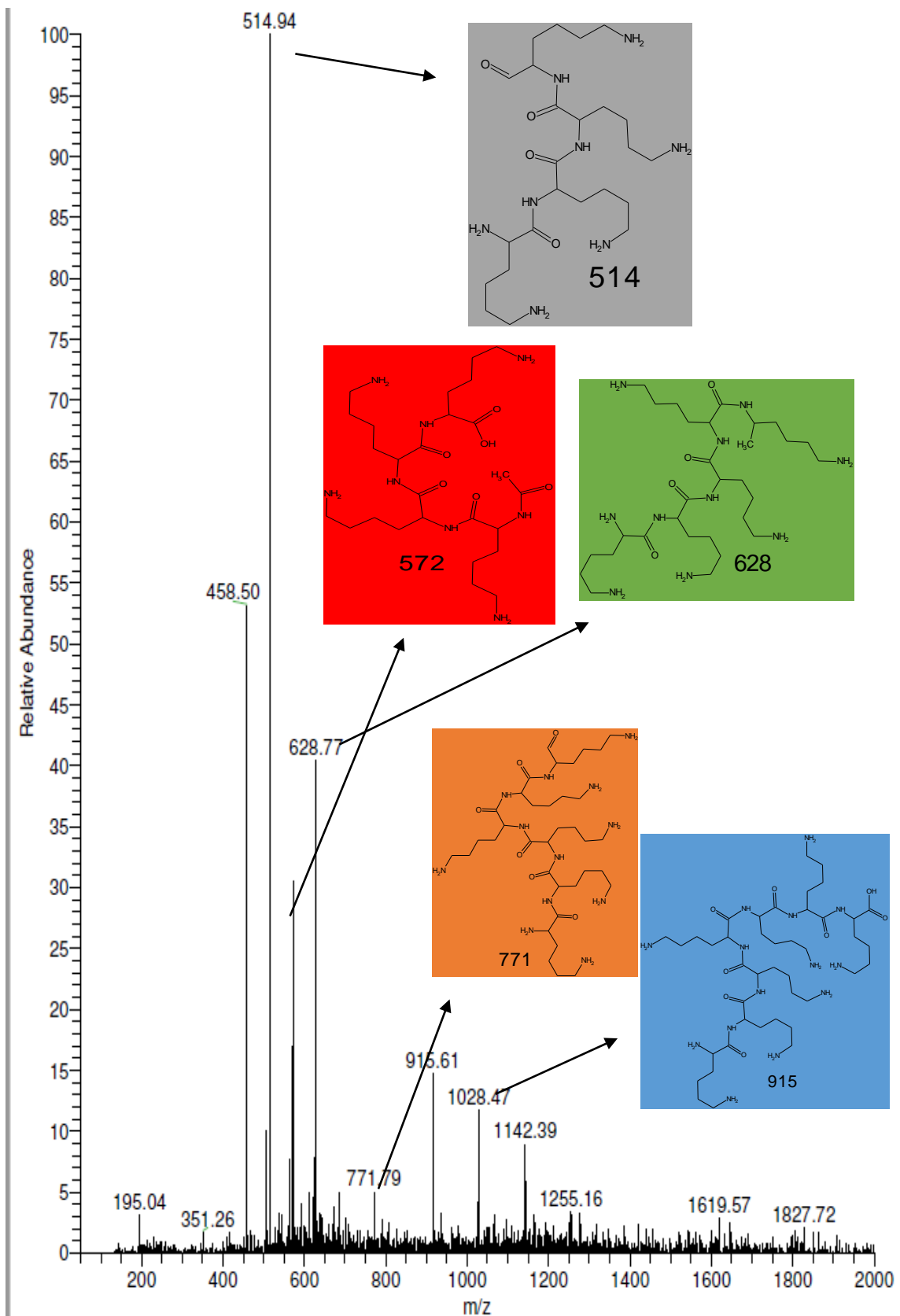


Figure 19a: Mass spectrum for peak at 15 min.

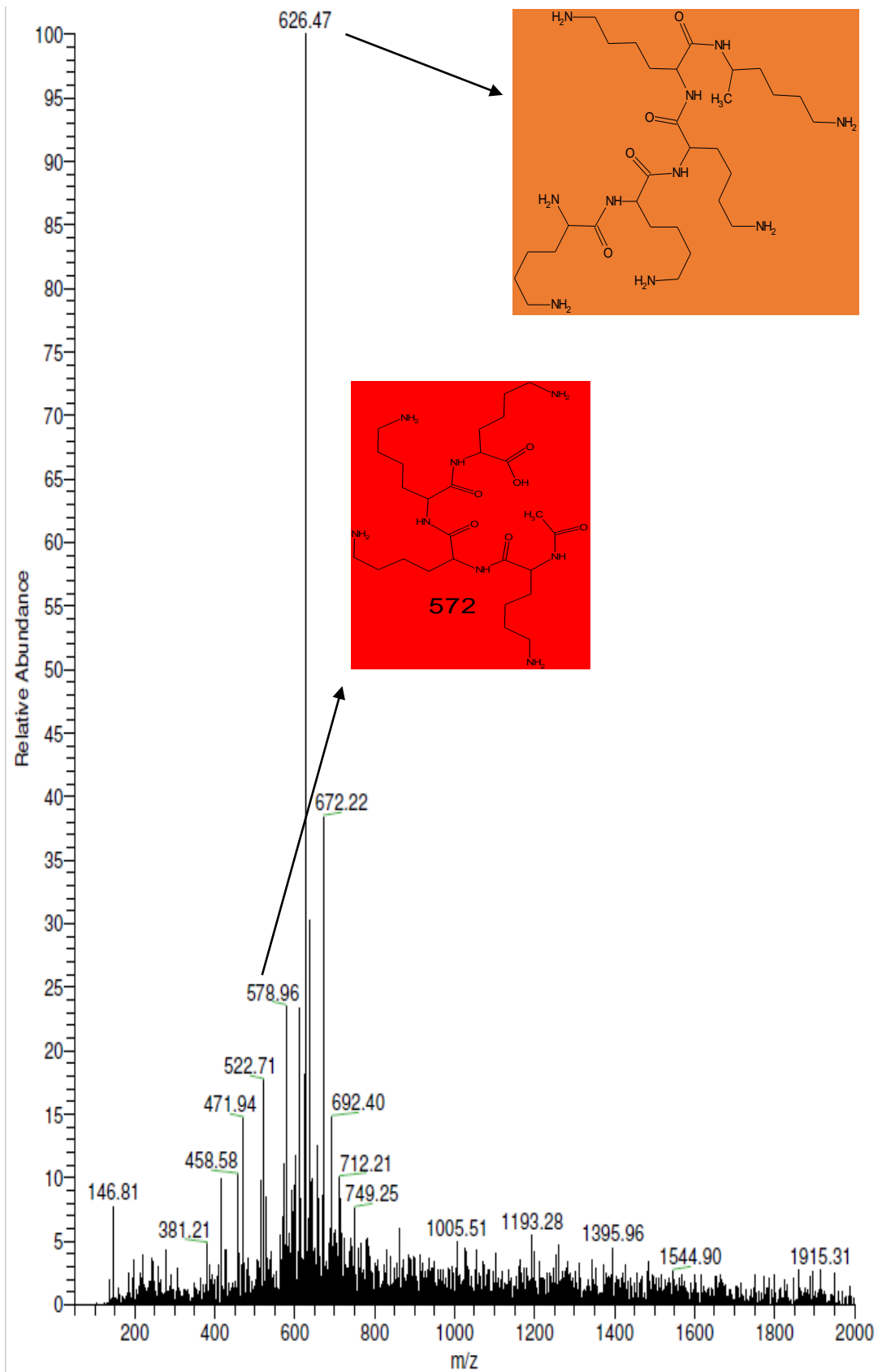


Figure 19b: Mass spectrum for peak at 17 min.

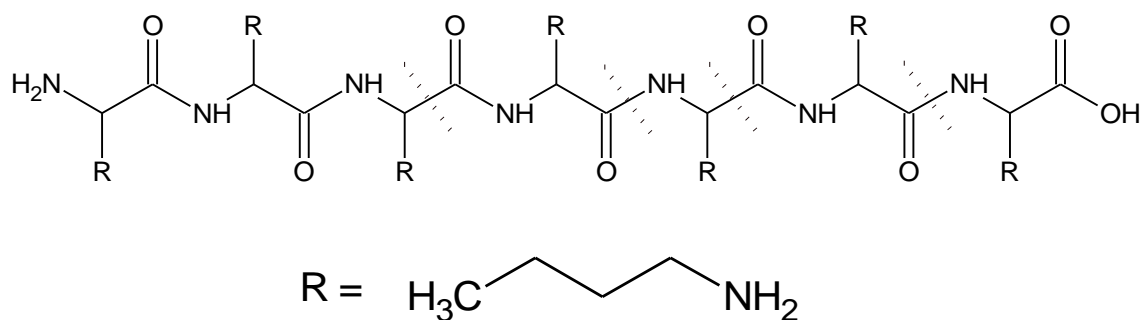


Figure 20: Diagram of the molecular structure of K7 peptide showing the locations around the carbonyl bonds where fragments occur. The R group represents the side groups.

HPLC analysis taken of the K7 peptide to work out the purity after the synthesis of the peptide synthesizer. To conclude, the sample of K7 peptide ran on the HPLC to work out the purification and on average, it exceeds 97%. Even though the actual purity of the peptide was not calculated, the HPLC data gave confident reading to allow the conjugation to C-dot and further analysis. Further analysis of the K7 peptide includes; determination of the molecular structure using NMR spectroscopy and the main functional groups present in the peptide, using IR spectroscopy.

### 3.1.2 NMR for K7 peptide

NMR is a useful tool to determine the molecular structure of different materials. Therefore, the K7 peptide was analysed once using NMR spectroscopy to discover what atoms are bonded together to make up the molecule of K7 peptide. Comparing the <sup>1</sup>H proton to the literature values for an oligo-poly-L-Lysine structure.<sup>67</sup> In literature, the oligo-poly-L-Lysine has 5 hydrogen environments with a total integration of 9 hydrogen nuclei. The structure in figure 21, illustrates using

the letters A-E, the position of the hydrogen environments. The  $^1\text{H}$  proton NMR shows 3 relevant multiplet peaks (excluding the  $\text{CDCl}_3$  solvent peak at 7.26 ppm) at the chemical shift values of 1.95 ppm, 1.28 ppm and 0.86 ppm. At 0.86 ppm, it shows the hydrogen region at position (b)  $\text{NH}_2\text{-CH}_2\text{-CH}_2\text{-CH}_2\text{-CH}_2$  which appears as a multiplet with an integration of 2. The peak at 1.28 ppm shows the hydrogen environment at position (c)  $\text{NH}_2\text{-CH}_2\text{-CH}_2\text{-CH}_2$  which also appears as a multiplet with integration of 2.47 (2). Lastly, the most concentrated peak at 1.98 ppm represents the hydrogen environments of the peak positions (e), (d) and (a). Each of the integrations of the individual peaks added up to 5 and matches the integration of 4.91 (5). These peaks are positioned closest to the nitrogen atoms. By using a  $^1\text{H}$  proton predictor<sup>68</sup>, it demonstrates that a carbon atom closest to the nitrogen atom has an increased chemical shift likely due to the higher electronegativity of the nitrogen atom.<sup>69</sup> The concentrated sample of K7 peptide and the size of the structure may be factors that causes the possible merging of peak positions.

$^1\text{H}$  NMR (400 MHz, Chloroform-*d*)  $\delta$  1.95 (dd,  $J = 14.1, 5.8$  Hz, 5H), 1.33 – 1.23 (m, 2H), 0.90 – 0.77 (m, 2H).

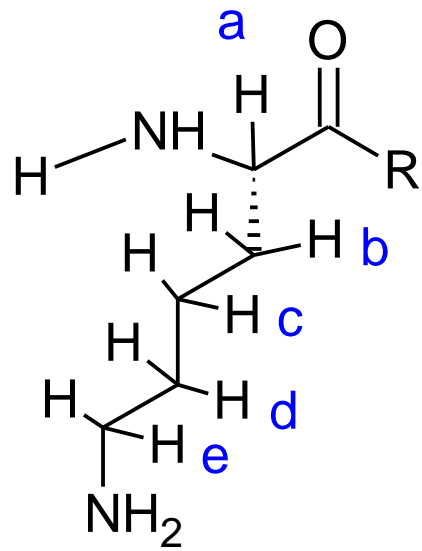
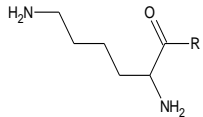


Figure 21: Structure of poly-L-Lysine.<sup>67</sup>

Table 4: NMR results.

Hydrogen environment	Integration (H)	Multiplicity	Chemical shift (ppm)
CDCl <sub>3</sub> (Solvent)	n/a	n/a	7.26
E – NH <sub>2</sub> -CH <sub>2</sub> D - NH <sub>2</sub> -CH <sub>2</sub> -CH <sub>2</sub>   A	4.91 (5)	Multiplet	1.95
C - NH <sub>2</sub> -CH <sub>2</sub> -CH <sub>2</sub> -CH <sub>2</sub>	2.47 (2)	Multiplet	1.28
D - NH <sub>2</sub> -CH <sub>2</sub> -CH <sub>2</sub> -CH <sub>2</sub> -CH <sub>2</sub>	2	Multiplet	0.86

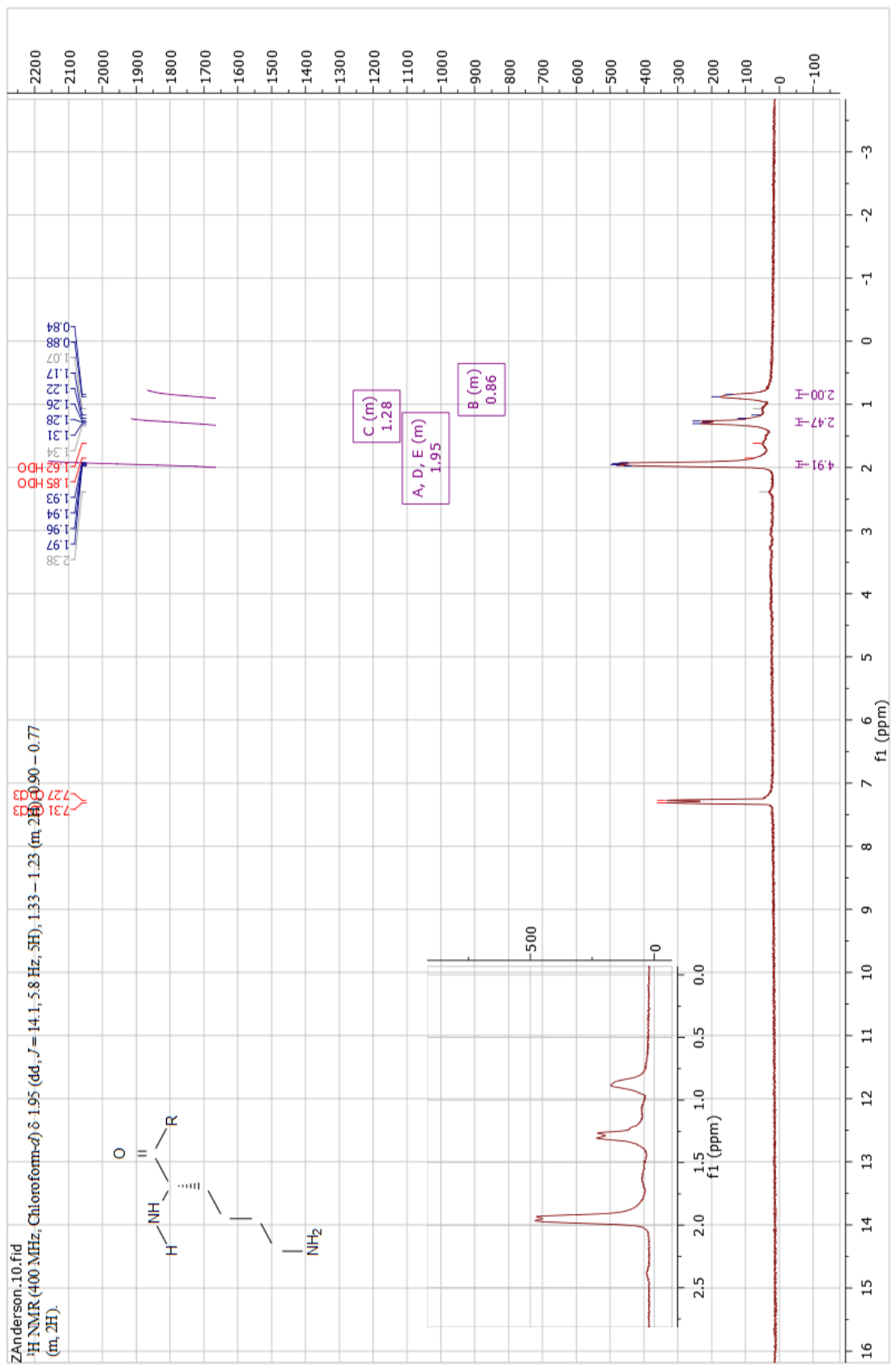


Figure 22: NMR spectrum of K7 peptide.

### 3.1.3 IR spectroscopy

The interaction of infrared radiation with a material is known as infrared spectroscopy. This experiment was convenient in the project to determine the main functional groups present in all the C-dot, C-dot/K7 peptide materials. It allows comparison of the IR spectrums to see the differences between the C-dot alone and K7 peptide alone and then how the spectrums appear once the attachment occurs to form the conjugated systems. A C-H stretch representing an alkane functional group is present in the spectrums of K7 peptide, C-dotK7A and C-dotK7B but not in the spectrum of C-dot. A broad COOH region at around  $3300\text{ cm}^{-1}$  wavelength is present in both IR spectrums of C-dot and C-dotK7B, this region not noticeable in the K7 and C-dotK7A spectrums. C-N IR stretch indicating presence of an amine functional group present in the C-dotK7B and K7 IR spectrums but not for the C-dot or C-dotK7A spectrums. O-H bending stretches linking to a carboxylic acid and a C-O stretch linking to an alcohol functional group shown in all the IR spectrums containing C-dot material but not for K7. The absorption peaks roughly at  $1500\text{-}1700\text{ cm}^{-1}$  are different for all the samples. The C=O stretch represents the presence of a carbonyl group. In the IR spectrums for both C-dot and C-dotK7B, the C=O stretch links a carbonyl to an acid group, whereas the K7 peptide and C-dotK7A spectrums show a C=O stretch linking a carbonyl group to the presence of an amide peptide bond. These differences in IR spectrums for the samples show evidence that the C-dot and K7 peptide conjugation occurs. It shows especially in C-dotK7A that a peptide bond forms representing the carbonyl peak at wavelength  $1700\text{ cm}^{-1}$ .

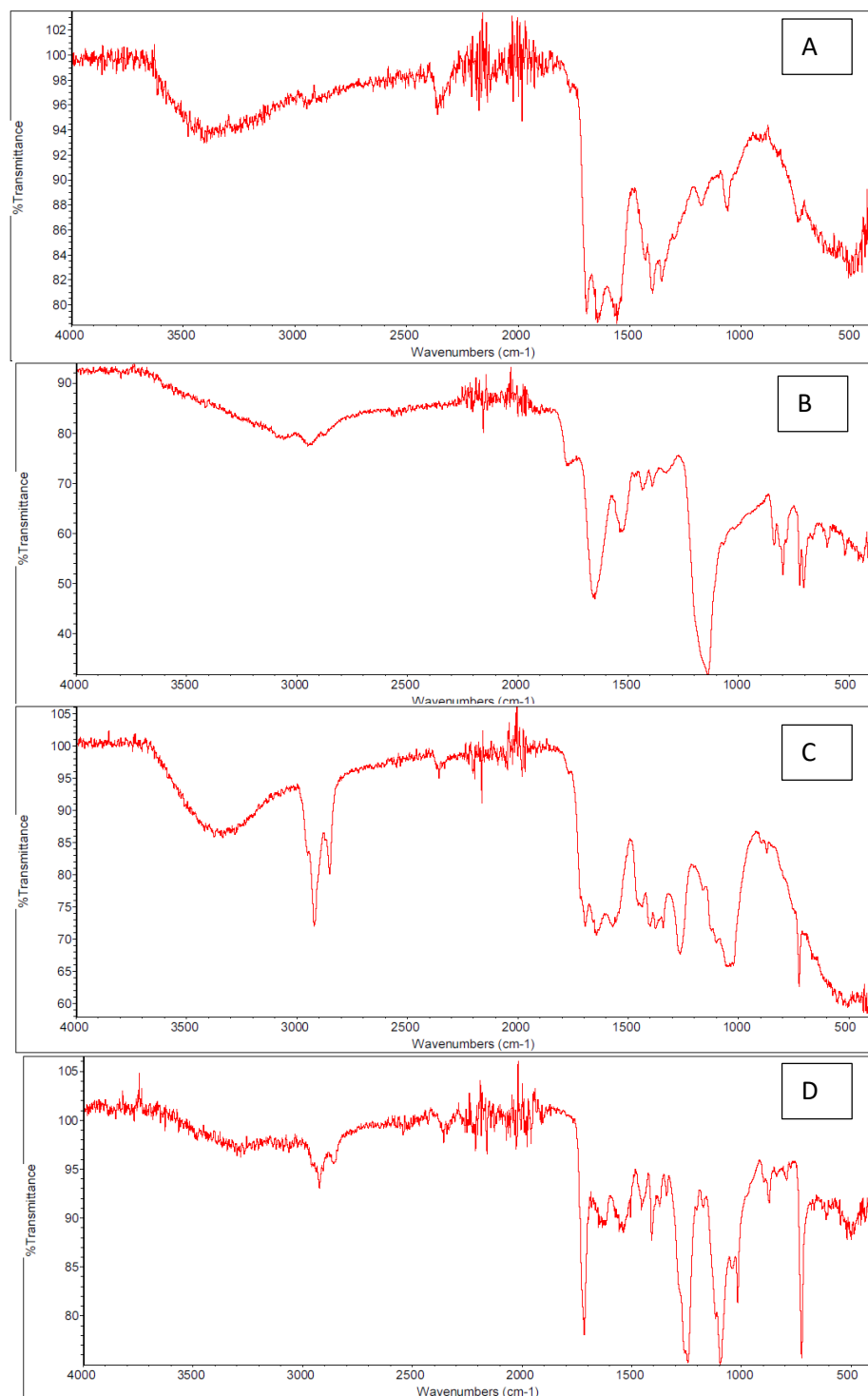


Figure 23: A) IR spectrum of C-dot B) IR spectrum of K7 peptide C) IR spectrum of C-dotK7B D) IR spectrum of C-dotK7A.

Table 5: Functional groups present in IR spectrums.

<b>Sample</b>	<b>Functional group and wavelength (cm<sup>-1</sup>)</b>
<b>C-dot</b>	O-H broad region represents COOH wavelength = 3420.68
	O-H bending stretch represents COOH wavelength = 1397.29
	C=O stretch (Acid) wavelength = 1693.73
	C-O stretch represents alcohol wavelength =1059.89
<b>K7 peptide</b>	C-H stretch represents alkane wavelength = 2947.52
	C-N stretch represents amine wavelength =1139.15
	C=O stretch amide 1 band wavelength =1651.35 represents peptide bond
	C=O stretch amide 11 band wavelength =1537.79
<b>C-dotK7A</b>	C-H stretch represents alkane wavelength =2923.57
	C-O stretch represents acid wavelength = 1244.56
	C-O stretch represents alcohol wavelength = 1016.61
	C-N stretch represents amine wavelength = 1096.10
	O-H bending stretch represents COOH wavelength = 1455.55
	C=O stretch Amide 1 band wavelength = 1716.35
	C=O stretch Amide 11 band wavelength = 1633.98
	N-H bending amine wavelength = 1651.81
<b>C-dotK7B</b>	O-H broad region represents COOH wavelength = 3300
	C-H stretch represents alkane wavelength = 2922.26
	C-O stretch represents acid wavelength = 1264.02
	C-O stretch represents alcohol wavelength = 1034.73
	C=O stretch (Acid) wavelength =1693.99
	N-H bending amine wavelength = 1644.64

### 3.1.4 Zetasizer

The intensity distribution can be used as a sensitive detector for the presence of large material particles in the K7 peptide. The K7 peptide gave 3 measurements each time it was scanned, and the test performed 3 times. In figure 24 down below, it appears that the size by intensity distribution of K7 shows one peak around 40nm and another peak around 300nm. This indicates two populations with hydrodynamic diameter 40nm and 300nm respectively. Poly (L-lysine)-DNA complexes diluted with HEPES buffer measured the size of the Poly (L-lysine) using a Zetasizer 300 system.<sup>78</sup> The size of all the complexes were in the range of 55-105 nm diameter <sup>78</sup> and the size of the K7 peptide diameter of 42 nm is relatively close to this range.

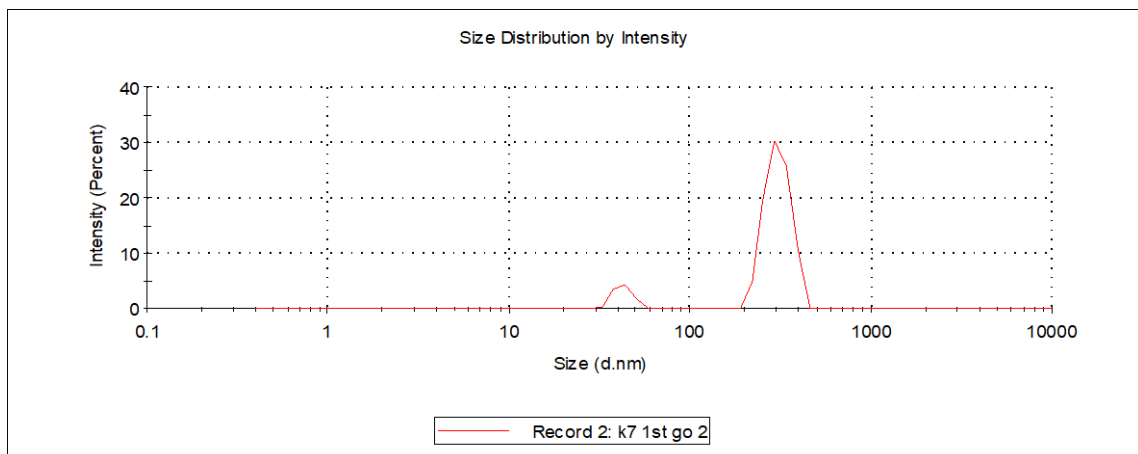


Figure 24): Size distribution by intensity for the zetasizer analysis of K7 peptide

### 3.1.5 Contact Angle Measurement

The results for the contact angle test describe the nature of the interaction of the micro glass surface to each of the test solutions, all dispersed in water in the same concentrations. Contact angle measurements were performed to explore the surface interaction of C-dot conjugated to K7 peptide with water. Firstly, in figure 25a) the C-dot material gave the lowest contact angle of  $12.30^{\circ}$ , therefore it spreads more evenly against the glass surface than the other materials. The figure 25b) of K7 peptide gave a contact angle of  $15.94^{\circ}$  and this explains why both C-dot and K7 are hydrophilic as they show wettability. The C-dot conjugates to the K7 peptide in two different ways to provide the C-dotK7A and C-dotK7B systems and the contact angles increase from  $12.30^{\circ}$  to  $23.15^{\circ}$  for C-dotK7B in figure 25c) and  $12.30^{\circ}$  to  $30.46^{\circ}$  for C-dotK7A in figure 25d). Tests against the surface found these contact ranges and it seems the conjugated systems have greater hydrophobicity, consistent with the nature of K7 peptide.

C-dot contact angle = 12.30 degrees

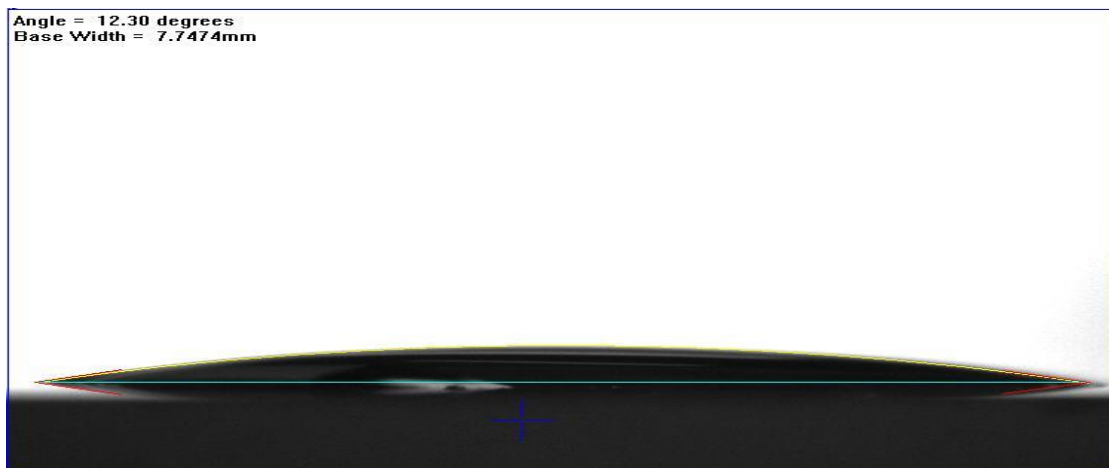


Figure 25a): Contact angle of C-dot.

K7 Peptide contact angle = 15.94 degrees



Figure 25b): Contact angle of K7.

C-dotK7B contact angle = 23.15 degrees



Figure 25c): Contact angle of C-dotK7B.

C-dotK7A contact angle = 30.46 degrees

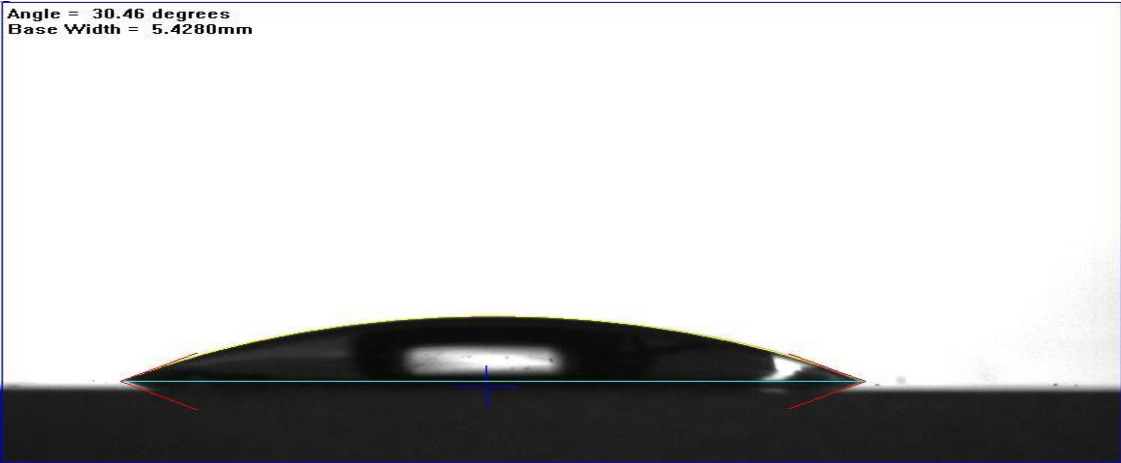


Figure 25d): Contact angle of C-dotK7A.

## 3.2 Optical properties of C-dot, K7 peptide and conjugates

### 3.2.1 Fluorescence properties

#### The four theoretical photoluminescence mechanisms

The photoluminescence spectra of the C-dot and the C-dotK7A/C-dotK7B are generally broad and show excitation wavelength emissions. The fluorescence band maximum shifts slightly with the excitation towards longer wavelengths and decrease of emission intensities. This wavelength dependent emission behaviour of C-dots is contributed by four possible PL mechanisms. However, the actual mechanism of the PL of fluorescent C-dots is still being widely researched and investigated. One possible PL contribution arises from the presence of  $sp^2$  islands within  $sp^3$  continuum.<sup>4,71</sup>

The second PL contribution stems from the presence of surface defects coupled with the passivation action of external moieties. Increasing the surface oxidation or modification of the C-dot surface can result in more surface defects, resulting in a red-shift emission. The surface state does not consist of isolated chemical groups, but determined by hybridization of the carbon backbone and connected chemical groups.<sup>72</sup> The first report of synthesized C-dots back in 2004, which were an oxidation-cut product with oxygen based chemical groups on the surfaces; most PL centres of the C-dots proven to be surface states.<sup>73</sup> The surface passivation of C-dots using PEG investigated by Sun and co-workers. They demonstrated that many organic molecules could provide surface passivation, which further proved that surface energy traps controlled the PL mechanism.<sup>74</sup> Many methods to prepare C-dots, combine oxygen-based groups onto the carbon core, which was the primary surface state of the C-dot.<sup>72</sup>

Colourful C-dots derived from oxidizing candle soot obtained by Mao and co-workers. The PL, which ranged from violet to red region, may have been induced by different surface oxidation.<sup>75</sup> By using the bottom-up carbonization method, C-dots with surface-state emission were achieved and by using different reaction conditions, the PL could be tuned from blue to green. Pang proved that the surface states of electrochemical C-dots were the main responsibility of tuning the luminescence.<sup>76</sup>

Another PL contribution originates from the presence of fluorophores units connected on the surface of the C-dots. These types of C-dots are prepared, when small fluorophore molecules are formed at low reaction temperatures. When the temperature increases, consumption of the fluorophores or dehydration of the initial molecules forms the carbon core. At low temperatures, the C-dots have strong PL emission with high QYs, whereas the carbon core state has weaker PL behaviour but with good photo stability. The formation mechanism investigated by *Giannelis and co-workers*, for the molecule and carbon core states of C-dots made using citric acid (CA) and ethanolamine (EA). The materials heated at 180 °C resulted in a molecular precursor with a strongly intense PL and high QY of 50%. When the material further heats to temperatures of 230 °C, a carbogenic core started forming and the PL was due to the presence of both molecular fluorophores and the carbon core, but the QY was only 15%. The low QY suggests that many of the fluorophore molecules were used as the building blocks of the carbon core. The C-dots that had PL emission arising from the carbon cores obtained at even higher temperatures (300-400 °C), and the QY decreased. The reduced emission of the PL centres observed in C-dots at high temperatures, could be a result of quenching of the carbon core structure.<sup>72</sup> Another PL mechanism theory of wavelength dependent emission of C-dots is

the crosslink-enhanced emission (CEE) effect. This explains that a special kind of C-dot known as non-conjugated polymer dots (PDs) possess aggregated polymer structures and the formation of these polymer aggregations promote PL behaviour.<sup>77</sup>

#### Results of the fluorescence data of C-dot, C-dotK7A and C-dotK7B solutions

The C-dot, C-dotK7A and C-dotK7B materials were all dispersed separately into water to make 0.1 mg/mL solutions. Fluorescence spectroscopy was used to analyse the fluorescence properties of the C-dot in each of the solutions. From literature, C-dots display high levels of photoluminescence, making them strong candidates for imaging applications.

The C-dots will likely be exposed to different environment conditions, so therefore the fluorescence properties were analysed of the C-dot material solutions at different pH levels.

The fluorescence intensity of the C-dot solution at pH 7.36 shown in figure 26 a), is roughly twice as high as the intensity of the C-dot solution at a much lower pH level of 0.90 (figure 26d). Increasing the acidity of the solution for C-dot seems to decrease the fluorescence, at neutral pH the fluorescence reached to over 160,000 on the intensity scale whereas, the fluorescence at pH 0.90 reached to almost half that at 60,000. The intensity at a higher pH of 12.97 viewed in figure 26 g) reached on the scale to over 120,000, which is much greater, compared to a low pH. The fluorescence data suggests that when the pH is low, the intensity is lowest, and as the pH value starts to increase to 7 and above, the intensity

reaches a maximum, in which then the intensity begins to drop as the pH further increases. No direct relation of pH to the synthesized C-dot and C-dotK7 system found in literature however, one report found out when the absorption/emission spectra of CQDs (not conjugated to a biomaterial) tested under different pH conditions, interesting observations are noted. Within the pH, range of 3-7 there was not any real variation in the peak position of absorption spectra. However, a red shift spotted when pH becomes more basic and this reflects in the emission spectra viewed in the figure below. The opposite effect of pH noticed in the CQD system compared to the C-dot/C-dotK7 system, where the fluorescence intensity decreases from acidic to basic environment (pH 3-12), indicates the CQDs are pH sensitive. The report assumes that the molecular state of the CQD is affected at extreme pH values and dissociation into smaller particles leads to low fluorescence.<sup>70</sup>

The fluorescence spectrums of both C-dotK7A (figure 26e) and C-dotK7B (figure 26f) at low pH values (0.85-0.87) show a decrease in intensity compared to when at higher pH. Therefore, as this comparison of low pH resulting in low intensity is presentable in all solutions of C-dot, C-dotK7A and C-dotK7B, it suggests that the C-dot material is pH sensitive. In addition, the fluorescence intensities are very low for both C-dotK7 samples compared to just C-dot (180,000 compared to 16,000 on the intensity scale y axis). The attachment of K7 peptide to the C-dot seems to influence the strength of fluorescence, leading to lower intensities when the peptide is attached.

C-dotK7A and C-dotK7B have some visible differences in each of the spectrums (at neutral pH). Firstly, for C-dotK7A, at a wavelength absorbance of 380 nm the

intensity is highest whereas, in C-dotK7B, the wavelength absorbance 410 nm has the highest intensity. Table 6 shows the  $\lambda_{Max}$  emissions of all peaks in each of the spectrums. The spectrums of C-dotK7A (figure 26e) and C-dotK7B (figure 26f) at pH 7, have different maximum emission values between the wavelengths 350-380nm. Two viable arguments that may explain the different intensity properties displayed for C-dotK7A and C-dotK7B, first the peptide itself may act differently when the method of conjugation is modified and adapted, the properties of peptide could influence C-dot behaviour. Second, the different method to conjugate peptide to C-dot might affect the graphite density and change the C-dots behaviour for fluorescence. The highest fluorescence intensity is at the same level for both samples of C-dotK7 neutral solutions and they show a trend of wavelength excitation dependent emission behaviour keeping with the characteristics expected for C-dots. On the other hand, when the pH solution of C-dotK7A decreases, the fluorescence pattern changes, the wavelength dependent emission is harder to distinguish and the maximum emission difficult to detect, the data not producible.

In table 6, the maximum emissions for C-dotK7B at neutral and high pH levels are the same. The maximum emission shifts outwards at lower wavelengths for low pH, but as the wavelength increases the maximum emissions start to match to the shifts in the other spectrums. Additionally, the fluorescence spectrum of C-dotK7B solution at high pH (12.93) exhibits an intensity peak at 350 nm, which shows very high fluorescence which appears as an anomaly. Surface passivation of the C-dots add the addition of amide groups and oxygen-based groups onto the surface of the C-dot and these groups can ultimately fluoresce themselves. Additional contributions coming from extreme pH most likely the amide and

oxygen-based groups change their electronic environments and this leads to possible increases in fluorescence intensity.

Table 6:  $\lambda$  max emissions at each wavelength.

	<b><math>\lambda</math> Max Emission</b>								
	<b>C-dot</b>			<b>C-dotK7A</b>			<b>C-dotK7B</b>		
<b>Emissio</b>	<b>pH</b>	<b>pH</b>	<b>pH</b>	<b>pH</b>	<b>pH</b>	<b>pH</b>	<b>pH</b>	<b>pH</b>	<b>pH</b>
<b>n</b>	<b>7.36</b>	<b>0.90</b>	<b>12.97</b>	<b>7.38</b>	<b>0.87</b>	<b>12.73</b>	<b>7.60</b>	<b>0.85</b>	<b>12.93</b>
<b>350</b>	475	480	475	440	430	435	420	490	420
<b>380</b>	470	500	475	445	440	460	470	510	465
<b>410</b>	510	510	490	495	n/a	480	495	520	500
<b>440</b>	520	520	515	530	n/a	515	530	530	530
<b>470</b>	545	555	540	555	n/a	540	555	555	555
<b>500</b>	565	565	575	575	n/a	565	575	570	575

Fluorescence graphs for C-dot, C-dotK7A and C-dotK7B solutions at neutral pH

(7)

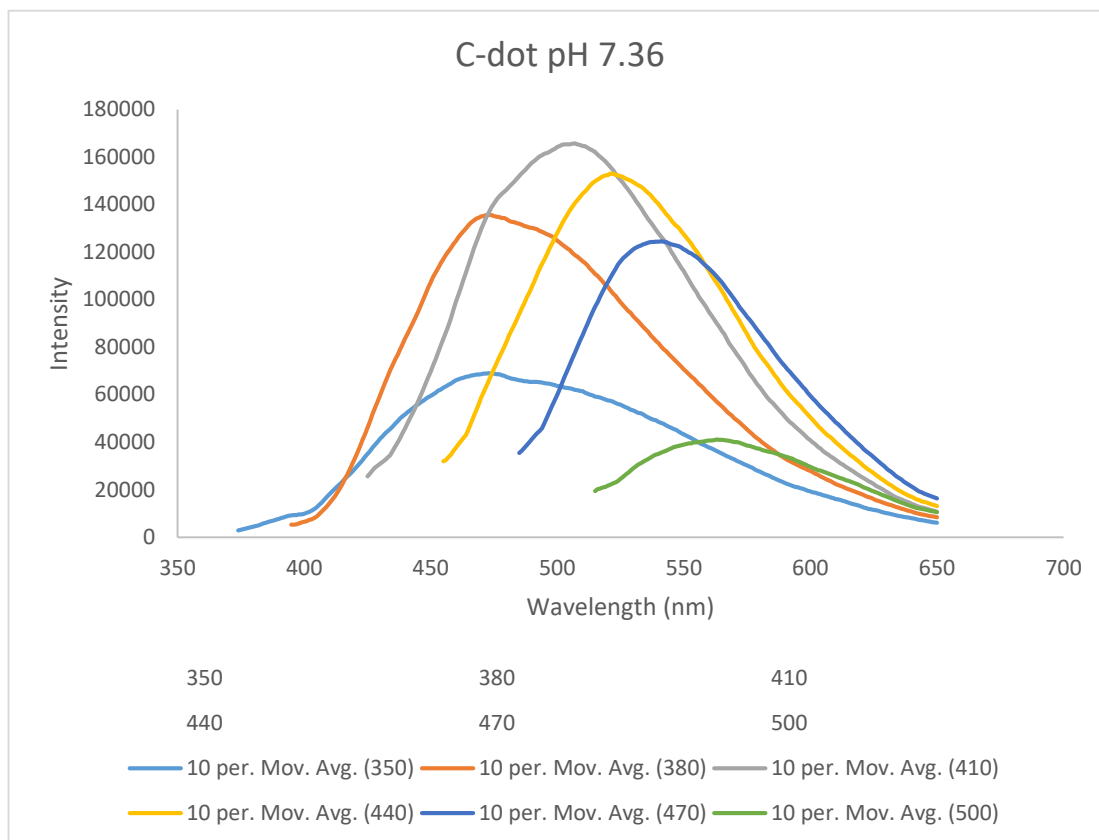


Figure 26a: Fluorescence spectrum of C-dot solution (0.1 mg/mL) at pH 7.36

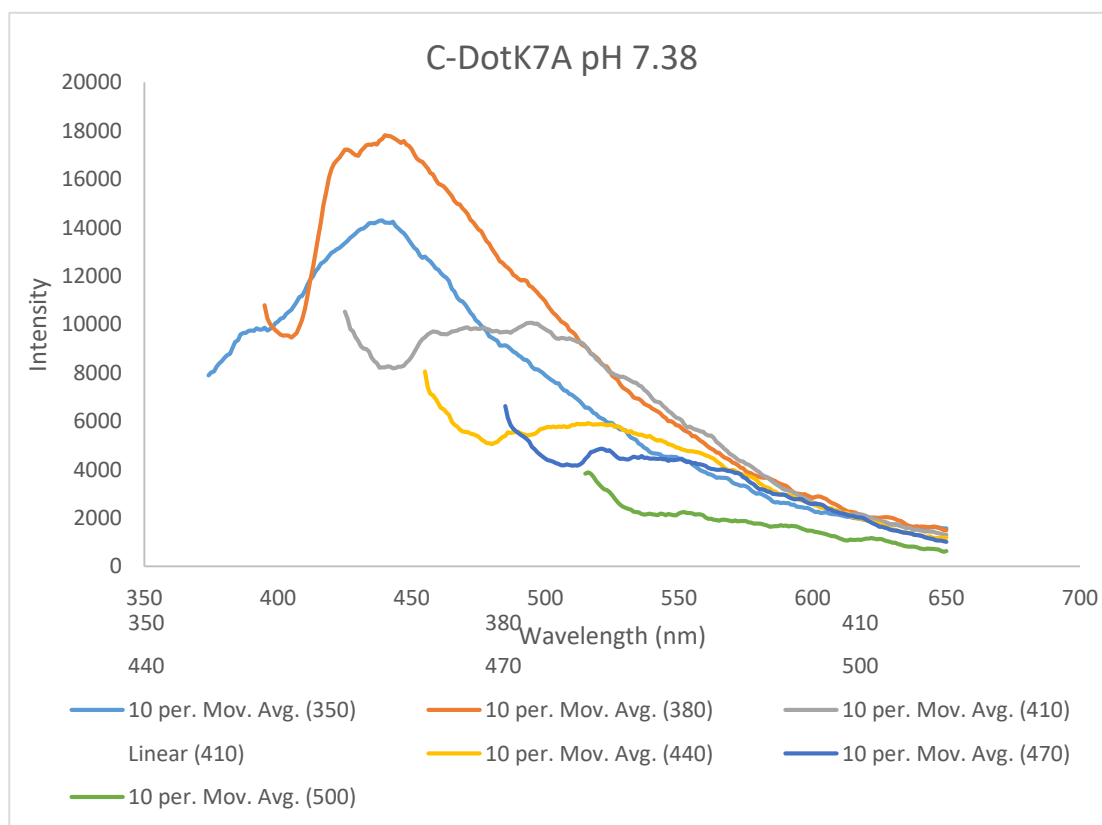


Figure 26b: Fluorescence spectrum of C-dotK7A solution (0.1 mg/mL) at pH 7.38

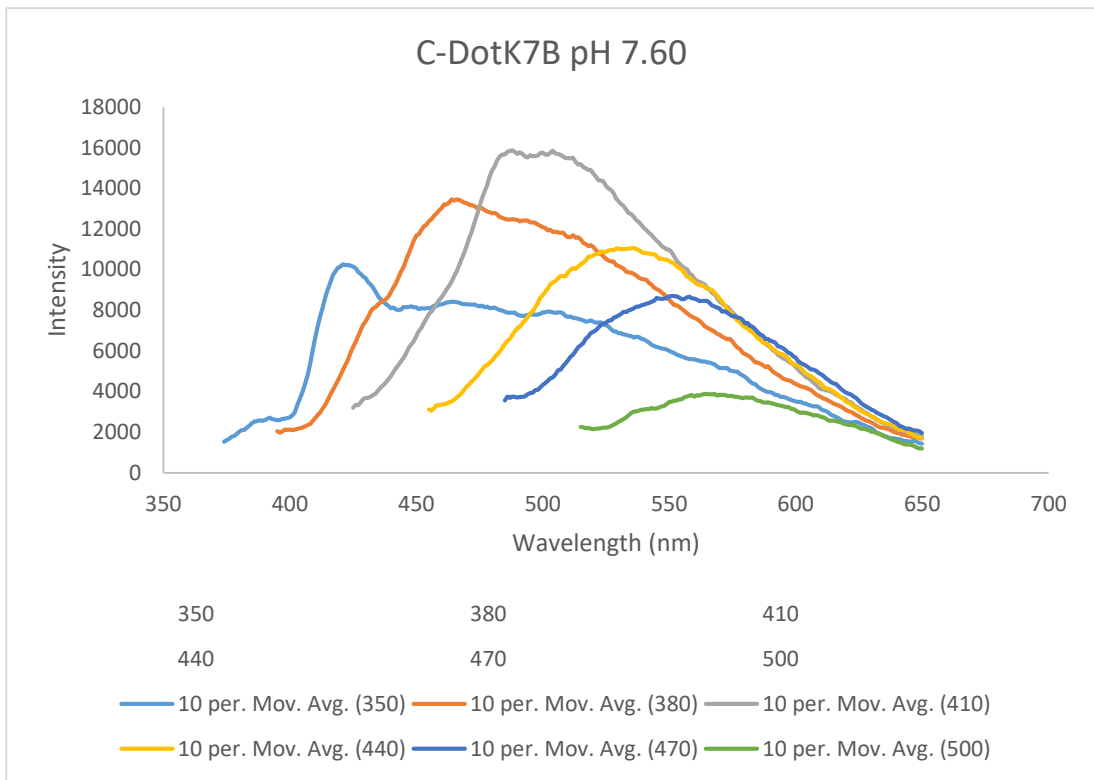


Figure 26c): Fluorescence spectrum of C-dotK7B solution (0.1 mg/mL) pH 7.60

**Fluorescence graphs for C-dot, C-dotK7A and C-dotK7B solutions at low pH (less than 7)**

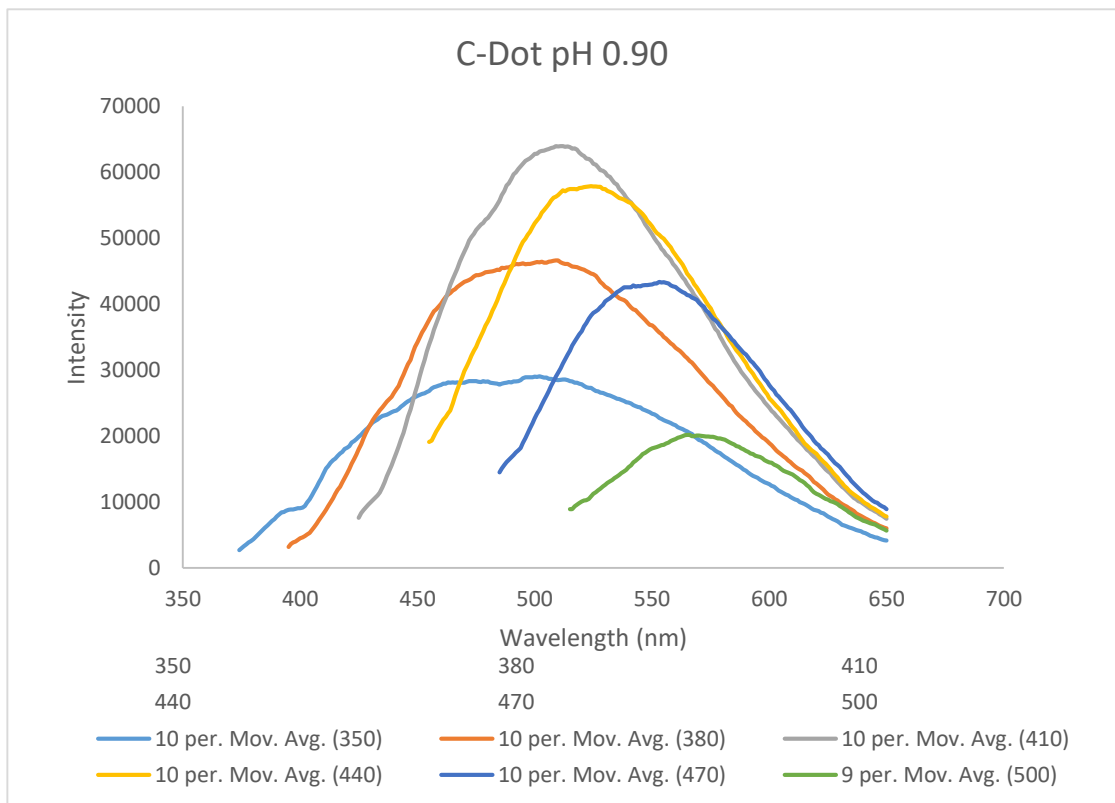


Figure 26d): Fluorescence spectrum of C-dot solution (0.1 mg/mL) at pH 0.90

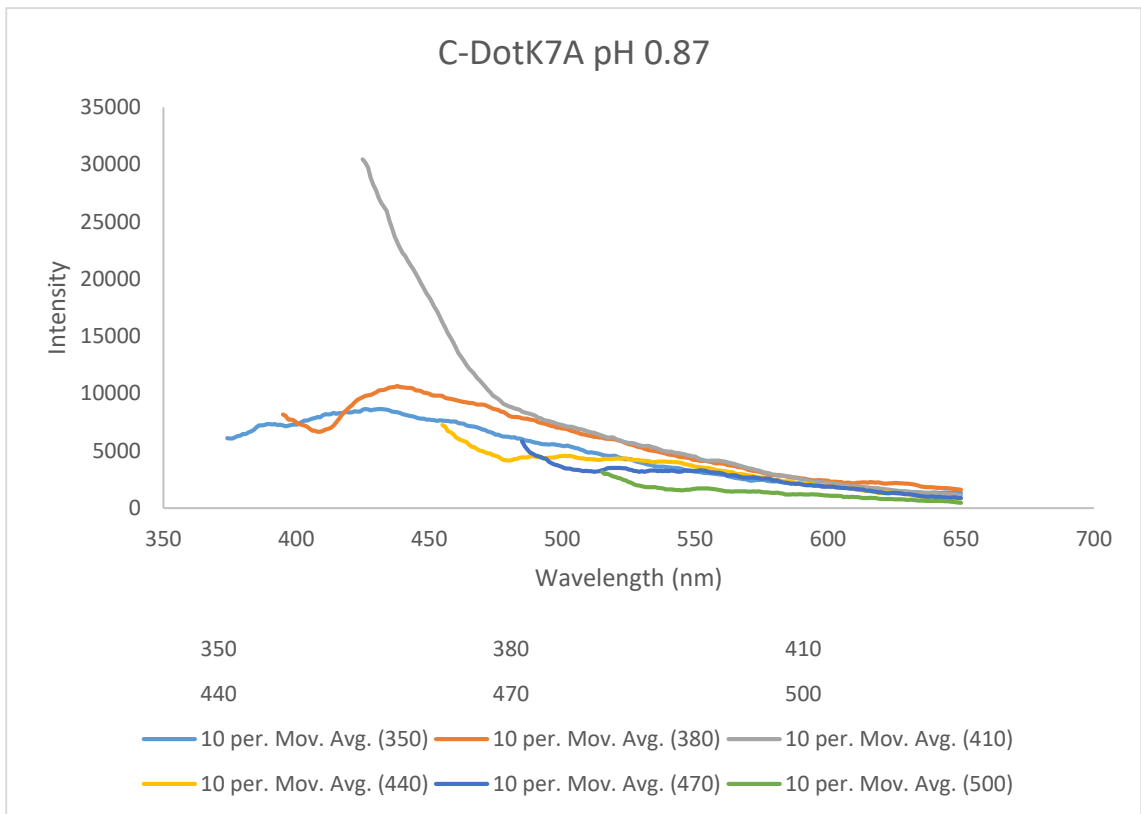


Figure 26e): Fluorescence spectrum of C-dotK7A solution (0.1 mg/mL) at pH 0.87

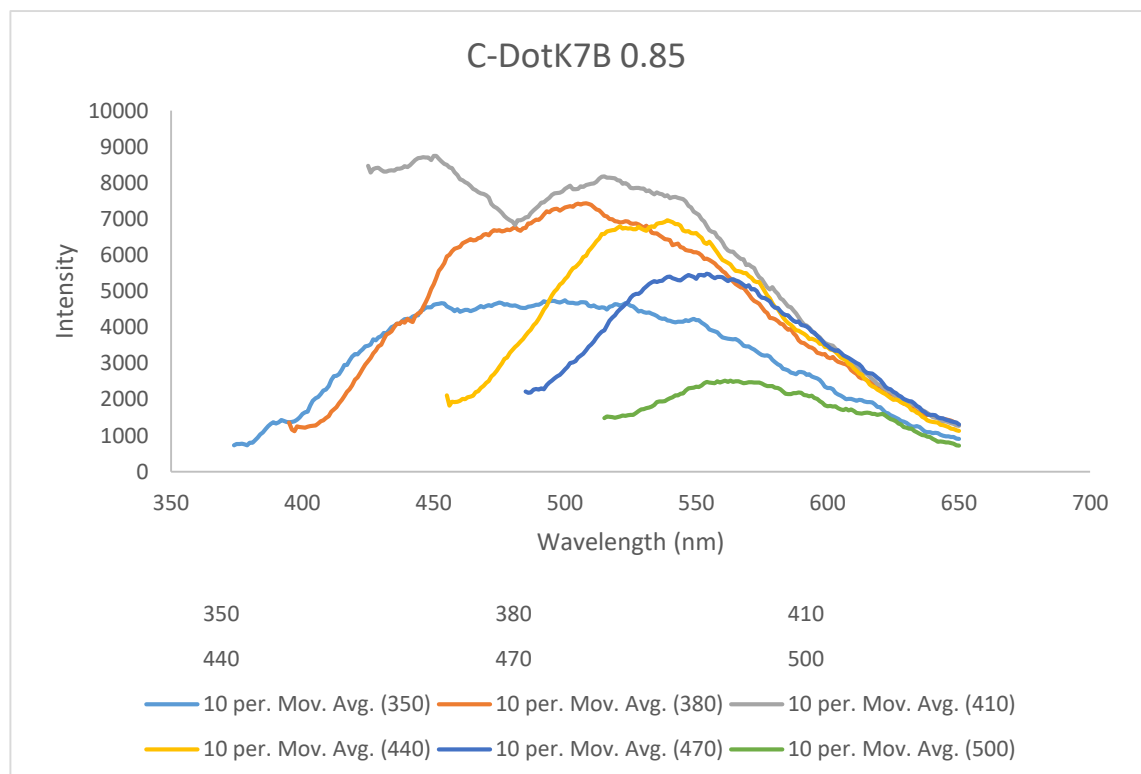


Figure 26f): Fluorescence spectrum of C-dotK7B solution (0.1 mg/mL) pH 0.85

Fluorescence graphs for C-dot, C-dotK7A and C-dotK7B solutions at high pH (greater than 7)

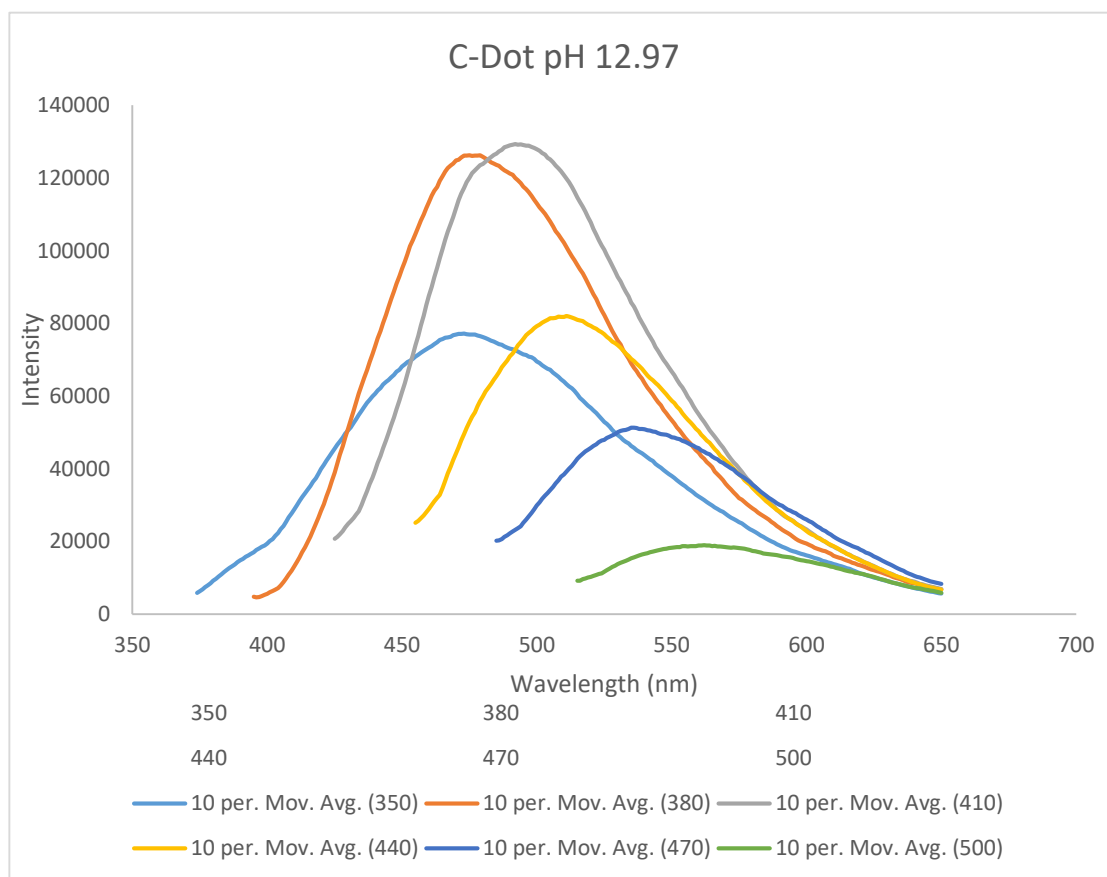


Figure 26g): Fluorescence spectrum of C-dot solution (0.1 mg/mL) at pH 12.97

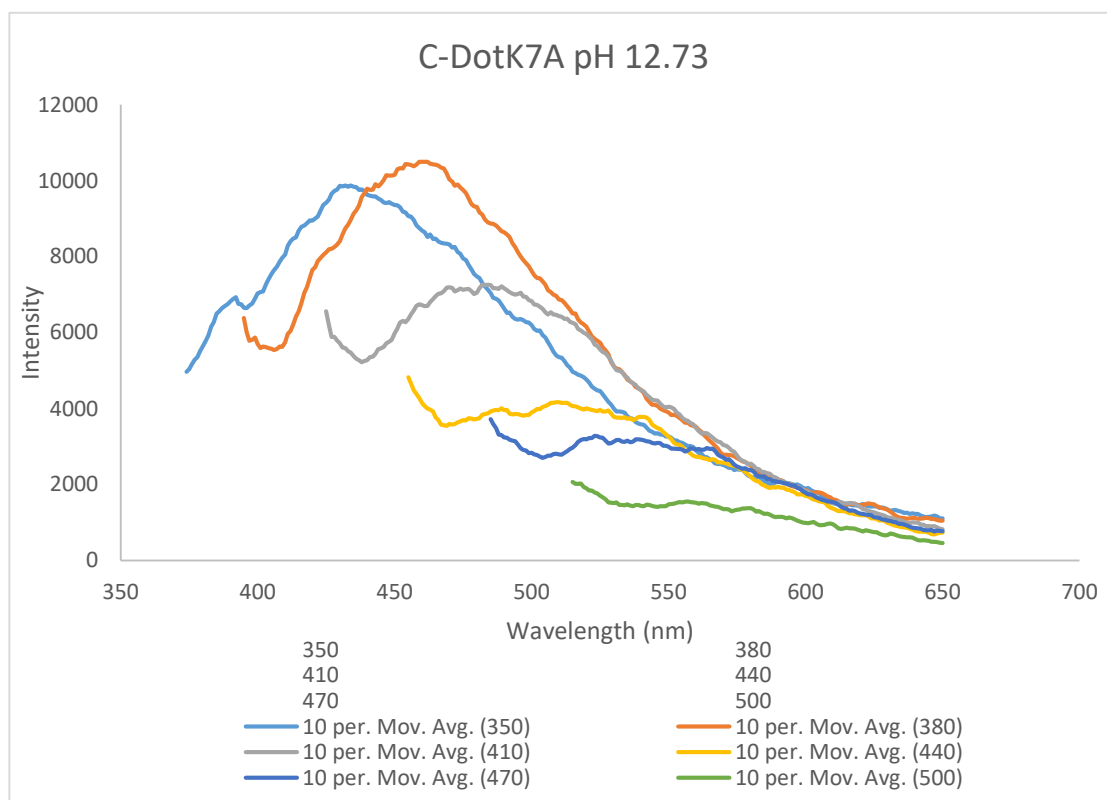


Figure 26h): Fluorescence spectrum of C-dotK7A solution (0.1 mg/mL) pH 12.73



### 3.2.2 UV-VIS analysis

Ultra-violet spectroscopy performed on all the C-dot material solutions to find out how they absorb or reflect in the ultraviolet region and it is a good test to compare with fluorescence data. The solutions of all C-dot materials dispersed in water had the same concentration of (0.1 mg/ml) and the K7 peptide solution had an unknown concentration. The image showing the colour of each sample solutions (darkest to lightest) reflects how they absorb in the ultra-violet light. For example, the C-dot solution has the darkest colour (dark brown) and on the UV graph (figure 27), the blue line representing the C-dot solution has the highest absorbance. On the other hand, the K7 peptide solution has no colour and has the lowest absorbance. When the K7 peptide attaches to the C-dot, the conjugated C-dotK7 systems display coloured solutions and absorbance values somewhere in-between. The absence of distinct, sharp peaks characteristic of aromatic rings is consistent with NMR data.

Both samples are water-soluble and show colloidal stability over a prolonged period of time. In a sample solution, if the particles do not all disperse, then large aggregates will start to form, these aggregates will absorb UV-light and absorbance values would be much greater. Solutions, which are transparent, tend to reflect light. The K7 peptide is still dispersible at a good level and this fits with the zetasizer information providing a diameter size of 42 nm.

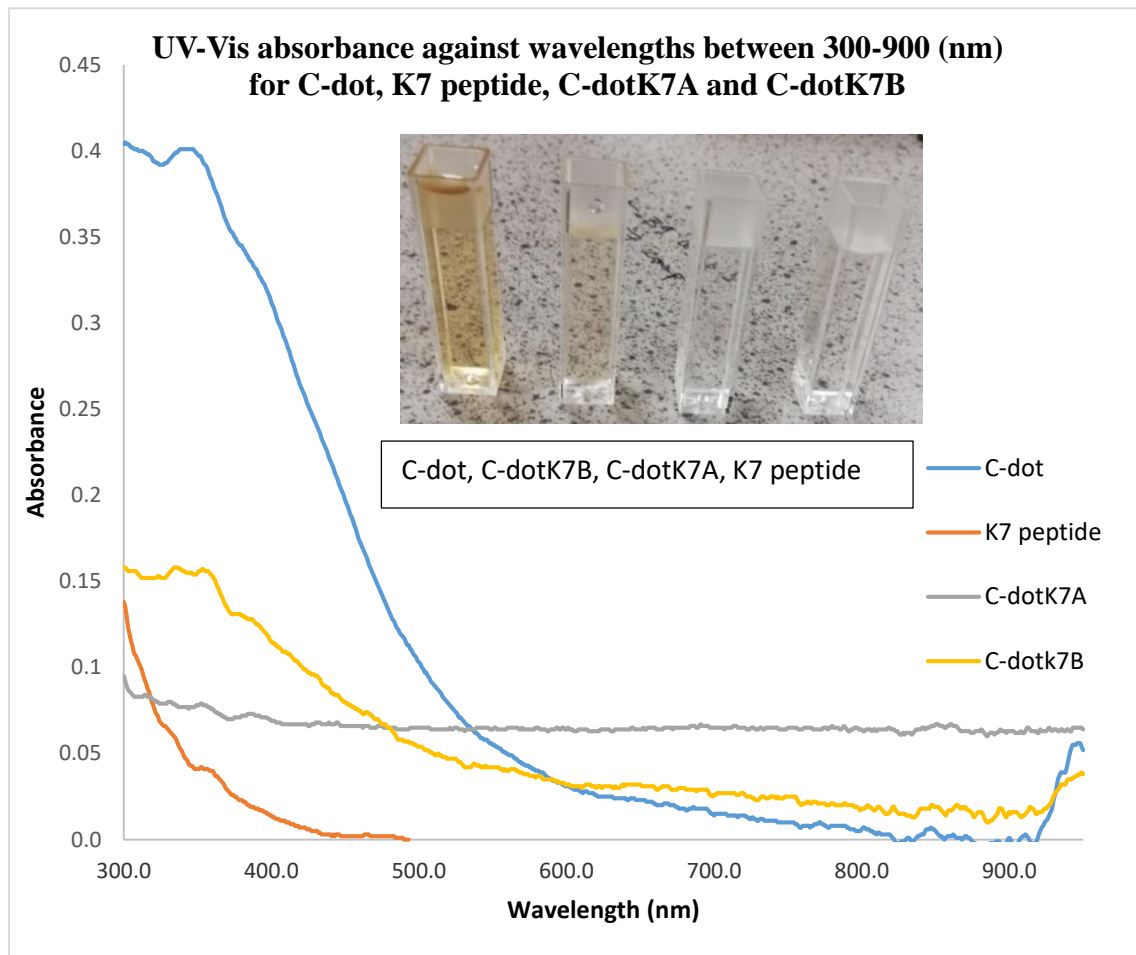


Figure 27: UV-Vis absorbance of solutions of C-dot, K7 peptide, C-dotK7A and C-dotK7B. The image shows the solutions inside the cuvette, left to right, C-dot, C-dotK7B, C-dotK7A and K7 peptide.

### 3.3 Sterility test

By observing all the petri dish images, each of the samples at both 24 hours and 48 hours do not display any sign of growth therefore, the samples are ready for antimicrobial testing.



Figure 28a): Petri dishes of C-dot material after 24 hours (left) and after 48 hours (right)

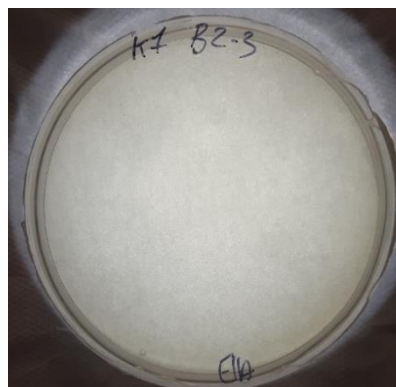
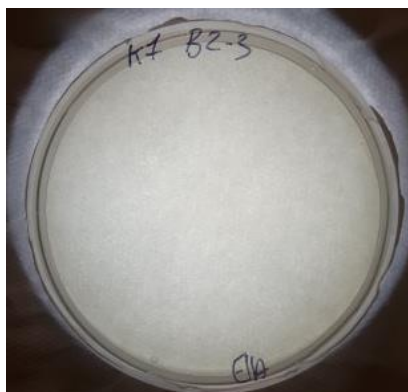


Figure 28b): Petri dishes of K7 peptide material after 24 hours (left) and after 48 hours (right)

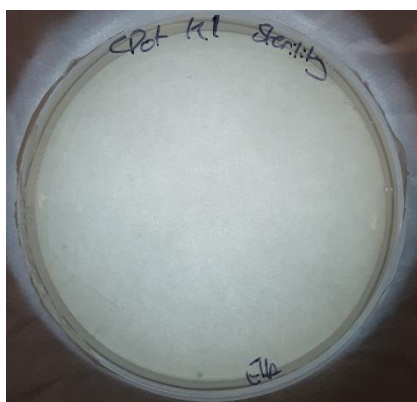


Figure 28c): Petri dishes of C-dotK7A material after 24 hours (left) and after 48 hours (right)

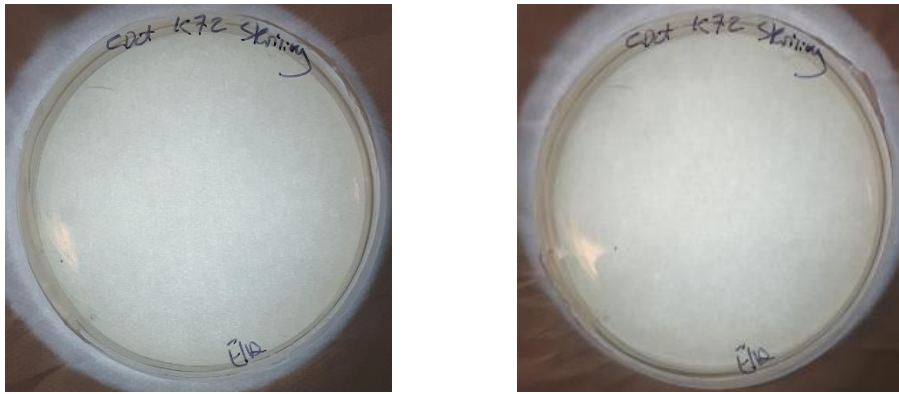


Figure 28d): Petri dishes of C-dotK7B material after 24 hours (left) and after 48 hours (right)

### 3.4. Haemolysis Test Method

A haemolysis test completed for all the samples three times, to determine whether they show any toxicity against RBCs. Haemolysis is the breaking down of red blood cells (RBCs), if RBCs are being destroyed, and then the substance is toxic against RBCs. Figure 29a) shows the negative and positive control, figure 29b) shows the haemolysis result for the K7 peptide and figure 29c) shows the haemolysis result for C-dot, C-dotK7A and C-dotK7B. All four samples produced no haemolysis at all so the samples do not break down any of the red blood cells. To go down the path of testing in biological applications, further toxicity testing is required, as some substances might not be toxic to RBCs but may be toxic to other cells.

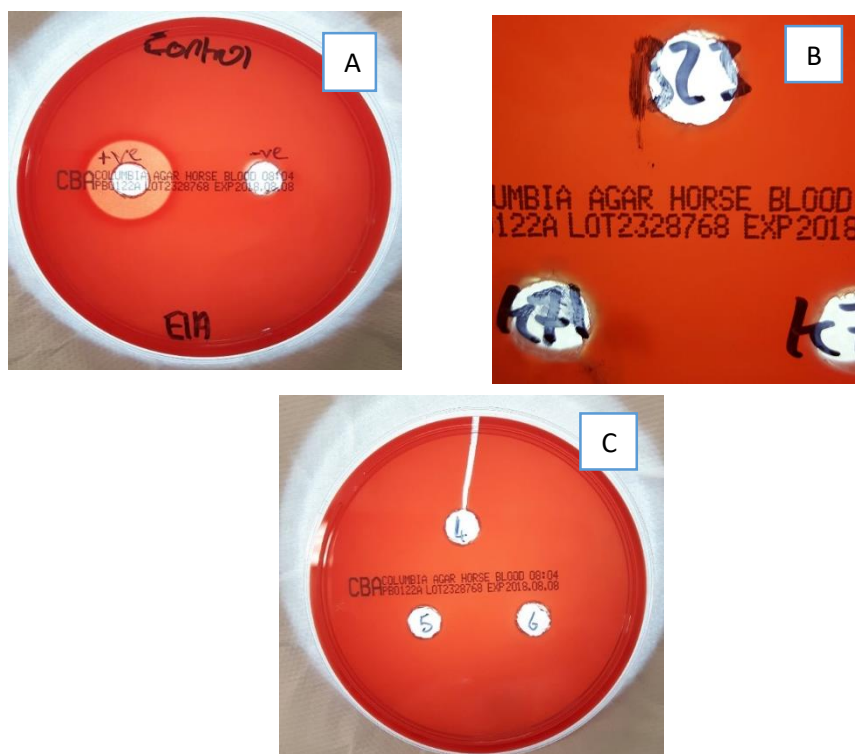


Figure 29): A) negative and positive control for the haemolysis test, B) haemolysis result for the K7 peptide and C) haemolysis result for C-dot (4), C-dotK7A (5) and C-dotK7B (6).

### 3.5 Nanoparticles with both bioimaging and antimicrobial properties

Many bioimaging materials show excellent antimicrobial properties and a few of the materials mentioned below, describe briefly the uses of both bioimaging and antimicrobial behaviour. The potential of the C-dotK7 conjugated materials for use in biomedical applications, made it of interest to go and explore their antimicrobial activity.

Nanosilver (Ag nanoparticles) is a commonly used engineered nanomaterial, which has attractive biomedical applications, taking advantage of its plasmonic/metallic and antimicrobial properties.<sup>81</sup> These properties will help in preventing infections and can be used as a diagnostic and therapeutic tool. Nanosilver particles release Ag<sup>+</sup> ions from their surface which can kill sulphur and

phosphorus containing groups such as DNA and proteins. This results in damage to the cell membrane and protein function, leading to cell death. The use of nanosilver in dental adhesives was effective against streptococci without disturbing the adhesive mechanical properties.<sup>81</sup> Nanosilver is an example of a plasmonic particle and can be detected by many optical microscopy techniques. An example of this, the attachment of nanosilver to iron oxide nanoparticles. These were incubated with macrophages and were easily detected by two-photon imaging after their cell uptake.<sup>81</sup>

The chemical grafting of a fluorescent carbon nanoparticle onto the surface of a fabricated zinc oxide nanorod, showed antimicrobial activity against gram-positive and gram-negative bacteria and displayed bioimaging properties. The fluorescent nanorod was incubated into the cell of *Staphylococcus* bacteria and was imaged successfully under fluorescent microscopy.<sup>82</sup>

### 3.6 Antimicrobial behaviour of C-dot, K7 peptide and conjugates

All samples of K7 peptide, C-dot, C-dotK7A and C-dotK7B underwent an antimicrobial test method to determine how efficient the materials were at killing or stopping the growth of microorganisms. The concentration used for the samples was 0.01 mg/ml and they were tested against two different types of bacteria strain, which consisted of *E.coli* in one culture and *Staphylococcus* in the other. Figures 30 shows the results of each sample to see how efficient they were at destroying the colonies of the two bacteria.

C-dot and K7 peptide materials tested for antimicrobial properties and individually they may show some contribution to antimicrobial effect. The blue chart in each of the figures 30) results, describes the percentage number of *E.coli* cell colonies destroyed by each material tested. C-dot and K7 peptide killed roughly 30% of

*E.coli* colonies and when the materials conjugate together, an average of 40% of colonies were destroyed which shows better antimicrobial efficiency. C-dotK7B system had 63% of *E.coli* bacteria growth inhibition and has greater antimicrobial effect on the bacteria than C-dotK7A. The yellow chart in each of the figure 30 results shows the percentage number of *Staphylococcus* cell colonies destroyed by each material tested. The C-dot material killed over 30% of colonies, whereas the K7 peptide killed 4% of *Staphylococcus* colonies. The percentage of *Staphylococcus* death increases to over 40% when the C-dot and K7 peptide materials conjugate together. Overall, it can be seen that there is a synergistic effect-taking place for the conjugated C-dotK7 systems. The antimicrobial effect is greater than average when C-dot and K7 attach together.

#### Statistics of microbiology results

Table 7 and table 8 show the statistical results for the antimicrobial testing performed three times on each of the materials against *E.coli* and *Staphylococcus* bacteria, respectively. The colony forming unit (CFU) is a measure of the number of bacteria colonies, present in the sample culture. The total dilution factor is a value that describes the overall dilution used and how the total dilution factor was achieved, can be seen in the appendix. Lastly, the total number of bacteria is calculated by multiplying the CFU value by the total dilution factor. An average was taken for the CFU value and the total number of bacteria for each of the sample materials and of the control. The average values were used to work out the number of bacterial colonies destroyed by each of the sample materials.

Table 7: Statistical results of C-dot/C-dot k7 materials against E.coli

Material	CFU ( $\times 10^{-6}$ )	Total dilution ( $\times 10^7$ )	Total number of bacteria
<b>K7 peptide</b>	83	2.5	2075
	65	2.5	1625
	80	2.5	2000
<b>C-dot</b>	68	2.5	1700
	76	2.5	1900
	72	2.5	1800
<b>C-dotK7A</b>	67	2.5	1675
	68	2.5	1700
	48	2.5	1200
<b>C-dotK7B</b>	22	2.5	550
	59	2.5	1475
	36	2.5	900
<b>Control</b>	101	2.5	2525
	113	2.5	2825
	110	2.5	2750

Table 8: Statistical results of C-dot/C-dot k7 materials against Staphylococcus

Material	CFU ( $\times 10^{-6}$ )	Total dilution ( $\times 10^7$ )	Total number of bacteria
<b>K7 peptide</b>	68	5	3400
	73	5	3650
	82	5	4100
<b>C-dot</b>	56	5	2800
	53	5	2650
	44	5	2200
<b>C-dotK7A</b>	40	5	2000
	51	5	2550
	41	5	2050
<b>C-dotK7B</b>	52	5	2600
	42	5	2100
	38	5	1900
<b>Control</b>	72	5	3600
	68	5	3400
	91	5	4550

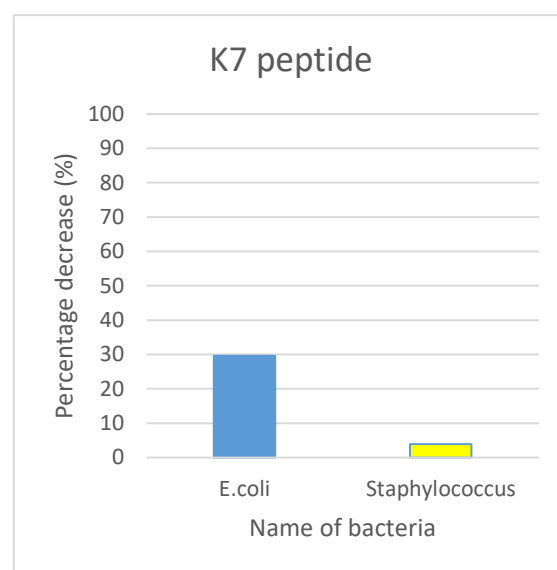
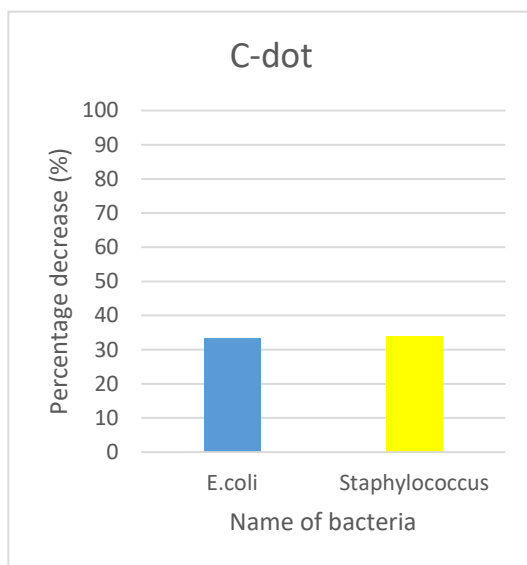


Figure 30 a-b): a) Percentage decrease of *E.coli* and *Staphylococcus* bacteria colonies for C-dot (left) and b) K7 peptide (right).

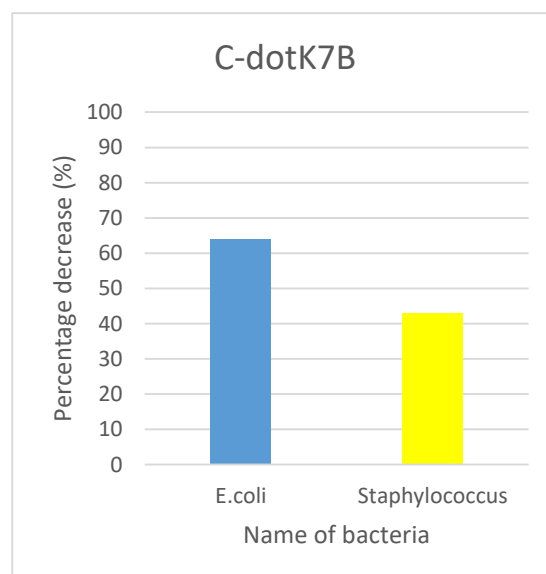
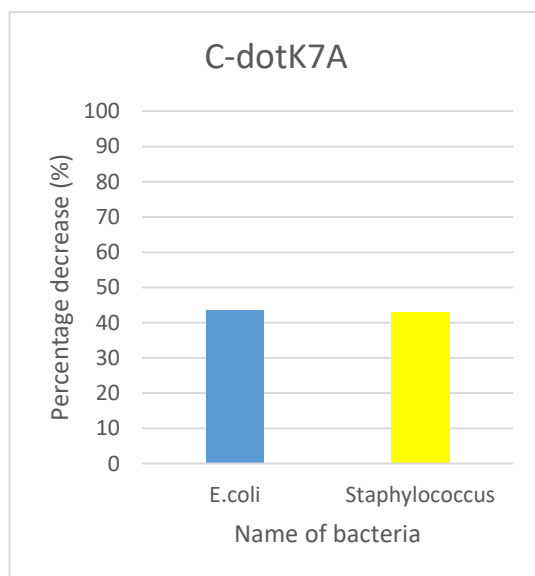


Figure 30 c-d): c) Percentage decrease of *E.coli* and *Staphylococcus* bacteria colonies for C-dotK7A (left) and d) C-dotK7B (right).

### 3.7 Comparison of results to literature data

The structural characterisation, optical properties and antimicrobial behaviour of the C-dot, K7 and C-dotK7 conjugates has been explained in detail throughout section 3. The results from a variety of tests performed on the materials can be compared to similar data explored from the literature. Firstly, the structural characterisation of K7 peptide to determine the size of its particles was performed, by measuring the dynamic light scattering effect using a zetasizer instrument. The main particle size of K7 peptide is 42nm in diameter and a similar polyLysine complex had comparable particle sizes. The poly(L-lysine)-DNA complexes had sizes in the range of 55-105 nm.<sup>78</sup> Moreover, the C-dot particle was functionalized with nitric acid to incorporate oxygen based functional groups onto its surface for the availability of attaching a K7 peptide. The surface functionality provided brilliant fluorescence emissions of the C-dot and C-dotK7 materials. A study by Sun *et al* also functionalised the surface of C-dots but with inorganic salts such as ZnO, ZnS. The fluorescence spectroscopy gave increased quantum yields and brighter fluorescence emissions, compared to the un-doped C-dots.<sup>11</sup> Furthermore, two different C-dot conjugated systems read in literature, showed interesting antimicrobial activity as well as the C-dot and C-dotK7 conjugates. A group of researchers developed a method of conjugating C-dots (C-dot-C<sub>12</sub>) with the quaternary ammonium compound lauryl betaine (BS-12).<sup>79</sup> A number of antimicrobial evaluations performed on the C-dots, BS-12 and conjugated C-dot-C<sub>12</sub> materials. The materials were tested against *Staphylococcus* (gram-positive) and *E.coli* (gram-negative) bacteria. Under the same conditions to C-dot/K7/C-dotK7 system, these tests showed that the individual C-dot material and BS-12 showed no antimicrobial activity against either bacteria not even when the concentration increased to 30 µg/mL. However,

when the C-dot and BS-12 attach together to form the C-dot-C<sub>12</sub> system, a synergistic effect happens were over 98.5% of *Staphylococcus* colonies killed at a concentration 10 µg/mL for C-dot-C<sub>12</sub> (figure 31a). For Gram-negative bacteria *E.coli*, the C-dot-C<sub>12</sub> system at a concentration of 25 µg/mL killed about 5% of *E.coli* bacterial colonies and at an increased concentration of 200 µg/mL, only 25% of colonies were killed<sup>79</sup> (figure 31b). Overall, comparing the two C-dot systems, C-dot/K7/C-dotK7 has stronger antimicrobial fight against gram-negative *E.coli* bacteria. The C-dot-C<sub>12</sub> system shows promising antimicrobial effects against *Staphylococcus* bacteria compared to the C-dot/K7/C-dotK7 system, however, only low concentrations of 10 µg/mL used for C-dot/K7/C-dotK7.

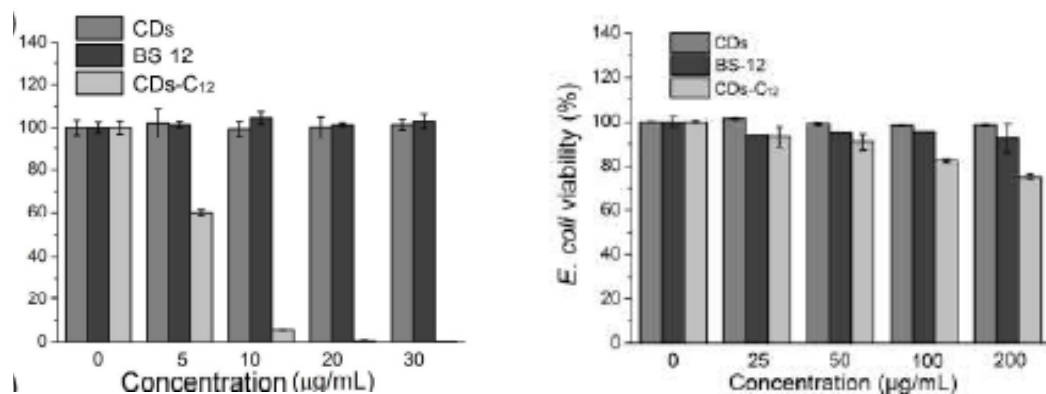


Figure 31: a) The left graph shows the concentration (µg/mL) vs the viability of *Staphylococcus* bacteria against CDs, BS-12 and CDs-C<sub>12</sub> materials. b) The right graph shows the concentration (µg/mL) vs the viability of *E.coli* bacteria against CDs, BS-12 and CDs-C<sub>12</sub> materials.<sup>79</sup>

The bactericidal activity of multi-walled carbon nanotubes (MWNTs) and MWNT-epilison-polyLysine (MEPs) at 20 mg l<sup>-1</sup> concentration in phosphate buffer saline (PBS) were reported in literature. The figure 32) below, describes that MWNTs kill 25.5, 34 and 22.5% of *E.coli*, *Ps. Aeruginosa* and *Staphylococcus* respectively.<sup>80</sup> The carbon nanotubes show a small amount of antimicrobial activity against both *E.coli* and *Staphylococcus* bacteria (25.5 and 22.5%), these values are similar to our C-dot material (33% death of both bacteria). The attachment of MWNTs to polyLysine to form MEPS increases the antimicrobial properties dramatically. MEPs kill 97.6, 91.5 and 88.5% of *E.coli*, *Ps. Aeruginosa* and *Staphylococcus* respectively.<sup>80</sup> Therefore, carbon nanoparticles on their own, do not exhibit great antimicrobial properties. Yet, when functionalized with polyLysine they significantly enhance the antibacterial activates against *E.coli* and *Staphylococcus*. The MEPs system displays larger percentages of bacteria death compared to the C-dotK7 systems, but higher concentrations of MEPs solutions used.

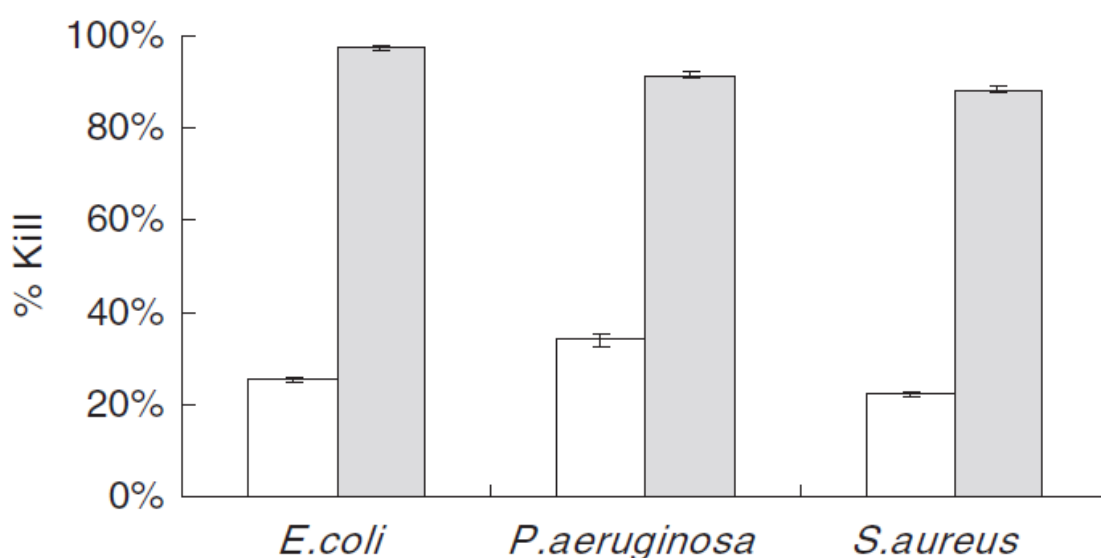


Figure 32) The killing percentages of multi-walled carbon nanotubes (MWNTs) (no background column) and MWNTepilison-polylysines (grey background column) against *E.coli*, *Pseudomonas aeruginosa* and *Staphylococcus aureus* in the 20 mg l<sup>-1</sup> concentration of suspensions, respectively.<sup>80</sup>

Due to timing issues, no bioimaging experiments were tested or analysed. However, described in the future work section, is a few proposed tests that can be used and investigated for the continuation of the research project.

#### 4. Conclusion

Well-defined C-dots were synthesized via pyrolytic treatment of citric acid monohydrate and ethanolamine and were characterized using FT-IR, elemental analysis and fluorescence spectroscopy. Elemental analysis provided information about the element composition of C-dot (60% C, 13.5% N, 7% H), FT-IR showed the relevant functional groups present on the surface of the C-dot, such as COOH, C-O and C=O. The fluorescence spectroscopy shows that the C-dots exhibit excitation-wavelength dependent emission. In the introduction section, literature research was carried out explaining that the synthesis of C-dots can be modified to tune and increase the photoluminescence emissions. For example, the surface functionalisation or heteroatom doping of C-dots can significantly increase the photoluminescence. Therefore, the synthesis of the C-dot in our research project, had its surface oxidised with nitric acid to increase its photoluminescence.

The cell-penetrating peptide K7 was synthesized, purified using HPLC analysis and characterised via NMR spectroscopy. The size by intensity distribution of K7 peptide using the zetasizer instrument, indicated two populations with hydrodynamic diameters of 40nm and 300nm respectively. Two different approaches were followed to allow the C-dot/peptide conjugation. First, method A was used to attach the C-dot to the end of the uncleaved peptide sequence as grown to the synthesizer. Second, method B focuses on the covalent attachment of C-dot to the cleaved peptide. FT-IR spectroscopy confirmed the successful conjugation of C-dot to K7 peptide. UV-VIS analysis proved the C-dot solution had the highest absorbance and the K7 peptide had lowest absorbance. Whereas, the C-dotK7 conjugates displayed coloured solutions and absorbance values somewhere in-between. Described also in the introduction section, are a

few unique examples of C-dot and QD nanoparticles attached to different peptides that can inhibit or slow down the fibrillation process of amyloid fibrils which causes Alzheimer's disease.

Both conjugated systems show promising antimicrobial properties against model Gram positive and Gram-negative strains, while demonstrating very low levels of haemolytic activity. Moreover, the conjugated systems display interesting optical properties, albeit less intense compared to the peptide-free analogues. The combination of those unique characteristics (e.g. supreme optical properties, minimal haemolytic activity, enhanced biocompatibility) make the C-dotK7 ideal candidates for bioimaging applications. Many bioimaging materials show excellent antimicrobial properties and the potential of the C-dotK7 conjugates for use in biomedical applications lead us to go and explore their antimicrobial activity. To assess their bioimaging capabilities it is important to explore how the properties of the conjugates work when used in different bioimaging experiments, especially on the focus for cancer cell imaging. Two bioimaging probes with suggestions of possible cancer cell incubation with the C-dotK7 conjugates are discussed further in the future section. Lastly, improvements and further progression for the project work, such as toxicity testing of the conjugates and the evaluation of their cell penetrating performance is highlighted.

## 5. Future Work

Firstly, we need to evaluate the cell-penetrating performance of the conjugates and it will be beneficial to compare against a different peptide that has been functionalised onto the C-dots surface. Secondly, we need to evaluate possible toxicity effects of the conjugates. One way is by performing an MTT assay. An MTT assay is a common colimetric assay for assessing cell metabolic activity.<sup>31</sup> An alternative test that can be performed on the conjugates is known as WST-1-Cell cytotoxicity assay. The WST-1 assay is a subtle and accurate assay for cell proliferation and cytotoxicity.<sup>83</sup> It is accomplished in a single tissue culture well and requires no washing or solubilisation of cells. The adherent or suspension cells are cultured on a microplate and then incubated with WST-1 and a spectrometer is used to screen the assay.<sup>83</sup> Thirdly, we need to assess their bioimaging capabilities and therefore, it is important to explore how the properties of the conjugates work when used in different bioimaging experiments, especially on the focus for cancer cell imaging. In one study, confocal laser scanning microscopy (CLSM) was used to investigate the uptake of C-dots-FA by HeLa cancer cells.<sup>25</sup> The images show that the HeLa cells incubated with C-dots-FA show bright fluorescence in both the cytoplasm and cell membrane, but not the nucleus. The technique in effect scans an object point by point using a focused laser beam to allow for a 3-D reconstruction.<sup>25</sup> CLSM is an ideal imaging tool to observe the possible fluorescence of different cancer and defected cells such as HeLa, A549, MCF- 7 when incubated inside the conjugate materials. A second bioimaging probe which works similarly to CLSM is known as two-photon microscopy (TPM). The technique uses a laser to excite a fluorescent tag within a sample and the detectors will measure light that is emitted. The lasers used in TPM, excite by using near simultaneous absorption of two long wavelength

(800nm) photons. The benefits of using longer wavelengths is that they are less damaging to the tissues but can also penetrate the tissues more deeply.<sup>84</sup> C-dots passivated with PPEI-EI agent for two-photon microscopy was reported by Cao *et al.*<sup>19</sup> The passivation leads to surface defects on the carbon particle surface acting as excitation energy traps, which allow human breast cancer MCF-7 cells to be brightly illuminated under the microscope with excitation at 800nm.<sup>19</sup> It is of curiosity to discover whether the supreme optical properties of the C-dotK7 conjugates can detect good, clear images of different cancer and defected cells such as MCF-7, HeLa or A549 cells etc. Therefore, the conjugates will be incubated with the different cancer cell lines and the bioimaging will be performed using both CLSM and TPM probes. The resolution of these probes will be compared against a standard such as quantum dots etc. Additionally, other imaging techniques like NIR fluorescence or therapies such as photodynamic therapy, can be performed using C-dotK7 as a PL material, to observe if it can image or help to kill cancer cells.

## 6. References

1. Hola K, Zhang Y, Wang Y, Giannelis EP, Zboril R, Rogach AL. Carbon dots-emerging light emitters for bioimaging, cancer therapy and optoelectronics. *Nano Today*. 2014;9(5):590-603.
2. Bhunia SK, Saha A, Maity AR, Ray SC, Jana NR. Carbon nanoparticle-based fluorescent bioimaging probes. *Sci Rep*. 2013;3:1473.
3. Fernandes D, Krysmann JM, Kelarakis A. Carbogenically coated silica nanoparticles and their forensic applications. *Chemical Communication*. 2016;52:8294-8296.
4. Krysmann MJ, Kelarakis A, Dallas P, Giannelis EP. Formation mechanism of carbogenic nanoparticles with dual photoluminescence emission. *J Am Chem Soc*. 2012;134(2):747-750.
5. Song Y, Zhu S, Yang B. Bioimaging based on fluorescent carbon dots. *RSC Advances*. 2014;4:27184-27200.
6. Krysmann MJ, Kelarakis A, Giannelis EP. Photoluminescent carbogenic nanoparticles directly derived from crude biomass. *Green Chem*. 2012;14(11):3141-3145.
7. Tucureanu V, Matei A, Avram AM. FTIR spectroscopy for carbon family study. *Crit Rev Anal Chem*. 2016;46(6):502-520.
8. Sk AM, Ananthanarayanan A, Huang L, Lim HK, Chen P. Revealing the tunable photoluminescence properties of graphene quantum dots. *Journal of Materials Chemistry C*. 2014;2:6954-6960.

9. Li L, Wu G, Yang G, P J, Zhao J, Zhu JJ. Focusing on luminescent graphene quantum dots: Current status and future perspectives. *Nanoscale*. 2013;5:4015-4039.
10. Lim YS, Shen W, Gao Z. Carbon quantum dots and their applications. *Chem Soc Rev*. 2015;44:362-381.
11. Luo GP, Sahu S, Yang TS, et al. Carbon "quantum" dots for optical bioimaging. *Journal of Materials Chemistry B*. 2013;1:2116-2127.
12. Goh J, E., Kim S, K., Kim R, Y., et al. Bioimaging of hyaluronic acid derivatives using nano-sized carbon dots. *Biomacromolecules*. 2012:1-27.
13. Qiao Z, Wang Y, Gao Y, et al. Commercially activated carbon as the source for producing multicolor photoluminescent carbon dots by chemical oxidation. *Chem Commun*. 2010;46(46):8812-8814.
14. Hu Y, Yang J, Tian J, Jia L, Yu J. Waste frying oil as a precursor for one-step synthesis of sulfur-doped carbon dots with pH-sensitive photoluminescence. *Carbon*. 2014;77:775-782.
15. Wang Y, Hu A. Carbon quantum dots: Synthesis, properties and applications. *Journal of Materials Chemistry C*. 2014;2:6921-6939.
16. Xu Q, Zhao J, Liu Y, et al. Enhancing the luminescence of carbon dots by doping nitrogen element and its application in the detection of Fe(III). *J Mater Sci*. 2015;50:2571-2576.
17. Zhao A, Chen Z, Zhao C, Gao N, Ren J, Qu X. Recent advances in bioapplications of C-dots. *Carbon*. 2015;85:309-327.

18. Xu M, He G, Li Z, et al. A green heterogeneous synthesis of N-doped carbon dots and their photoluminescence applications in solid and aqueous states. *Nanoscale*. 2014;6(17):10307-10315.
19. Cao L, Wang X, Meziani MJ, et al. Carbon dots for multiphoton bioimaging. *J Am Chem Soc*. 2007;129(37):11318-+.
20. Yan F, Zou Y, Wang M, Mu X, Yang N, Chen L. Highly photoluminescent carbon dots-based fluorescent chemosensors for sensitive and selective detection of mercury ions and application of imaging in living cells. *Sens Actuator B-Chem*. 2014;192:488-495.
21. Mehta VN, Jha S, Basu H, Singhal RK, Kailasa SK. One-step hydrothermal approach to fabricate carbon dots from apple juice for imaging of mycobacterium and fungal cells. *Sens Actuator B-Chem*. 2015;213:434-443.
22. Wang L, Li B, Li L, et al. Ultrahigh-yield synthesis of N-doped carbon nanodots that down-regulate ROS in zebrafish. *J Mat Chem B*. 2017;5(38):7848-7860.
23. Zheng M, Liu S, Li J, et al. Integrating oxaliplatin with highly luminescent carbon dots: An unprecedented theranostic agent for personalized medicine. *Adv Mater*. 2014;26(21):3554-3560.
24. Zhu C, Zhai J, Dong S. Bifunctional fluorescent carbon nanodots: Green synthesis via soy milk and application as metal-free electrocatalysts for oxygen reduction. *Chem Commun*. 2012;48(75):9367-9369.

25. Song Y, Shi W, Chen W, Li X, Ma H. Fluorescent carbon nanodots conjugated with folic acid for distinguishing folate-receptor-positive cancer cells from normal cells. *Journal of Materials Chemistry*. 2012;22(25):12568-12573.
26. Li S, Amat D, Peng Z, et al. Transferrin conjugated nontoxic carbon dots for doxorubicin delivery to target pediatric brain tumor cells. *Nanoscale*. 2016;8(37):16662-16669.
27. Li H, Qian Z. Transferrin/transferrin receptor-mediated drug delivery. *Med Res Rev*. 2002;22(3):225-250.
28. Li M, Tang Z, Lv S, et al. Cisplatin crosslinked pH-sensitive nanoparticles for efficient delivery of doxorubicin. *Biomaterials*. 2014;35(12):3851-3864.
29. Sharma V, Tiwari P, Mobin SM. Sustainable carbon-dots: Recent advances in green carbon dots for sensing and bioimaging. *J Mat Chem B*. 2017;5(45):8904-8924.
30. Chong Y, Ma Y, Shen H, et al. The in vitro and in vivo toxicity of graphene quantum dots. *Science direct Biomaterials*. 2014;35:5041-5048.
31. Yang L, Jiang W, Qiu L, et al. One pot synthesis of highly luminescent polyethylene glycol anchored carbon dots functionalized with a nuclear localization signal peptide for cell nucleus imaging. *Nanoscale*. 2015;7(14):6104-6113.
32. Yang L, Wang Z, Wang J, et al. Doxorubicin conjugated functionalizable carbon dots for nucleus targeted delivery and enhanced therapeutic efficacy. *Nanoscale*. 2016;8(12):6801-6809.

33. Yang Y, Wang X, Liao G, et al. iRGD-decorated red shift emissive carbon nanodots for tumor targeting fluorescence imaging. *J Colloid Interface Sci.* 2018;509:515-521.
34. Soto C, Sigurdsson E, Morelli L, Kumar R, Castano E, Frangione B. Beta-sheet breaker peptides inhibit fibrillogenesis in a rat brain model of amyloidosis: Implications for alzheimer's therapy. *Nat Med.* 1998;4(7):822-826.
35. Xia Y, Padmanabhan P, Gulyas B, Murukeshan VM. *Peptides functionalized carbon dots for in vitro fluorescent imaging of amyloid fibrils.* ; 2017.
36. Levine H. Thioflavine T interaction with synthetic Alzheimers's disease beta-amyloid peptides: Detection of amyloid aggregation in solution. *Protein Science.* 1993;2:404-410.
37. Xiao S, Zhou D, Luan P, et al. Graphene quantum dots conjugated neuroprotective peptide improve learning and memory capability. *Biomaterials.* 2016;106:98-110.
38. Thakur G, Micic M, Yang Y, et al. Conjugated quantum dots inhibit the amyloid beta(1-42) fibrillation process. *International Journal of Alzheimer's Disease.* 2011:1-15.
39. Xu C, Xie J, Kohler N, Walsh EG, Chin YE, Sun S. Monodisperse magnetite nanoparticles coupled with nuclear localization signal peptide for cell-nucleus targeting. *Chemistry-an Asian Journal.* 2008;3(3):548-552.
40. Zhang M, Ju H, Zhang L, et al. Engineering iodine-doped carbon dots as dual-modal probes for fluorescence and X-ray CT imaging. *International Journal of Nanomedicine.* 2015;10:6943-6953.

41. Merrifield B, R. Solid phase peptide synthesis. I. the synthesis of a tetrapeptide. *Institute of Industrial Medicine*. 1963;85:2149-2154.
42. Glasfeld A. Overview of solid-phase peptide synthesis (SPPS) and secondary determination by FTIR. 2015  
people.reed.edu/~glasfeld/Chem392/lab/Exp2\_peptide.pdf.
43. Introduction to fmoc solid phase peptide synthesis.  
<https://cdn2.hubspot.net/hubfs/.../904001902-Intro%20to%20Fmoc%20SPPS-1.pdf?t>.
44. FIELDS G, NOBLE R. Solid-phase peptide-synthesis utilizing 9-fluorenylmethoxycarbonyl amino-acids. *Int J Pept Protein Res*. 1990;35(3):161-214.
45. Carpino A, L., Han Y, G. The 9-fluorenylmethoxycarbonyl amino-protecting group. *J. Org. Chem*. 1972;37:3404-3409.
46. El-Faham A, Albericio F. Peptide coupling reagents, more than a letter soup. *Chem Rev*. 2011;111(11):6557-6602.
47. Vasconcelos L, Parn K, Langel U. Therapeutic potential of cell-penetrating peptides. *Future Science*. 2013;4(5):573-591.
48. Sigma Aldrich. Poly-lysine | sigma-aldrich.  
<https://www.sigmaaldrich.com/technical-documents/articles/biofiles/poly-lysine.html>. Accessed 25th September, 2018.

49. Dabbousi B, RodriguezViejo J, Mikulec F, et al. (CdSe)ZnS core-shell quantum dots: Synthesis and characterization of a size series of highly luminescent nanocrystallites. *J Phys Chem B*. 1997;101(46):9463-9475.
50. Lei Y, Tang H, Yao L, Yu R, Feng M, Zou B. Applications of mesenchymal stem cells labeled with tat peptide conjugated quantum dots to cell tracking in mouse body. *Bioconjug Chem*. 2008;19(2):421-427.
51. Biju V, Muraleedharan D, Nakayama K, et al. Quantum dot-insect neuropeptide conjugates for fluorescence imaging, transfection, and nucleus targeting of living cells. *Langmuir*. 2007;23(20):10254-10261.
52. Li Z, Huang P, Lin J, et al. Arginine-glycine-aspartic acid-conjugated dendrimer-modified quantum dots for targeting and imaging melanoma. *Journal of Nanoscience and Nanotechnology*. 2010;10(8):4859-4867.
53. bio synthesis. Solid phase peptide synthesis.  
<https://www.biosyn.com/tew/solid-phase-peptide-synthesis.aspx>. Accessed 26th September, 2018.
54. Kreuzer G, A., Salveson J, P. Standard practices for fmoc-based solid phase peptide synthesis in the nowick laboratory (version 1.6.1). 2015.
55. Bakalyar S, Mcilwrick R, Roggendorf E. Solvent selectivity in reversed-phase high-pressure liquid-chromatography. *J Chromatogr*. 1977;142(NOV):353-365.
56. Sellergren B, Hall J, A. Fundamental aspects on the synthesis and characterisation of imprinted network polymers. In: B. Sellergren, ed. *Molecular imprinted polymers*. 1st ed. Elsevier; 2000:22-57.

57. Povrozin Y, Barbieri B. Fluorescence spectroscopy. In: Kurtz M, ed. *Handbook of measurement in science and engineering*. 1st ed. Wiley; 2013:2475-2499.
58. Gurumurthy B, R., Bhatia D, Ramesh K, P. Structural analysis of merino wool, pashmina and angora fibers using analytical instruments like scanning electron microscope and infra-red spectroscopy. *International Journal of Engineering Technology Science and Research*. 2017;4(8):2394-3386.
59. Tomaszewska E, Soliwoda K, Kadziola K, et al. Detection limits of DLS and UV-vis spectroscopy in characterization of polydisperse nanoparticles colloids. *Journal of Nanomaterials*. 2013:1-10.
60. Diehl B. Principle in NMR spectroscopy. In: Ulrike H, Wawer I, Diehl B, eds. *NMR spectroscopy in pharmaceutical analysis*. Elsevier Science; 2008:4-40.  
<https://doi.org/10.1016/B978-0-444-53173-5.X0001-7>.
61. Sotheeswaran S. Assay for hemolytic activity. *Journal of Chemical Education*. 1988;65:161-162.
62. Goldberg I, W. Dynamic light scattering. *American Association of Physics Teachers*. 1999;67:1152-1160.
63. Pusey PN. Brownian motion goes ballistic. *Science*. 2011;332(6031):802-803.
64. Yuan Y, Randall Lee T. Contact angle and wetting properties. In: Holst B, Bracco G, eds. *Surface science techniques*. Springer-Verlag Berlin Heidelberg; 2013. 10.1007/978-3-642-34243-1\_1,.

65. Barrett C, G., Elmore T, D. Mass spectra of free peptides. In: *Amino acids and peptides*. Cambridge University Press; 1998:61-65.  
<https://doi.org/10.1017/CBO9781139163828>.
66. Hurteau R. Separation of peptide standards using formic acid as a mobile phase additive. [https://www.agilent.com/cs/library/.../5991-8597EN\\_Peptide\\_Plus\\_application.pdf](https://www.agilent.com/cs/library/.../5991-8597EN_Peptide_Plus_application.pdf). Accessed 28th September, 2017.
67. Xuan Y, Jiang G, Li Y, Yang L, Zhang X. Biodegradable oligo (poly-L-lysine) as a high performance hydration inhibitor for shale. *RSC Advances*. 2015;5:84947-84958.
68. Institute of chemical sciences and engineering. Predict 1H proton NMR spectra. [http://www.nmrdb.org/new\\_predictor/index.shtml?v=v2.95.0](http://www.nmrdb.org/new_predictor/index.shtml?v=v2.95.0). Accessed 25th September, 2018.
69. Allred L, A., Hensley L, Jr. Electronegativities of nitrogen, phosphorus, arsenic, antimony and bismuth. *J.Inorg. Nucl Chem*. 1961;17:43-54.
70. Bharathi D, Siddlingeshwar B, Krishna RH, et al. Green and cost effective synthesis of fluorescent carbon quantum dots for dopamine detection. *J, Fluoresc*. 2018;28(2):573-579.
71. Kelarakis A. Graphene quantum dots: In the crossroad of graphene, quantum dots and carbogenic nanoparticles. *Elsevier*. 2015;20:354-361.
72. Zhu S, Song Y, Zhao X, Shao J, Zhang J, Yang B. The photoluminescence mechanism in carbon dots (graphene quantum dots, carbon nanodots, and polymer dots): Current state and future perspective. *Nano Research*. 2015;8(2):355-381.

73. Xu X, Ray R, Gu Y, et al. Electrophoretic analysis and purification of fluorescent single-walled carbon nanotube fragments. *J Am Chem Soc.* 2004;126(40):12736-12737.
74. Sun Y, Zhou B, Lin Y, et al. Quantum-sized carbon dots for bright and colorful photoluminescence. *J Am Chem Soc.* 2006;128(24):7756-7757.
75. Liu H, Ye T, Mao C. Fluorescent carbon nanoparticles derived from candle soot. *Angew Chem -Int Edit.* 2007;46(34):6473-6475.
76. Bao L, Zhang Z, Tian Z, et al. Electrochemical tuning of luminescent carbon nanodots: From preparation to luminescence mechanism. *Adv Mater.* 2011;23(48):5801.
77. Zhu S, Wang L, Zhou N, et al. The crosslink enhanced emission (CEE) in non-conjugated polymer dots: From the photoluminescence mechanism to the cellular uptake mechanism and internalization. *Chemical Communications.* 2014;50(89):13845-13848.
78. Symonds P, Murray J, Hunter A, Debska G, Szewczyk A, Moghimi S. Low and high molecular weight poly(L-lysine)s/poly(L-lysine) - DNA complexes initiate mitochondrial-mediated apoptosis differently. *FEBS Lett.* 2005;579(27):6191-6198.
79. Yang J, Zhang X, Ma Y, et al. Carbon dot-based platform for simultaneous bacterial distinguishment and antibacterial applications. *ACS Appl Mater Interfaces.* 2016;8(47):32170-32181.

80. Zhou J, Qi X. Multi-walled carbon nanotubes/epsilon-polylysine nanocomposite with enhanced antibacterial activity. *Lett Appl Microbiol.* 2011;52(1):76-83.
81. Soltiriou, Georgios A; Pratsinis, Sotiris E. Engineering nanosilver as an antibacterial, biosensor and bioimaging material. *Curr. Opin.Chem.Eng*, 2011, 1, 1, 3-10.
82. Mitra,Shouvik; Chandra,Sourov; Laha,Dipranjan; Patra,Prasun; Debnath,Nitai; Pramanik,Arindam; Pramanik,Panchanan; Goswami,Arunava. Unique chemical grafting of carbon nanoparticles on fabricated ZnO nanorod: Antibacterial and bioimaging property. *Mater. Res.Bull*, 2012, 47,3,586-594,
83. G-Biosciences CytoScan™ WST-1 Cell Cytotoxicity Assay Colorimetric Assay for Quantitation of Cellular Cytotoxicity & Proliferation. 2017, [www.thco.com.tw/comm/upfile/p\\_160421\\_04270.pdf](http://www.thco.com.tw/comm/upfile/p_160421_04270.pdf)
84. Masters,BR; So,PTC Antecedents of two-photon excitation laser scanning microscopy *Microsc.Res.Tech*, 2004, 63, 1, 3-11,

Appendix:



*Appendix 1: UV-light image of C-dot in water.*



*Appendix 2: UV-light image of C-dotK7A in water*



*Appendix 3: UV-Light image of C-dotK7B in water*

### The total dilution factor

Wanted to find out the total dilution factor for the E.coli and S. aureus cultures.

The cultures suspended overnight.

Diluted the test cultures to get the desired absorbance. E.coli multiplied by 1000 and S.aureus x 2000.

200  $\mu$ L taken out of 10 ml onto each of the discs. x 50

The 200  $\mu$ L then placed into 9.8 ml Ringers (10 ml total). x 50

Serially diluted x times. Serial dilutions x (However many dilutions)

100  $\mu$ L taken out of 1ml. x 10

Total dilution factor for E.coli  $2.50 \times 10^7$  x serial dilution x by CFU

Total dilution factor for S.aureus  $5.00 \times 10^7$  x by serial dilution x by CFU

